Max-Planck-Institut für Meteorologie
Max Planck Institute for Meteorology

Sea Ice Export through Fram Strait: Variability and Interactions with Climate

Torben Königk

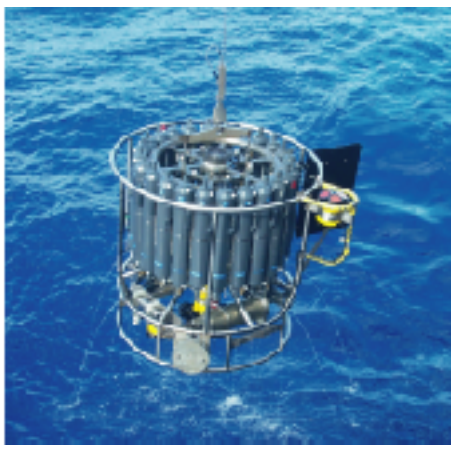

Berichte zur Erdsystemforschung 12/2005

Reports on Earth System Science

Hinweis

Die Berichte zur Erdsytemforschung werden vom Max-Planck-Institut für Meteorologie in Hamburg in unregelmäßiger Abfolge herausgegeben.

Sie enthalten wissenschaftliche und technische Beiträge, inklusive Dissertationen.

Die Beiträge geben nicht notwendigerweise die Auffassung des Instituts wieder.

Die "Berichte zur Erdsystemforschung" führen die vorherigen Reihen "Reports" und "Examensarbeiten" weiter.

Notice

The Reports on Earth System Science are published by the Max Planck Institute for Meteorology in Hamburg. They appear in irregular intervals.

They contain scientific and technical contributions, including Ph. D. theses.

The Reports do not necessarily reflect the opinion of the Institute.

The "Reports on Earth System Science" continue the former "Reports" and "Examensarbeiten" of the Max Planck Institute.

Anschrift / Address

Max-Planck-Institut für Meteorologie
Bundesstrasse 53
20146 Hamburg
Deutschland

Tel.: +49-(0)40-4 11 73-0
Fax: +49-(0)40-4 11 73-298
Web: www.mpimet.mpg.de

Layout:

Bettina Diallo, PR & Grafik

Titelfotos:
vorne:
Christian Klepp - Jochem Marotzke - Christian Klepp
hinten:
Clotilde Dubois - Christian Klepp - Katsumasa Tanaka

Berichte zur Erdsytemforschung 12/2005

Meereisexport durch die Framstraße: Variabilität und Wechselwirkungen mit dem Klima

Sea Ice Export through Fram Strait: Variability and Interactions with Climate

Dissertation zur Erlangung des Doktorgrades der Naturwissenschaften
im Fachbereich Geowissenschaften der Universität Hamburg
vorgelegt von

Torben Königk

aus Kiel

Hamburg 2005

Reports on Earth System Science 12/2005

ISSN 1614-1199

Torben Königk
Max-Planck-Institut für Meteorologie
Bundesstrasse 53
20146 Hamburg
Germany

Als Dissertation angenommen
vom Fachbereich Geowissenschaften der Universität Hamburg

auf Grund der Gutachten von
Prof. Dr. J. Meinke
und
Dr. U. Mikolajewicz
Hamburg, den 13.Juli 2005
Professor Dr. Helmut Schleicher
Dekan des Fachbereiches Geowissenschaften

ISSN 1614-1199

Sea Ice Export through Fram Strait: Variability and Interactions with Climate

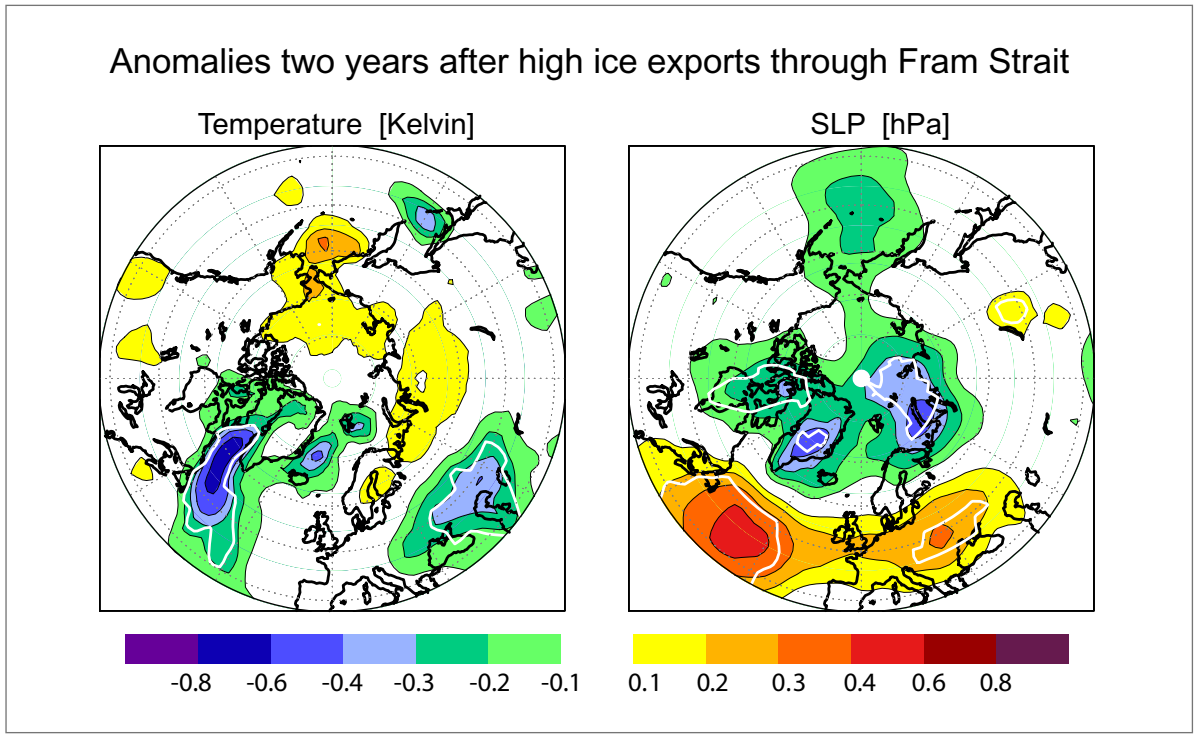

Torben Königk

Hamburg 2005

Contents

Abstract

The Fram Strait is an important interface for the transfer of Arctic climate signals to the North Atlantic Ocean. This thesis investigates the variability of the sea ice export through Fram Strait and its impact on northern hemispheric climate. For this purpose a 500-year control integration of the global coupled atmosphere-ocean-sea ice model ECHAM5/MPI-OM is analysed and sensitivity experiments are performed. The model provides a realistic mean Arctic climate and reproduces the observed variability well. The simulated mean Fram Strait ice export amounts to 97000 m^3/s. It is highly variable at interannual to decadal time scales. This variability is mainly determined by variations in the sea level pressure gradient across Fram Strait and thus geostrophic wind stress. The North Atlantic Oscillation has no significant influence on the ice export in this model. In contrast, variations in the stratospheric polar vortex and atmospheric planetary waves turned out to be of considerable importance for the wind stress in Fram Strait.

A combination of anomalous northerly winds in Fram Strait and increased sea ice thickness leads to particularly large ice exports. After such events the ice/fresh water signal propagates southward in the East Greenland Current and reaches the Labrador Sea one to two years later. This negative salinity anomaly decreases or even suppresses oceanic convection in the Labrador Sea. The associated cooler sea surface and increased sea ice cover reduce the ocean heat release to the atmosphere, which has a significant impact on air temperatures and atmospheric circulation. Sea level pressure anomalies respond in large areas of the high northern latitudes to oceanic perturbations in the Labrador Sea.

A decadal climate mode could be identified in the Arctic: it is characterised by wind forced formation of ice thickness anomalies at the Siberian coast, their subsequent propagation across the Arctic towards Fram Strait in 4 to 5 years and enhanced ice export. Negative ice thickness anomalies are generated at the Siberian coast simultaneously with the enhanced export. They reach Fram Strait another 4 to 5 years later. Furthermore, there is a feedback of the ice anomalies on the atmospheric circulation. However, it is rather weak compared to atmospheric variability. The mode is thus strongly damped.

Sensitivity studies show that the isolated effect of a prescribed ice/fresh water anomaly in Fram Strait explains a large part of the climate variability in the Labrador Sea. The ice export through Fram Strait can thus be used for predictability of Labrador Sea climate for the next two years.

Zusammenfassung

Die Framstraße stellt eine wichtige Verbindung für den Transport von Klimasignalen aus der Arktis in den Nordatlantik dar. Diese Arbeit untersucht die Variabilität des Framstraßeneistransportes und deren Einfluss auf das nordhemisphärische Klima. Dazu werden eine 500-jährige Modellsimulation und Sensitivitätsexperimente des global gekoppelten Atmosphäre-Ozean-Meereis Modells ECHAM5/MPI-OM verwendet. Das Modell stellt das mittlere arktische Klima relativ realistisch dar und reproduziert einen Großteil der beobachteten Variabilität. Der mittlere Framstraßeneistransport beträgt 97000 m^3/s und zeigt ausgeprägte interannuale und dekadische Schwankungen. Diese werden zu einem erheblichen Anteil von dem Luftdruckgradienten über der Framstraße und somit von dem geostrophischen Windstress bestimmt. Die Nordatlantische Oszillation hat in diesem Modell keinen signifikanten Einfluss auf den Framstraßeneistransport. Im Gegensatz dazu sind die stratosphärische, polare Vortex und die planetaren Wellen von großer Bedeutung für den Windschub in der Framstraße.
Besonders starke Eisexporte treten bei einer Kombination aus anomalen Nordwinden und dickem Eis auf. Die mit solchen Ereignissen verbundenen Eis/Süßwasseranomalien werden im Ostgrönlandstrom nach Süden transportiert und erreichen nach ein bis zwei Jahren die Labradorsee. Dies führt zu einer Abschwächung der ozeanischen Konvektion und nachfolgend kälteren Wassertemperaturen sowie einer erhöhten Eisbedeckung. Als Konsequenz verringert sich der Wärmefluss in die Atmosphäre, was einen signifikanten Einfluss auf die Lufttemperatur und die atmosphärische Zirkulation hat. Weite Teile der hohen nördlichen Breiten reagieren mit Luftdruckanomalien auf die ozeanischen Störungen in der Labradorsee.
Im Bereich der Arktis konnte ein dekadischer Klimamode identifiziert werden. Wesentliche Charakteristiken dieses Modes sind die windgetriebene Bildung einer Eisdickenanomalie an der sibirischen Küste, deren anschließende Propagation durch die Arktis zur Framstraße in vier bis fünf Jahren und einem darauf folgenden anomalen Eisexport in den Nordatlantik. Gleichzeitig ensteht eine negative Eisdickenanomalie an der Sibirischen Küste, die die Framstraße nach weiteren vier bis fünf Jahren erreicht. Die Eisanomalien üben eine schwache Rückwirkung auf die atmosphärische Zirkulation aus. Aufgrund der ausgeprägten atmosphärischen Variabilität ist der Klimamode jedoch stark gedämpft.
Mit Sensitivitätsexperimenten wird gezeigt, dass der isolierte Einfluss von Eisanomalien in der Framstraße einen erheblichen Anteil der Klimavariabilität in der Labradorsee erklärt. Daher ist der Eisexport durch die Framstraße ein geeignetes Vorhersageinstrument für das Klima in der Labradorsee der folgenden zwei Jahre.

1 Introduction

The Arctic consists of the large northern polar region of land and sea embracing the Arctic Ocean and the northern parts of Europe, Asia and North America (fig. 1.1). The southern boundary of the Arctic region is commonly placed at the Arctic Polar Circle (66°N). Besides this, there are other definitions of the Arctic: the area north of the tree line or the area with an average summer temperature of below 10°C. Nevertheless, the central Arctic Ocean is ice-covered year-round and snow and ice are present on land for most of the year.

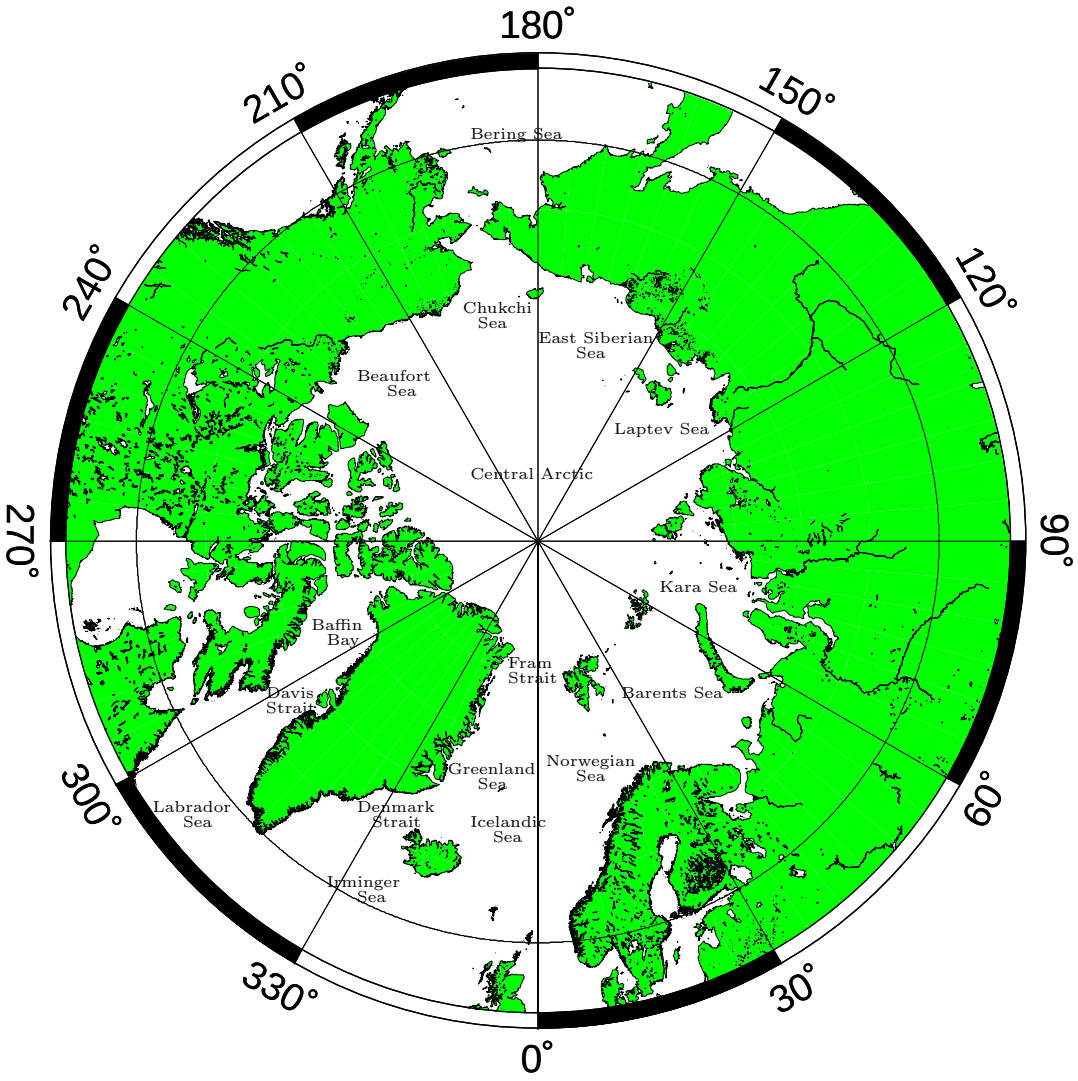

Figure 1.1: The Arctic and its periphery.

As an interface between ocean and atmosphere, the rather thin layer of sea ice controls most of the heat, momentum and matter transfers. Its low thermal conductivity prevents the relatively warm ocean to loose heat to the much colder atmosphere in the non-summer months. The ice effectively reflects the incoming solar radiation but acts almost as perfect black body radiator for the outgoing terrestrial radiation. Thus, in summer the sea ice cover reduces the energy absorbed at the surface because its albedo is much higher than that of sea water. Sea ice contributes to a colder local climate and stabilises the atmospheric stratification.

In the history of the earth, the sea ice extent varied considerably. Sometimes the Arctic was completely without ice while the ice extended as far as the mid-latitudes during ice ages. Thus, sea ice has not only an important impact on climate but also reacts sensitively to climate changes. This large sensitivity can primarily be attributed to the temperature - albedo - feedback. An initial surface warming of the polar atmosphere is amplified by less reflection of solar radiation due to a reduced ice cover. Climate models predict the largest changes for an increased greenhouse effect in the polar regions (Holland and Bitz, 2003). Therefore, a global warming would be detectable early in the sea ice cover. Although the number of observations in the Arctic is still poor, a growing interest of the Arctic climate in the last two to three decades could be noticed. Satellite observations (e.g. Kwok (2000)) and model studies (e.g. Hilmer and Lemke (2000)) have indicated a large decrease of sea ice extent in the last thirty years. Since model simulations suggest that Arctic sea ice volume varies on decadal to multi-decadal time scales (Goosse et al., 2003), there is still discussion whether the recent ice decrease is due to global warming or natural variability. Analysis of ship logs and meteorological observations since 1864 by Vinje (2001a) showed a 33 % - decrease of reconstructed sea ice extent in the Nordic Seas in the last 135 years with the occurrences of extreme events each 12-14 years.

Only a small part of the salt is included in the sea ice during the freezing of sea water while the majority is released into the underlying ocean layer. The density of the sea water is thus increased, which leads to a destabilisation of the ocean stratification. This constitutes the initial step for the deep water formation in regions without a halocline during winter time. Melting of sea ice represents a fresh water input into the upper layer of the ocean, reducing the density and stabilising the ocean stratification. Meincke et al. (1997) analysed the Arctic Ocean Nordic Seas thermohaline system and showed that a considerable part of the world ocean deep water is formed in the Nordic Seas. This occurs in direct vicinity of strong gradients in the surface salinity, which are due to melting and freezing of sea ice. Besides the cooling of the salty Atlantic inflow local ice formation and ice transports also affect the convection in the Nordic Seas. Thus, it is of great importance for the ocean where the ice is freezing and melting. As

sea ice can exist for several years, the formation area is not necessarily the same as the melting area. The transport of ice along with associated fresh water and negative latent heat plays a critical role in the climate system.

The transport of sea ice is determined by wind forcing, ocean currents and sea surface gradient. The wind forcing in the Arctic is mainly controlled by the large scale atmospheric circulation, which is dominated by the Arctic Oscillation (AO) and North Atlantic Oscillation (NAO), respectively. The AO (Thompson and Wallace, 1998) is the most important mode of atmospheric variability for the entire northern hemisphere. The AO-index is defined as the time series of the first Empirical Orthogonal Function (EOF, see Appendix A.4) of the northern hemispheric sea level pressure (SLP). The NAO (Hurrel and van Loon, 1997) describes the varying SLP difference between the Azores (alternatively Lissabon) and Iceland. A dipole with anomalous low pressure over Iceland and anomalous high pressure over the Azores occurs during a positive NAO-index. This leads to intensified westerlies over the North Atlantic and south-westerlies in the Norwegian and Barents Seas and vice versa during a negative NAO-index. Since the pressure difference between Iceland Low and Azores High is most dominant and most variable in winter seasons, the NAO-index is normally formed as winter mean (December, January, February) SLP difference. Figure 1.2 shows a negative trend in the NAO-index between 1950 and 1970 and a positive trend thereafter. The AO-pattern is nearly identically to the NAO-pattern over the North Atlantic area but the northern pole extends over large areas of the Arctic Ocean. Additionally, the AO-pattern shows a third pole over the Aleutian Islands with the same sign as the Azores High. The correlation between NAO and AO-index is very high. Thus, there is an ongoing discussion about the separability of NAO and AO (Rogers, 2002; Lin et al., 2002). Recent studies by Deser et al. (2000) and Dickson et al. (2000) highlighted an important relationship between the two oscillation phenomena and the mean state of sea ice in the Arctic. Rigor et al. (2002) showed that the AO is significantly correlated with the sea ice motion in most parts of the Arctic Basin between 1979 and 1998.

The sea ice drifts in latitudes where the ice is melting due to increased solar radiation and higher air and sea surface temperatures. The export of ice out of the Arctic Basin through Fram Strait into the Greenland Sea is especially large. Therefore, it presents a very important flux of fresh water into the North Atlantic Ocean. After passing Fram Strait, the sea ice/fresh water propagates along the east coast of Greenland into the Labrador Sea and influences the convection. As a consequence, the ice export through Fram Strait might be crucial for the thermohaline circulation. Dickson et al. (1988) and Belkin et al. (1998) suggested that the Great Salinity Anomaly (GSA) observed in the Labrador Sea in the early 70's was caused by large positive anomalies in the ice export through Fram

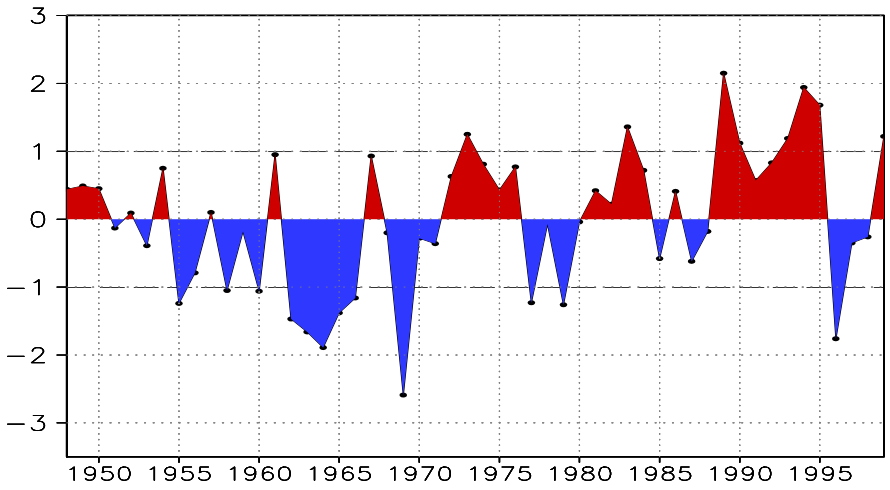

Figure 1.2: Winter means (DJF) of the NAO-index as defined by Hurrel (1995).

Strait, which propagated via the East Greenland Current to the Labrador Sea. Häkkinen (1999) used idealised fresh water pulses in the East Greenland Current to simulate this process. Her model reproduced the observed salinity anomalies in the Labrador Sea as well as the decrease in oceanic convection. It took several years until the convection in the Labrador Sea recovered in the simulation. Haak et al. (2003) concluded, from simulations with the ocean model MPI-OM (Marsland et al., 2003), that the GSA's in the 80's and 90's were caused by anomalous large ice exports through Fram Strait as well. These findings are confirmed by results from Koeberle et al. (1999). In contrary, Houghton and Visbeck (2002) emphasised the role of local processes in the production of GSA's.
The ice export through Fram Strait has a considerable effect on the ice cover in the Greenland Sea (Walsh and Chapman, 1990) and can lead to large and long lasting anomalies. The advective character of this process modifies the close local connection between direct atmospheric forcing and sea ice variability (Wang and Ikeda, 2000; Dickson et al., 2000).
Observational analysis of Deser et al. (2000) suggests a northward shift in the storm track as a consequence of low ice concentration in the Greenland Sea. They argued that SLP in the Greenland Sea is decreased as result of enhanced heat fluxes from ocean to atmosphere in areas of reduced sea ice.
In contrary, model results of Magnusdottir et al. (2004) and Deser et al. (2004) show a negative NAO pattern as response to extended sea ice cover in the Greenland and Barents Seas.

Because observations in the Arctic only exist for rather short intervals, recent studies have mainly focused on a few extreme events like the formation of the GSA in the 70's. Most observations took place in the last few decades, which saw

an unusual state of the general atmospheric circulation and large trends in Arctic climate parameters including sea ice cover, ice volume and temperature. Therefore, it is difficult to assess general statements about the interannual to decadal variability of the Arctic climate system. To avoid the above mentioned difficulties in this study, a global coupled atmosphere-ocean-sea ice model is used. In contrast to uncoupled ocean or atmosphere models, the coupled model provides the possibility to analyse interactions and possible feedbacks among ocean, sea ice and atmosphere.
Due to the importance of the Arctic within the entire climate system and the context of a potentially changing environment, it is essential to understand the physical mechanisms of climate variability in the Arctic and the teleconnections to the climate of lower latitudes. The ice export through Fram Strait is - as the largest source of fresh water export from the Arctic into the North Atlantic Ocean - a very reasonable mechanism to pass Arctic climate signals southwards.

This thesis focusses on the ice export through Fram Strait. The local and large scale response of climate on varying fresh water input through Fram Strait is investigated and the physical mechanisms of this response are analysed. Also the temporal and spatial variability of the Fram Strait ice export is considered. According to Kwok and Rothrock (1999), it is related to the sea level pressure gradient across Fram Strait. Since 1978, the ice export and the SLP gradient have been highly correlated with the NAO-index (Jung and Hilmer, 2001). This thesis seeks to determine the influence of large scale atmospheric circulation and regional processes on the ice export. Moreover, the question of a dominant time scale in the ice export variability is addressed. In this context, the aim is to find out whether dominant coupled modes exist in the Arctic climate system on an interannual to decadal time scale.
Another point of interest is whether the results gained in this context could be applied for climate predictability. The conditions and limitations for such a predictability will be analysed.
From the considerations presented in this chapter, the thesis is organised as follows: in chapter 2 a short description of the global coupled atmosphere-ocean-sea ice model ECHAM5/MPI-OM is given. The following two chapters present the mean simulated Arctic climate and its variability. The results are compared to observations and reanalysis to give an overview of the reliability of the model. A 500-year control integration of the model is used for statistical analyses. Here, the climate response to variations in the ice export through Fram Strait is investigated and the responsible physical processes shall be identified (chapter 5). Chapter 6 provides mechanisms for the variability of the ice export, a separate analysis of the atmospheric forcing and studies the influence of sea ice thickness on the ice export. The results from these analyses present some key regions and processes explaining the Arctic climate variability. To further investigate

these processes, three sensitivity studies are performed with the coupled model (chapter 7). In chapter 8 the predictability of Labrador Sea climate using the Fram Strait ice export as a predictor is addressed. The thesis is completed by a summary and conclusions (chapter 9). Some results of this thesis are presented by Koenigk et al. (accepted). The statistical tools applied in this study are described in detail in the appendix.

2 Model

The model used in this study is the Max-Planck-Institute for Meteorology global atmosphere - ocean - sea ice model ECHAM5/MPI-OM. It consists of the atmosphere model ECHAM5 (ECmwf HAMburg) and the ocean model MPI-OM (Max-Planck-Institute Ocean Model). A 500-year control integration of the ECHAM5/MPI-OM model is used for a large part of the investigations. Latif et al. (2004) used this control run for analyses of multi-decadal scale changes in the North Atlantic thermohaline circulation. The analysis of Arctic - North Atlantic interactions by Jungclaus et al. (in press) is based on the same run as well. Furthermore, the ECHAM5/MPI-OM is used to perform three sets of sensitivity experiments. A detailed description of the experiments is given in chapter 7.

2.1 Atmosphere Model ECHAM5

The atmospheric part of the coupled model is the atmospheric general circulation model ECHAM5. It belongs to the fifth cycle of a model series, which has been adapted for climate applications from the spectral weather prediction model of the European Centre for Medium Range Weather Forecast (ECMWF). A detailed description of the model characteristics is given by Roeckner et al. (2003). In the following, only a brief summary of the main features is presented.

The ECHAM model is based on primitive equations, which use the following prognostic variables: vorticity, divergence, temperature, the natural logarithm of surface air pressure, specific humidity and the mixing ratio of total cloud water. With exception of the water components, these variables are represented in the horizontal by a series of truncated spectral harmonics. In this model setup, a triangular truncation at wave number 42 (T42) is used. This results in a horizontal resolution of about $2.8° \times 2.8°$. The northern- and southern-most grid points are on a latitude of 87.8°. In the vertical, a hybrid sigma-pressure coordinate is used. It is discretized in 19 irregularly distributed levels and exhibits the highest vertical resolution in the atmospheric boundary layer. The top level reaches 10 hPa and thus the middle stratosphere.
The prognostic equations are integrated according to the semi-implicit method. Linear terms are calculated implicitly using their spectral transform while the nonlinear terms are treated explicitly on a Gaussian grid and spectrally transformed afterwards.
The initial state for the atmosphere was generated from the ECMWF-reanalysis data for 1st January 1978.

2.2 Ocean Model MPI-OM

The ocean model MPI-OM (Marsland et al., 2003) is a global version of the Hamburg Ocean Primitive Equation model (HOPE). The model is a z-coordinate global general circulation model with 23 vertical levels in this configuration and is based on primitive equations for a Boussinesq-fluid on a rotating sphere. It includes parameterisations of sub-grid scale mixing processes like isopycnal diffusion of the thermohaline fields, eddy-induced tracer transport and a bottom boundary layer slope convection scheme. The surface of the model is free and the grid is based on an Arakawa C-grid. The resolution is about 2.8° but with an increasing refinement between 30°N and 30°S up to 0.5° at the equator from 10°N to 10°S (fig. 2.3).

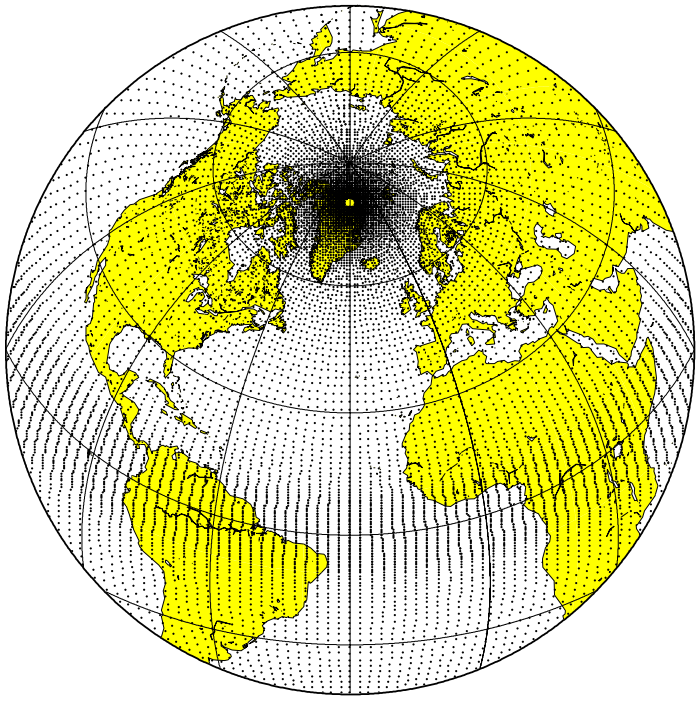

Figure 2.3: Grid of the ocean model MPI-OM.

The MPI-OM model gives the possibility to arbitrarily place the model's poles on the orthogonal curvilinear grid, which has two major advantages over conventional latitude/longitude grids. Firstly, placement of the poles over land removes the numerical singularity associated with the convergence of meridians at the geographical North Pole. The configuration used in this study places the north pole over northern Greenland at 80°N and 30°W. The model's South Pole is shifted to 80°S, 30°W. Secondly, the choice of non-diametric poles allows the construction of regionally high-resolution models to maintain a global domain. Another advantage of the placement of the grid poles is relatively high resolution in the

deep water formation regions of the Greenland and the Labrador Sea.
A dynamic, thermodynamic sea ice model is embedded in the ocean model code (Legutke et al., 1997). The dynamics of sea ice are formulated using a viscous-plastic rheology following Hibler (1979). The thermodynamics relate sea ice thickness changes to a balance of radiant, turbulent and oceanic heat fluxes. The sea ice coverage is fractional within grid cells and is related to the thickness according to subgridscale parameterisation of lateral versus vertical ablation and accretion following Stössel (1992). The considerable insulating effects of snow accumulation on sea ice are included, along with snow-ice formation when the snow/ice interface sinks below the sea level due to snow loading. The importance of sea ice dynamics in global climate models has been pointed out by Vavrus and Harrison (2003) who investigated the sensitivity of Arctic climates to sea ice motion.
The initial fields for the ocean are taken from the output of model year 150 of the climatologically forced experiment described in Marsland et al. (2003). This uncoupled run was initialised with temperature and salinity data from the World Ocean Atlas 1998 (Levitus et al., 1998).

2.3 OASIS - Coupler

The atmosphere model and the sea ice - ocean model are connected by the OASIS coupler. The coupler transfers the fluxes of momentum, heat, and freshwater from the atmosphere to the ocean and performs the interpolation onto the ocean grid. It transmits sea surface temperature, sea ice thickness, sea ice concentration and snow thickness from the ocean to the atmosphere. The climate model includes a river runoff scheme (Hagemann and Dümenil, 1998; Hagemann and Dümenil-Gates, 2003). The river runoff is transferred together with the precipitation into the ocean. Glacier calving is included in such a way that the amount of snow falling on Greenland and Antarctica is instantaneously transferred into the ocean.
In this climate model, no flux adjustment is used. Thus, problems and consequences of climate restoring (Zhang et al., 1998) are avoided. A detailed description of the OASIS coupler can be found in Terray et al. (1998).

3 Mean Arctic Climate in the Model

This chapter describes the simulated mean state of key parameters of northern high latitudes and compares the coupled model climate to observational data and other studies. Deficiencies in the model simulations are shown and discussed. The mean state of the model simulation is obtained by averaging the years 51 through 500 of the control integration. The first 50 years are regarded as spinup of the model and thus neglected.

3.1 Sea Level Pressure

Figure 3.1 shows a comparison between annual mean SLP in the 500-year control run and in the NCEP/NCAR reanalysis from 1948 to 2001 (Kalnay et al., 1996; Kistler et al., 2001). The large scale atmospheric circulation in the reanalysis is determined by high pressure systems over the subtropical North Atlantic and North Pacific as well as over Siberia. Low pressure systems occur over Iceland and the Aleutian Islands. The Iceland Low extends quite far into the Barents and Kara Seas while a ridge of the Siberian High extends from eastern Siberia to the Canadian coast. Together with the Aleutian Low, an anticyclonic wind field in the Central Arctic as well as wind stress from the west Siberian coast across the Arctic to Fram Strait and northern Greenland are produced. The pressure systems, especially the Siberian High, are particularly pronounced in winter seasons and are much weaker in summer. As a consequence, winds in the Arctic are weaker in summer, as well. The transition of the Arctic circulation state from the summer to the winter state has been specified by Miletta Adams et al. (2000).
The simulated SLP (fig. 3.1 b)) reproduces the main features of the SLP distribution in the reanalysis. However, some larger differences have to be pointed out. The Aleutian Low is much deeper in the reanalysis than in the model while the Pacific subtropical high is too pronounced in the model. Nevertheless, the resulting pressure gradient and associated winds over the North Pacific are in rather good agreement. Over the North Atlantic the subtropical high is slightly too strong and the Iceland Low extends not as far into the Barents Sea as in observations. This is partly due to a shift in the observed Iceland Low towards the northeast since the late 70's (Hilmer and Jung, 2000).
Furthermore, the Siberian High is slightly too pronounced and extends too close to the Pacific coast and into the Arctic. The mean SLP in the Arctic is therefore overestimated in the model. This leads to slightly underestimated transpolar winds from the Siberian coast to the Canadian Archipelago and the north of Greenland.

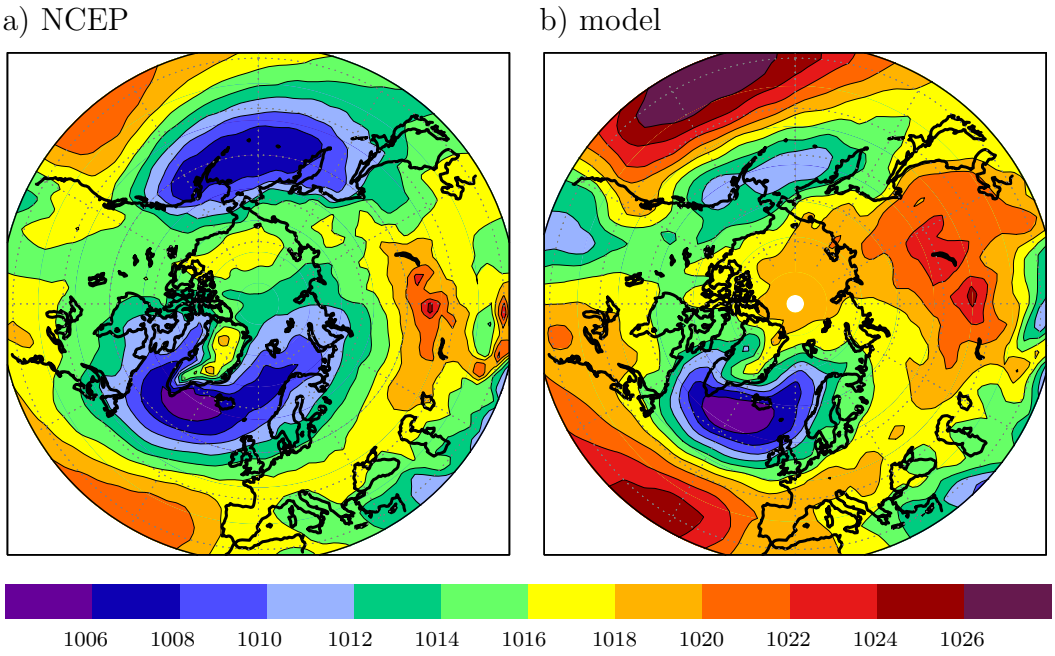

Figure 3.1: Annual mean SLP in hPa. a) NCEP data, b) control integration of the model.

3.2 Air Temperature

The annual mean two meter air temperature, averaged over 54 years of NCEP reanalysis (fig. 3.2 a), displays the typical north-south gradient. Temperature varies between less than $-15°$ C in the Central Arctic and Greenland and up to $20°$ C in the subtropics. A tongue of warm air in the northeastern North Atlantic and colder temperatures over Asia are the main deviations from the zonal distribution. The warm temperatures in the northeastern North Atlantic are due to both the heat transport of the North Atlantic Current and the southwesterly winds. An extraordinary strong temperature gradient occurs between this warm air and the cold air masses over the Arctic and Greenland. The large landmass of Asia leads to strong cooling in winter which maintains colder annual mean temperatures than the zonal mean. Temperatures over North America are colder as well but not as pronounced as in Asia. In the northeastern Pacific, a comparable effect to the northeastern Atlantic leads to slightly warmer temperatures. The simulated air temperature of the model captures the main features of the distribution in the reanalysis, but most parts of the polar regions are slightly too cold. The largest discrepancies can be seen over Siberia, in the Barents Sea and along the south coast of Alaska. Here, the simulated temperatures are up to 6 Kelvin colder than in the NCEP reanalysis data.

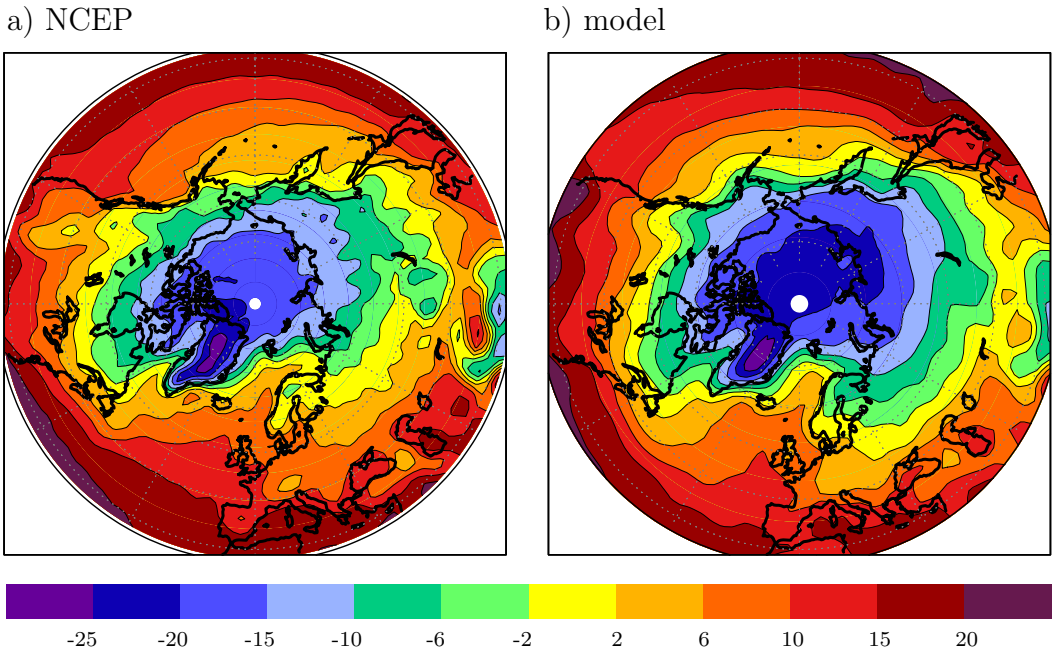

Figure 3.2: Annual mean 2 meter air temperature in ° Celsius. a) NCEP data, b) control integration of the model.

3.3 Precipitation

Figure 3.3 compares simulated annual mean precipitation with precipitation in the NCEP reanalysis. One has to keep in mind that precipitation in the reanalysis is not as reliable as e.g. SLP or temperature. Precipitation is calculated as 6-hour forecast and in contrary to SLP and air temperatures, no observations are used for the estimations. Mo and Higgins (1996) and Ruprecht and Kahl (2003) showed that the local error in the NCEP reanalysis may be quite large, especially in mountainous regions (Rasmusson and Mo, 1996) and high latitudes (Trenberth and Guillemot, 1998; Cullather et al., 2000).
However, the large scale pattern in the simulations agree well with the reanalysis. In the entire Arctic Basin precipitation is low with values of 10 to 30 mm/month. Most of the precipitation in the Arctic is falling during summer, whereas winter precipitation is less than 10 mm/month in most areas (not shown). In central Asia and the inner parts of North America, the amount of precipitation is also small. In contrast, amounts of up to 150 mm/month are reached over the mid-latitude oceans, especially over the Gulf Stream and the Kuroshio as well as at the mountainous west coast of North America. In middle and eastern Europe the model produces slightly less precipitation than in the reanalysis. In parts of Russia, it is not able to resolve the mountain ranges properly, but as pointed out before, reanalysis are erroneous in mountain regions anyway.

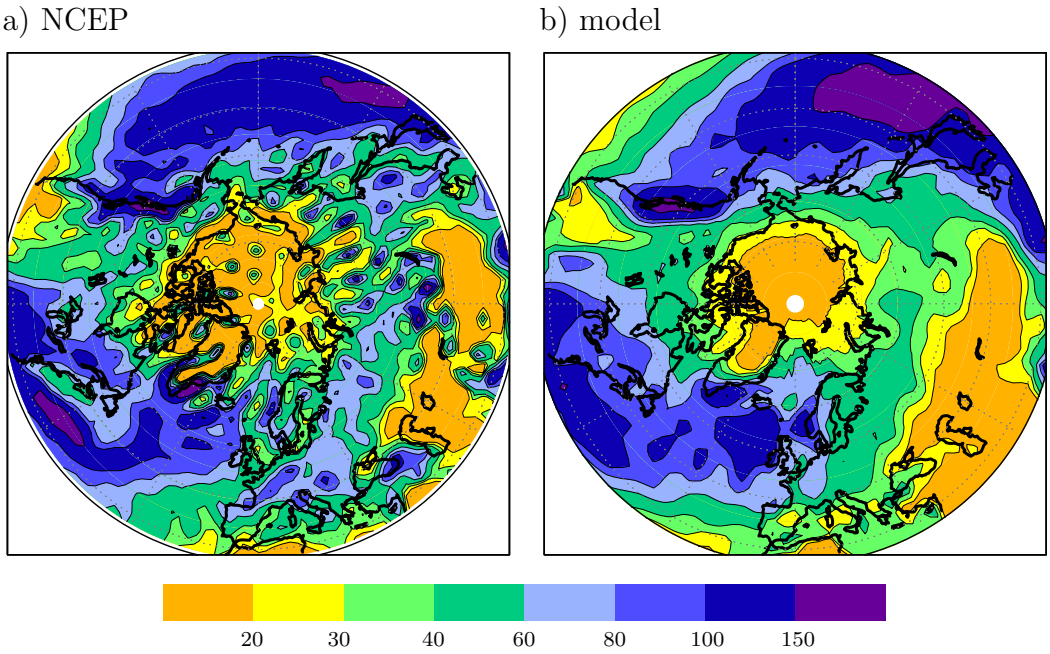

Figure 3.3: Annual mean precipitation in mm/month. a) NCEP data, b) control integration of the model.

3.4 Salinity

To compare the simulated surface salinity (10 m) to observations, the mean salinity of the Polar Science Center Hydrographic Climatology (PHC) is used (Steele et al., 2001). The PHC data set evolved by merging results from the World Ocean Atlas (Antonov et al., 1998; Boyer et al., 1998) and the Arctic Ocean Atlas (EWG, 1997, 1998) for the time period from 1950 to 1989. Because sea ice concentration is lowest in late summer, most of the observations have taken place then. Thus, observed and simulated surface salinities of August are compared (fig 3.4).
The observations show a pronounced east - west gradient in the North Atlantic. The North Atlantic Current transports warm and salty water with a salinity of 35 to 36 psu to the northeast Atlantic (Orvik and Niiler, 2002). In contrast, fresher and colder water is transported from the Arctic to the northwest Atlantic. The salinity gradient is strongest near the ice edge in the Greenland Sea. The simulated salinity shows a too pronounced fresh water tongue east of Newfoundland. Otherwise the observed pattern in the North Atlantic is quite well reproduced.
The surface salinity in the Arctic Basin is determined by the inflow of large amounts of fresh water from the Siberian and Canadian rivers and by melting and freezing of sea ice. Additionally, the amount of precipitation, although quite small, exceeds the evaporation in the Arctic area. This results in low salinities in the entire Arctic Basin. Especially fresh are surface waters at the coast of Siberia

and Canada. Near the mouths of the large Siberian and Canadian rivers, the observed surface salinity obtains less than 30 psu. The areas of low salinity at the Arctic coasts are well captured in the model, but the surface in the Central Arctic and the Chukchi Sea is too salty.
Although the simulated sea surface salinity shows some deficits, the ECHAM5/MPI-OM provides a reasonable salinity distribution compared to other ocean models (e.g. Häkkinen, 2002).

a) observations b) model

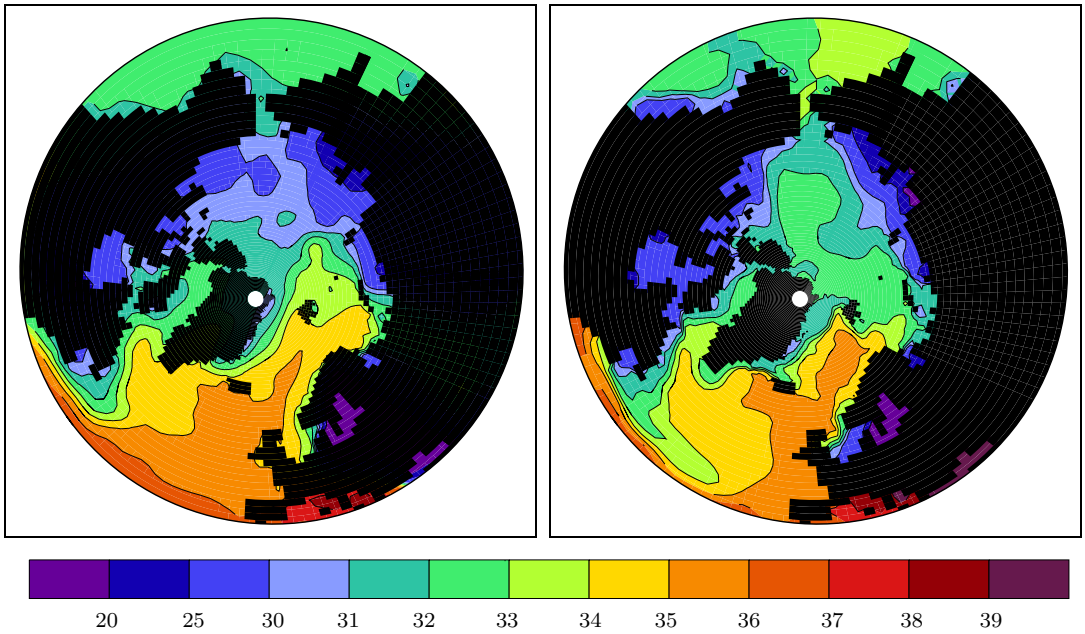

Figure 3.4: August surface salinity concentration in psu. a) Polar Science Center Hydrographic Climatology, b) control integration of the model.

3.5 Deep Water Formation and Meridional Overturning

Oceanic convection in the Nordic Seas and the Labrador Sea is the main source of deep water formation in the entire world ocean and an important drive for the thermohaline circulation. The Greenland Sea convection is mainly due to cooling of the ocean surface layer from the atmosphere (Pickart et al., 2000) while the primary precondition for Labrador Sea convection is very sensitive to surface salinity. The mixed layer depth is a good indicator for the strength of convection. Figure 3.5 a) shows the mean late winter mixed layer depth (February, March, April) of the control integration. It reaches 2000 m in the Greenland Sea and up to 1800 m in the Labrador Sea. In the Irminger Sea, it has a thickness of up to 1000 m. Convection also occurs east of Kamschatka in the Bering Sea. Bacon et al. (2003) showed that Irminger Sea convection was about 1000 meters in the

winter 1996/97. Lavender et al. (2002) used floats to estimate the mixed layer depth in the Labrador Sea in the winters 1996/97 and 1997/98. They found a mixed layer depth of more than 1300 m in the first winter whereas it was not thicker than 1000 m in the second winter. Rudels et al. (1989) observed a convection depth of 1250 m in the Greenland Sea in February 1988. Wadhams et al. (2002, 2004) found in March 2001 and May 2003 a deep convective chimney with a depth of 2500 m. Other observations (e.g. Morawitz et al. (1996); Alekseev et al. (1994)) estimated a convection depth that is varying between 1000 m and 2000 m.

a) mixed layer depth

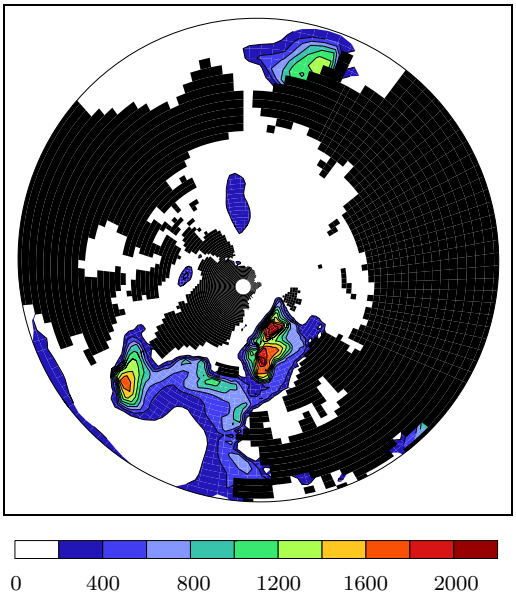

b) MOC

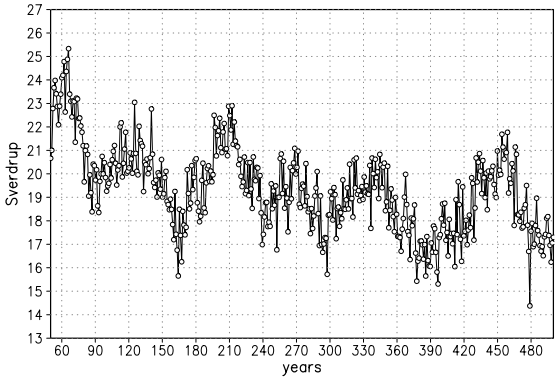

Figure 3.5: a) Late winter (February, March, April) mixed layer depth in m in the control integration, b) annual mean meridional overturning in Sverdrup at $30°N$.

The meridional overturning circulation (MOC) at $30°N$ is shown in fig. 3.5 b). The mean over the entire control integration (years 51 to 500) is 19.3 Sverdrups (Sv). This agrees well with observational estimates by Hall and Byrden (1982) and Römmich and Wunsch (1985). They found a MOC of 17 to 18 Sv. The time series of the overturning in the control integration shows a marked multi-decadal oscillation with a time scale of 80 years in average. The underlying processes are discussed in detail by Jungclaus et al. (in press). The difference between high and low phase of the overturning circulation is about 3 to 4 Sv and thus much more pronounced than interannual or decadal signals. The control integration shows a clear negative trend in the overturning circulation. This trend is particularly large before year 100 and is probably due to the turn into process of the model.

3.6 Sea Ice Concentration

The simulated sea ice concentration in the Arctic is compared with satellite observations from 1978 to 1998 (Johannessen and Myrmehl, 2002). The observational data set has a horizontal resolution of 25 km. This allows the resolution of some small islands in the Canadian Archipelago, which are unresolved in the model. Furthermore, no observations are available north of $85°N$. For a better comparison, the observations have been interpolated on the model grid.

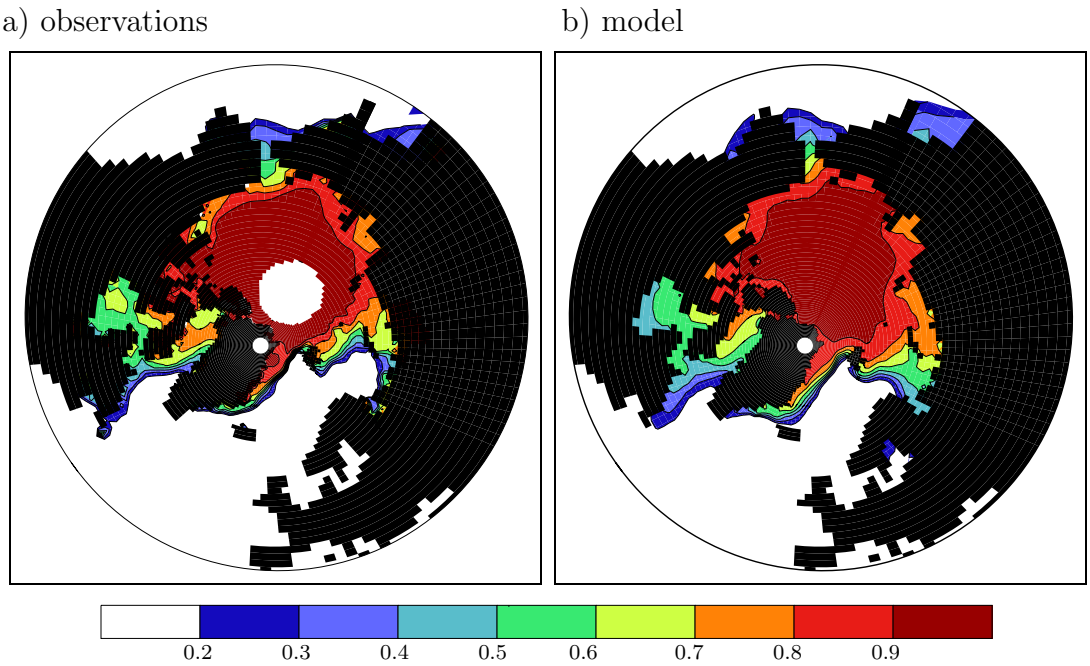

Figure 3.6: Annual mean sea ice concentration in parts. a) Johannesen et al. (2002), mean 1978-1998, b) control integration of the model.

The annual mean sea ice concentration in the observations and the control run are shown in fig. 3.6. The large scale pattern of the simulated sea ice extent agrees well with the observations. Nevertheless, the model tends to overestimate the ice content in the Barents Sea, where the observations show almost no ice at all. A slight overestimation of ice concentration is obvious in the Labrador and Greenland Seas as well. However, one has to take in account that observations are only available since the late 70's. This period was dominated by high NAO-indexes, which is associated with unusually low sea ice extent in the Barents Sea (Deser et al., 2000; Hilmer and Jung, 2000). Altogether, the ice extent in the Arctic comes out to be slightly larger in the model than in observations.
Both model simulations and observations show the largest ice extent in March while minimum values occur in September. The seasonal cycle is well reporduced by the model. A detailed description of the sea ice and its trends in different Arctic areas is presented by Parkinson et al. (1999).

3.7 Sea Ice Thickness

The distribution of sea ice thickness in the Arctic is poorly known. There are only few observations which cover small areas and short time periods (Hvidegaard and Forsberg, 2002). Rothrock et al. (1999) estimated the annual mean sea ice thickness to be 2 to 3.5 meters in the deep water portion of the Arctic. Wadhams and Comiso (1991) used remote sensing technique from submarines and aircrafts to estimate the ice thickness in the Central Arctic. They suggest a thickness of 3 to 4 meters. Simulations with an ice model of Hilmer et al. (1998) showed an ice thickness from 1 to 2 meters in the eastern Arctic, 3 to 4 meters at the North Pole and up to 6 meters north of Greenland. Haas and Eicken (2001) conducted drill holes and electromagnetic induction measurements in the Siberian and Central Arctic Seas in three different summer seasons. They found values between 1.25 to 1.85 meters in the Laptev Sea and up to 2.5 meters in the Central Arctic.

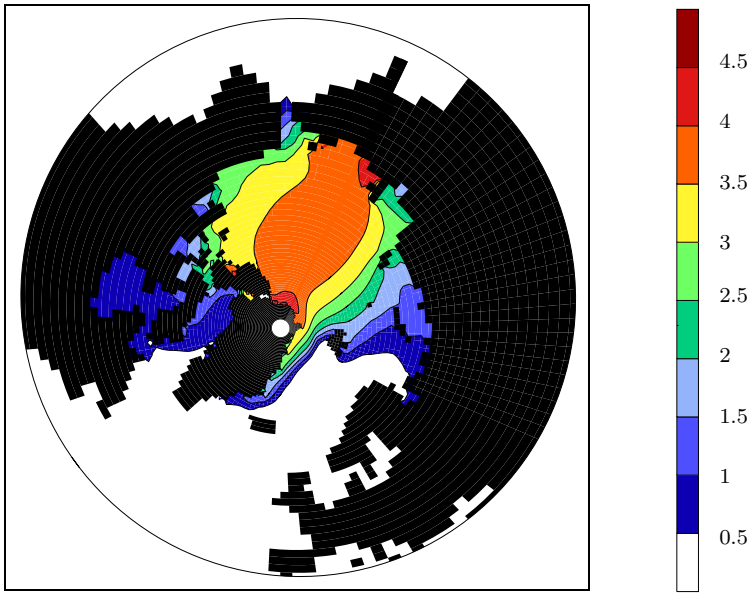

Figure 3.7: Annual mean sea ice thickness in m in the control integration.

The mean ice thickness in the 500-year control run shows a maximum of 4 to 4.5 meters north of Greenland and in the western East Siberian Sea. In a band from Greenland across the Arctic to the East Siberian coast, it reaches 3.5 to 4 meters (fig. 3.7). Towards Beaufort Sea it decreases to about 3 meters. A rapid decline can be seen from the North Pole to the European Arctic and the west Siberian coast. In the Kara Sea the ice has a thickness of 1 to 2 meters.
Obviously, the modelled ice thickness is in the range of estimations and observations in most parts of the Arctic. But the model seems to overestimate the

thickness at the East Siberian Coast. This is a common problem in coupled atmosphere-ocean-sea ice models (e.g. Goosse et al., 2002; Weatherly et al, 1998). Bitz et al. (2002) found for the atmospheric models that participated in the Atmospheric Model Intercomparison Project (AMIP) generally a too high SLP in the Arctic. This pattern creates anomalous winds, which transport too little ice from the East Siberian Sea to the Canadian Archipelago. As indicated before, the atmosphere model used in this thesis suffers under the same problem (fig. 3.1).

3.8 Sea Ice Transport

Figure 3.8 a) shows the mean sea ice transport in the Arctic in the control run. It is characterised by a clockwise ice transport in the Beaufort Gyre and transports from the Siberian coast across the North Pole to Fram Strait via the Transpolar Drift Stream (TDS). In this model, the largest transports in the entire Arctic occur in the area of Fram Strait and in the East Greenland Current (EGC). Thus, the main export of ice out of the Arctic Basin takes place through Fram Strait. Smaller amounts are exported over the Barents Shelf, through the Canadian Archipelago into the North Atlantic and through Bering Strait into the North Pacific. In Baffin Bay, Davis Strait and Labrador Sea, a southwards ice transport can be observed. The sea ice transport in the control run agrees well with model results of other studies (Häkkinen, 1993; Proshutinsky and Johnson, 1997). A comparison of the ice transport pattern to the mean SLP-field (fig. 3.1) shows that the ice is mainly driven by the wind. The ridge into the Arctic of the Siberian High, the Iceland Low and the Aleutian Low together determine the mean ice transport. As indicated above, SLP is overestimated in the Central Arctic in this model. As a consequence, the Beaufort Gyre and the TDS are slightly shifted towards the Central Arctic, Kara and Barents Sea, respectively.

The mean ice transport is divergent in almost the entire Arctic Basin (3.7 b). Largest divergences can be seen at the coasts of Barents and Kara Seas, at the northwestern coast of Greenland and in parts of the Canadian Archipelago. Furthermore, the Central Arctic shows up as a region with a quite large divergent ice transport. Convergent ice transports occur in the Barents and Greenland Seas and in the EGC as well as in the Labrador Sea and Bering Strait. As no significant trends in sea ice volume of the Arctic could be found, a convergent ice transport is associated with a negative net freezing rate and vice versa. This means that most net ice formation takes place in the coastal regions of west Siberia, northwestern Greenland, the Canadian Archipelago and in the Central Arctic, while the ice is mainly melted in the EGC south of Fram Strait, the Barents Sea, Labrador Sea and Bering Strait.

a) ice transport b) divergence

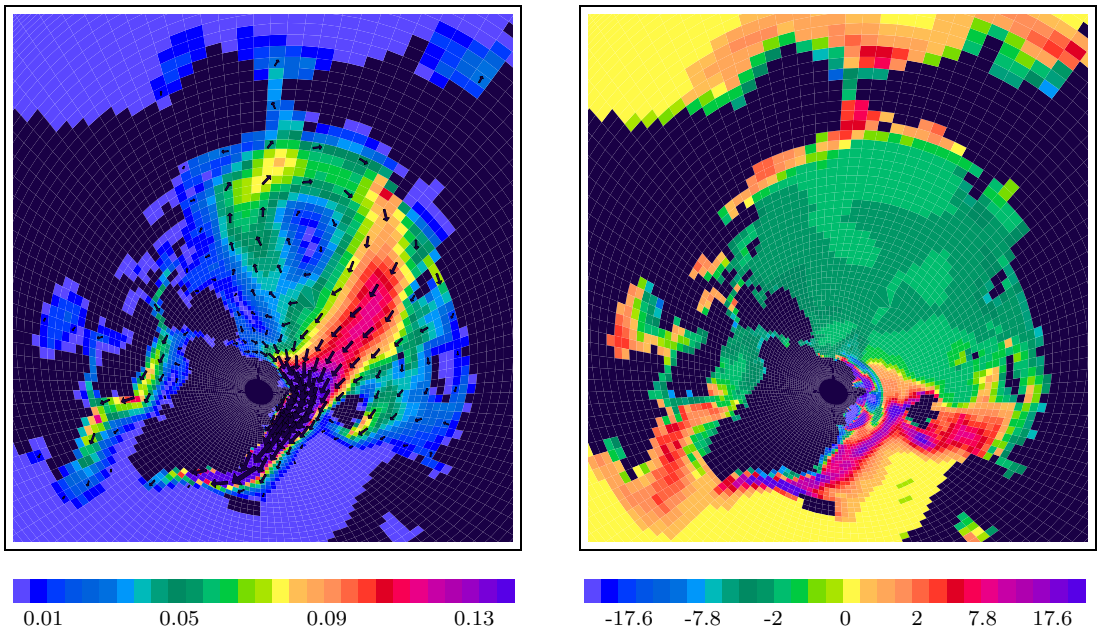

Figure 3.8: a) Annual mean sea ice transport in m^2/s in the control integration. b) Annual mean divergence of sea ice transport in $10^{-8}m/s$.

To study the ice transports and the regions of freezing and melting in detail, the Arctic has been divided into eight sub areas (Barents Sea, Kara Sea, Laptev Sea, East Siberian Sea, Chukchi Sea, Beaufort Sea and Central Arctic). The sub areas and the ice transport across their boundaries are shown in figure 3.9 together with the net freezing rate in each region. The largest ice transports take place from the Chukchi Sea into the East Siberian Sea and further to the Laptev Sea with values of about 50000 m^3/s and from the Laptev and Kara Seas into the Central Arctic. A considerable amount of ice is transported from the Central Arctic into the Barents Sea but most ice is exported through Fram Strait into the North Atlantic. The average ice export through Fram Strait in the control integration of the model is 97000 m^3/s. This is much larger than the sum of all other exports out of the Arctic Basin.
As shown before, the ice transport in the Arctic Basin is predominantly divergent. More ice is frozen than melted in all Arctic sub regions, except for Barents Sea. The net freezing rate is particularly large in the Laptev Sea, Kara Sea and in the Central Arctic with 60 to 70 cm per year. In the Barents Sea 20 cm/year are more melted than formed on average. The ice excess in the Arctic Basin is exported mostly into the North Atlantic and a smaller amount into the North Pacific to melt there.

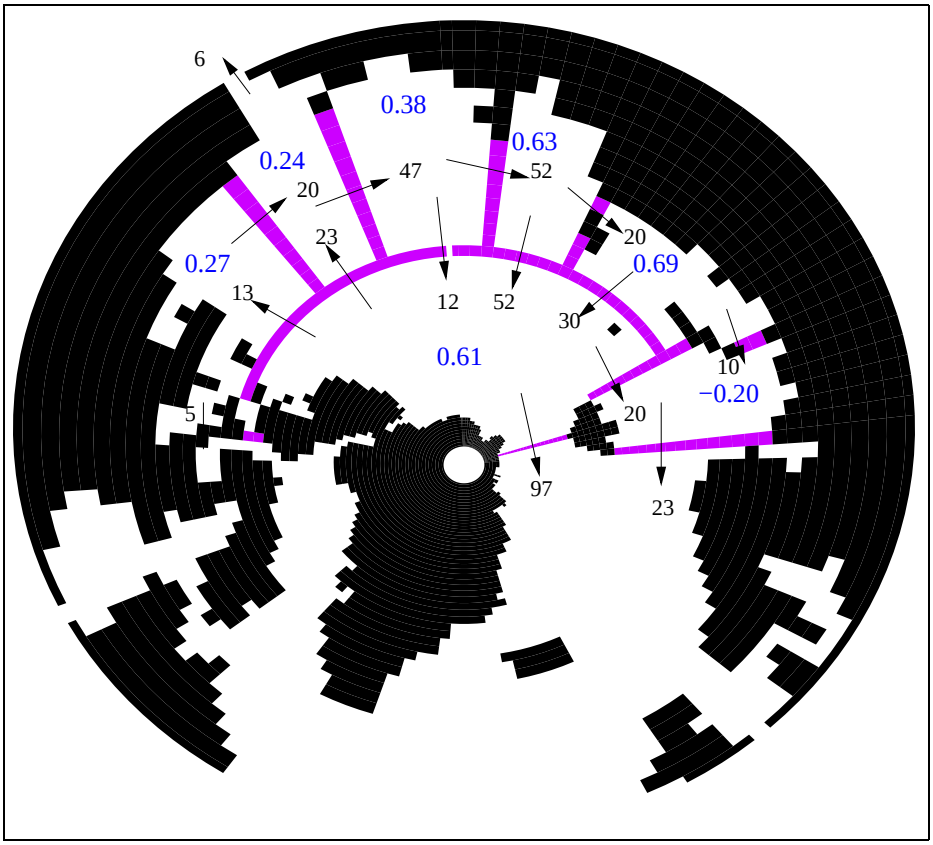

Figure 3.9: Mean ice transport through the boundaries (purple) of the Arctic sub-regions in 1000 m^3/s (black) and annual mean net freezing rate in m (blue).

4 Arctic Climate Variability

In the previous chapter, it has been shown that the 500-year control integration provides a realistic mean climate state in high northern latitudes. In this chapter, the variability of the simulated Arctic climate is compared to reanalysis data and observations. To study the variability, standard deviations and EOF analyses (compare appendix A.4) of annual mean values (August to July) of the most important parameters for this study are calculated.

4.1 Sea Level Pressure

Figure 4.1 displays the standard deviations of the simulated and observed (NCEP reanalysis) annual mean SLP in high northern latitudes. Both the reanalysis and the model simulation show high standard deviations with more than 1.5 hPa in the Nordic Seas and the Arctic Basin. The maximum of the reanalysis is situated in the Central Arctic while it is centered in the Greenland Sea in the model. The standard deviation is small over the continents of North America and central Asia. In the reanalysis, a second maximum can be observed over the North Pacific with 2 to 2.5 hPa while only about 1.5 hPa are reached in the simulation. However, the main features of the reanalysis are reproduced by the model.

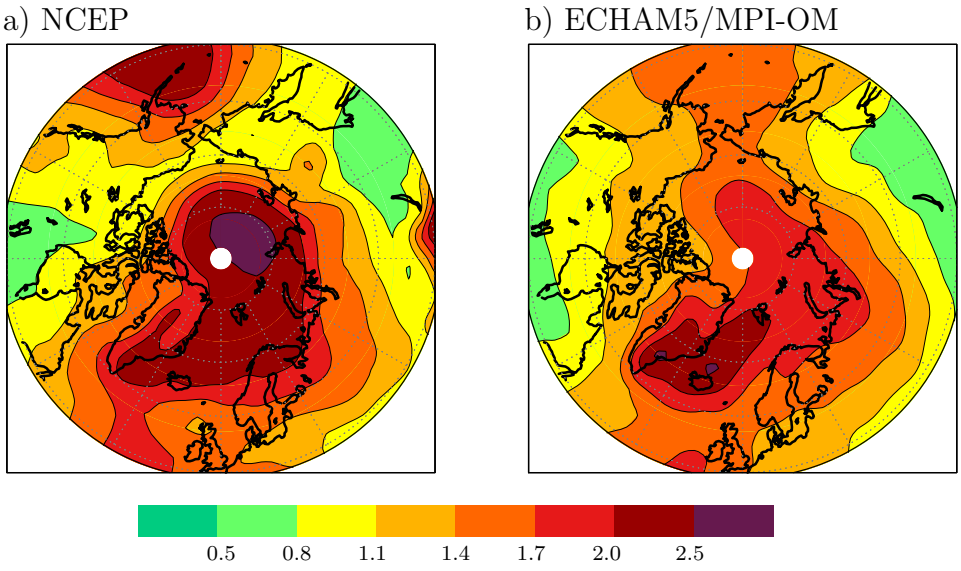

Figure 4.1: Standard deviation of annual mean SLP in hPa. a) NCEP data; b) control integration.

The first EOF of the modelled annual mean SLP north of $50°N$ (fig. 4.2 a) explains one third of the total SLP variance. The signal carries the same sign over

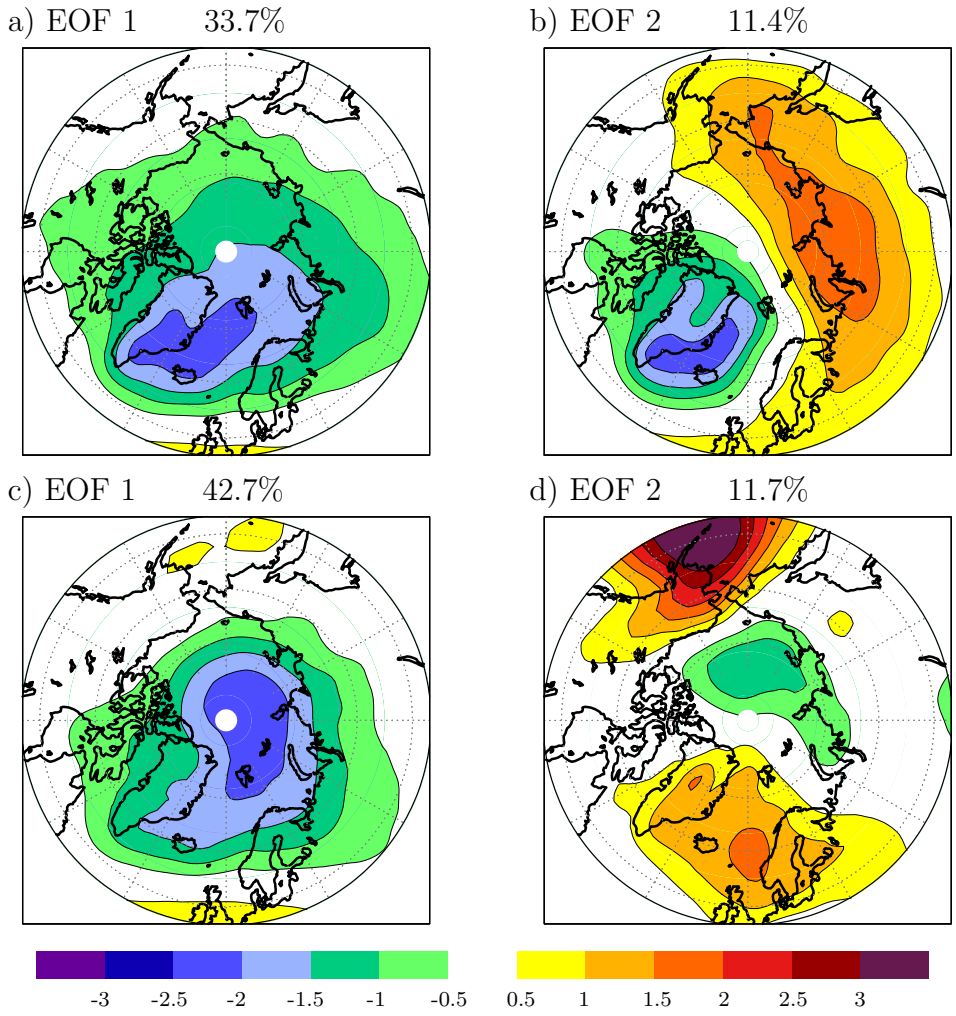

Figure 4.2: EOF 1 and 2 of annual mean SLP in the control integration (top) and the NCEP reanalysis data (bottom).

the entire Arctic Basin, the Nordic Seas and Siberia. Maximum values occur in the Nordic Seas and Greenland. The pattern is similar to the one of the standard deviation (fig. 4.1) in the Nordic Seas and the Central Arctic. The strongest SLP gradient can be seen over the North Atlantic. This distribution compares well to the pattern of the Arctic Oscillation (Christiansen, 2002; Lin et al., 2002; Itoh, 2002) north of $50°N$. The principal component (PC) of the first EOF is strongly positively correlated (r=0.7) with the AO-index in the control integration. A high AO-index is associated with anomalous west to southwest winds over the North Atlantic, which increases the transport of warm air to the north over the eastern North Atlantic. At the same time, anomalous northerly winds advect cold air into the Labrador Sea.

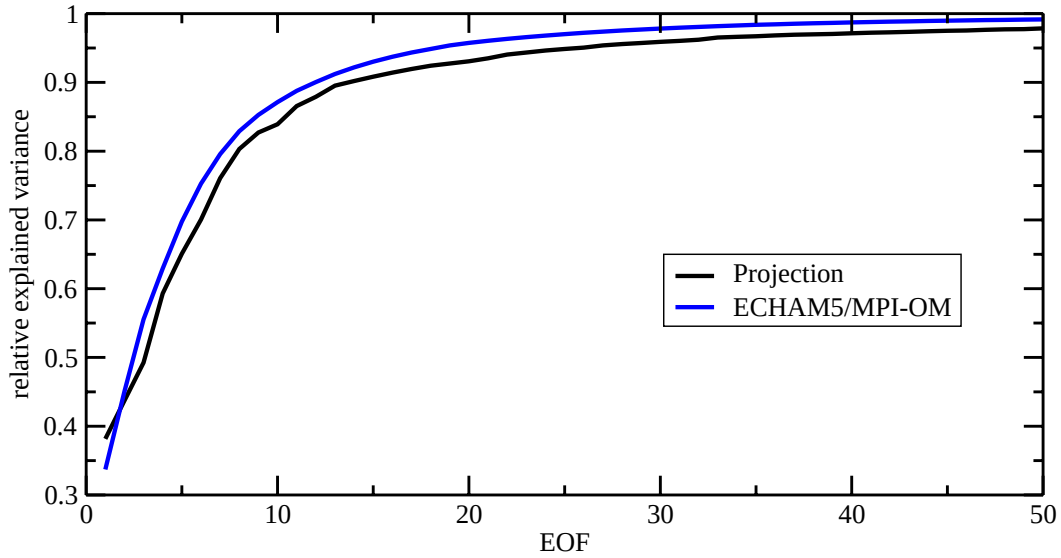

Figure 4.3: Cumulated relative explained variance of the first 50 EOF's of annual mean SLP north of $50°N$. Blue: ECHAM5/MPI-OM, black: projection of NCEP reanalysis on the EOF's of ECHAM5/MPI-OM.

The first EOF in the NCEP reanalysis shows a similar pattern. However, the center of the anomaly is shifted to the north. This leads to a stronger pressure gradient in the Arctic while the gradient over the North Atlantic is less pronounced. A spectral analysis of the first PC shows a significant peak at a time scale of about 3 years. In contrast the first PC of the control run does not indicate any significant spectral variability.
The second EOF of the control run explains about 11% of the total SLP variance and is characterised by a dipole pattern. The negative pole is situated with its center between Greenland and Iceland and the positive pole extends along the Siberian coast. For positive PC's, anomalous winds blow from the Barents Sea across the Arctic to the Chukchi Sea. The second EOF of the reanalysis provides a totally different pattern. Positive anomalies occur over the northern North Pacific as well as over northern Europe and the Nordic Seas while negative anomalies can be seen in the Central Arctic. However, disagreeing EOF patterns do not necessarily mean that the model is not able to capture the observed variability. Because the EOF's do not provide physical but mathematical modes, the variability may be differently distributed on several EOF's. To analyse how much of the observed total SLP variance is reproduced by the model, a projection of the NCEP reanalysis on the modelled EOF's is carried out. The dot product of each EOF, $\mathbf{e^n}$, with the anomalous SLP field of the NCEP reanalysis, $\mathbf{X}$, is formed for each year and one obtains the projected PC's:

$$\mathbf{e^n} \cdot \mathbf{X} = PCproj_n, \qquad n = 1, ..., 448 \tag{4.1}$$

Figure 4.3 shows the cumulated relative explained variance of the first 50 EOF's of the model and the projection. The first 10 EOF's explain slightly more than 80 % of the total variance while the first model EOF's explain about 5 % more. Obviously, the model captures a large part of the SLP variance in the reanalysis and provides a realistic SLP variability in the northern high latitudes.

4.2 Air Temperature

The standard deviation of the simulated air temperatures compares well to the one of the NCEP reanalysis data (fig. 4.4). Both patterns indicate maxima in the Labrador, Greenland and Barents Seas with a standard deviation of 2 Kelvin and more. The model shows an additional maximum in the Bering Sea, which is much weaker and shifted to the north in the reanalysis. The maxima are all located at the ice edge. Here, small variations in the ice cover can lead to large changes in the ocean heat release and hence in the air temperature. Furthermore, the sensitivity to the variations in wind direction is very high. Southerly winds advect warm air over the open water while northerly winds advect very cold air from the ice covered ocean.

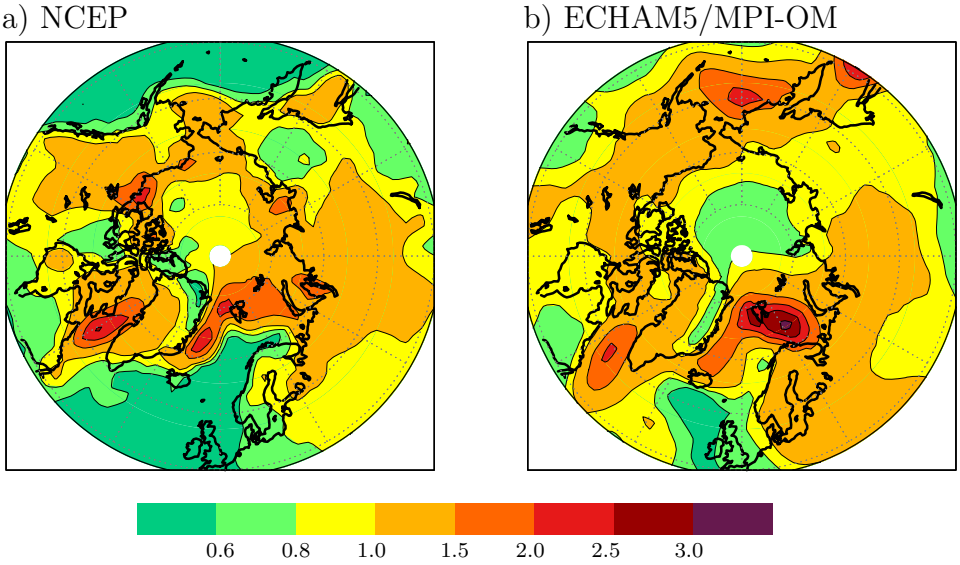

Figure 4.4: Standard deviation of annual mean 2m air temperature in Kelvin. a) NCEP data; b) control integration.

The patterns of the first EOF (fig. 4.5) of air temperatures in the reanalysis and the model simulation are alike. They show a dipole with positive anomalies in the Labrador Sea and negative anomalies in the Greenland and Barents Seas. In the

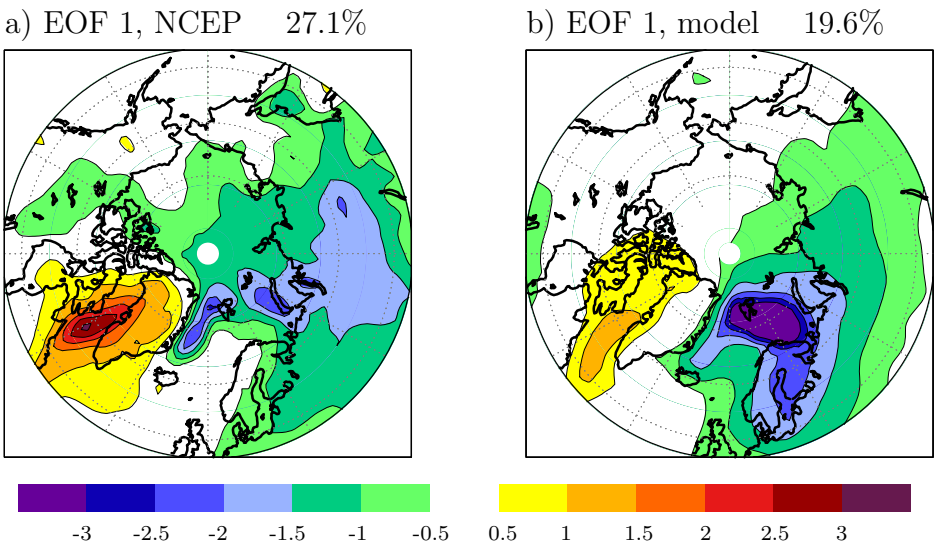

Figure 4.5: EOF 1 of annual mean 2 m air temperature. a) NCEP data; b) control integration.

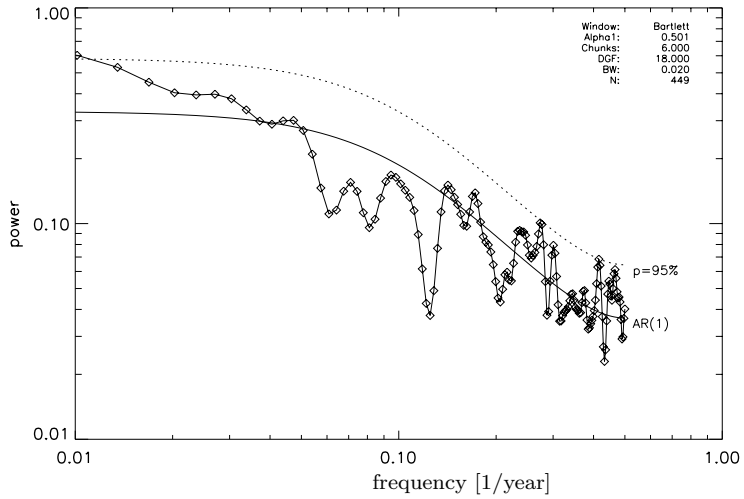

Figure 4.6: Power spectrum of the first PC of annual mean 2m air temperature of the 500-year control integration.

model, this negative pole is more pronounced than in the reanalysis and extends towards Scandinavia.
The simulated first PC is highly correlated with the first PC of the SLP (r=-0.63) as well as with the AO (r=-0.53) and NAO (r=-0.41). Apparently, the AO/NAO plays an important role for the air temperature variability. As described before

a high AO-index is related to the advection of warm air to Scandinavia and the Barents Sea. Additionally, anomalous warm surface waters are transported to the Barents Sea and lead to a decrease in ice cover of the Barents Sea, which responds with an increased ocean heat release. Thompson and Wallace (1998) analysed different historical data sets and showed an increase of surface air temperature up to two Kelvin per standard deviation AO-index over Siberia and slightly more than one Kelvin in the Labrador Sea. Holland (2003) simulated the effect of the AO with the global coupled atmosphere - ocean - sea ice model CCSM2 and found comparable results. Wettstein and Mearns (2002) indicated that the AO affects temperatures of North America as well.
In contrast to the first PC of SLP, the first PC of air temperature shows a much more pronounced multi-decadal signal (fig. 4.6). This indicates that other processes than SLP need to be considered to explain temperature variations on longer time scales. The first PC is significantly positively correlated (r=0.38) with the MOC indicating possible interactions between the MOC and Arctic climate variability on longer time scales.

4.3 Salinity

Figure 4.7 displays the standard deviation of the annual surface salinity (10 m) in the control run. By far the largest variability occurs at the coasts of Laptev and East Siberian Seas as well as at the mouth of the Mackenzie River. Here, standard deviations of more than 1 psu are reached. A tongue with large salinity variability extends from the coast of the Laptev Sea far into the Central Arctic.

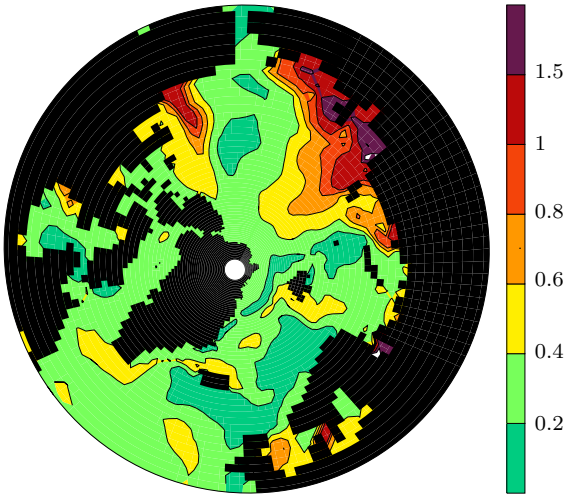

Figure 4.7: Standard deviation of the annual mean surface salinity (10 m) in the control integration in psu.

Something similar can be seen at the mouth of the Mackenzie River. These results are in good agreement with findings of Polyakov et al. (2003). They used salinity measurements from Russian winter surveys of the central Arctic Ocean between 1973 and 1979 and 40 years of summer and winter observations in the Laptev Sea. They demonstrated that the Laptev-East Siberian Sea shelfs are the largest source of strong surface salinity variations, which indicated the Lena River as major source of fresh water input and variability. Furthermore, Polyakov et al. (2003) found that centers of strong winter salinifications are often associated with leads and polynyas. The surface salinity anomalies are then advected eastward to the East Siberian Sea and northward into the Central Arctic.
In the western North Atlantic the standard deviation varies between 0.2 and 0.6 psu while the standard deviation does not excced 0.2 in most parts of the eastern North Atlantic.

4.4 Sea Ice Transport and Thickness

The mean sea ice transport is highly dependent on the mean state of the atmospheric circulation (see chapter 3.8). Several studies approved this relation (e.g. Martin and Martin (submitted); Thorndike and Colony (1982)). Polyakov and Johnson (2000) using reanalysis data and results from an ocean - sea ice model found a relation between ice motion in the Arctic and atmospheric circulation anomalies on a decadal time scale. Consistent with them, Proshutinsky and Johnson (1997) suggest the existence of two atmospheric circulation regimes in the Arctic Ocean. The wind driven motion alternates between anticyclonic and cyclonic circulation, with each regime existing for 5 to 7 years.

The first EOF (fig. 4.8 a) of sea ice transport in the 500-year control run explains about 25% of the total variability. It is characterised by a cyclonic circulation in the Arctic Basin. The pattern does not fit to the first EOF of the SLP. Nevertheless, the first PC of the sea ice transport is highly correlated with the SLP in the Central Arctic (not shown). Correlation coefficients of up to -0.8 are reached and the correlation pattern compares well to the anticyclonic and cyclonic wind regimes in the Arctic proposed by Proshutinsky and Johnson (1997). The power spectrum of the first PC (fig. 4.9) indicates a pronounced multi-decadal variability and a peak at a time scale of 10 years. Although this peak is not significant at the 95 % level, it fits well to the time scale found by Polyakov and Johnson (2000).
The spatial pattern of the second EOF shows anomalous ice transport from the Greenland Sea across the Arctic to the Chukchi and Siberian Seas for positive PC's. The largest variability can be seen in the area of Fram Strait. Obviously, this EOF is highly related to the ice export through Fram Strait. The associated PC is well correlated with the second PC of the SLP (r=0.55) indicating the importance of SLP variability for the ice export through Fram Strait. The power

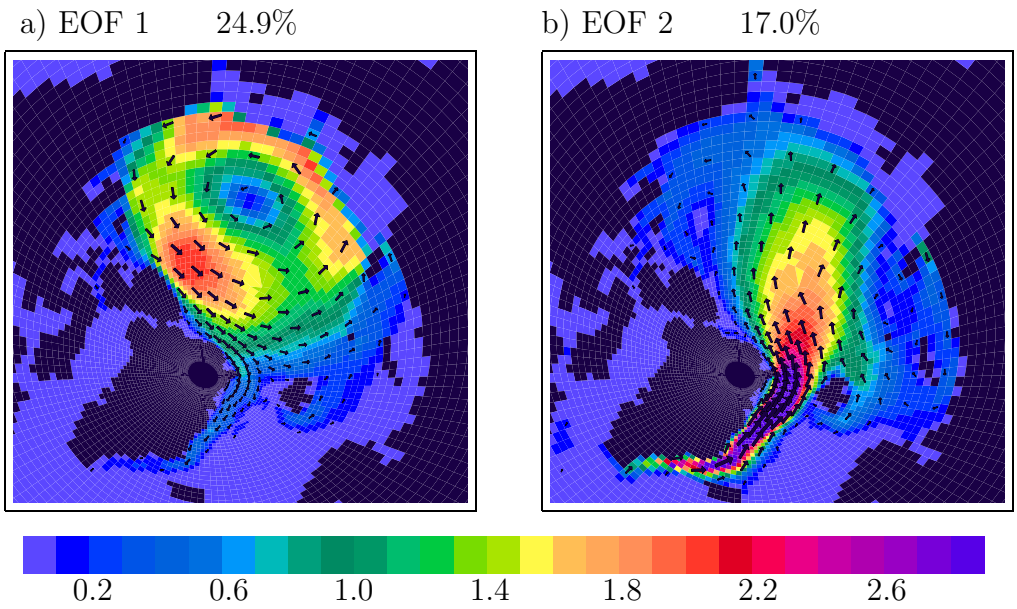

Figure 4.8: EOF 1 and 2 of annual mean sea ice transport in the control integration.

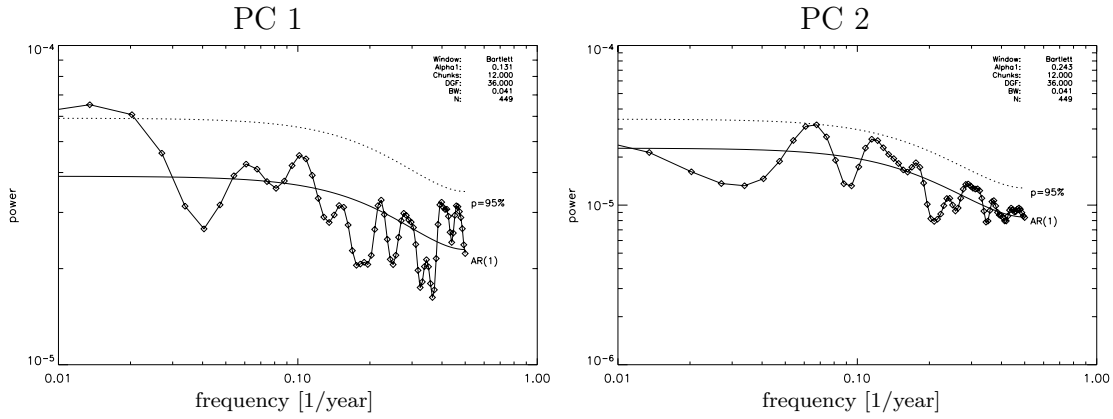

Figure 4.9: Power spectra of the first two PC's of annual mean sea ice transport in the control integration.

spectrum of the PC (fig. 4.9) shows two peaks at time scales of about 9 and 15 years, which reach the 95 % significance level. A detailed analysis of the ice export variability through Fram Strait is presented in chapter 6.

Figure 4.10 shows the first two EOF's of sea ice thickness in the control run. The first EOF explains 28% of the total variability and is positive in the entire Arctic. Variations are largest at the Siberian coast and decrease continuously towards Barents Sea, Fram Strait and Canadian Archipelago. The correlation of the associated PC with the AO-index is small with -0.12. But the PC is well

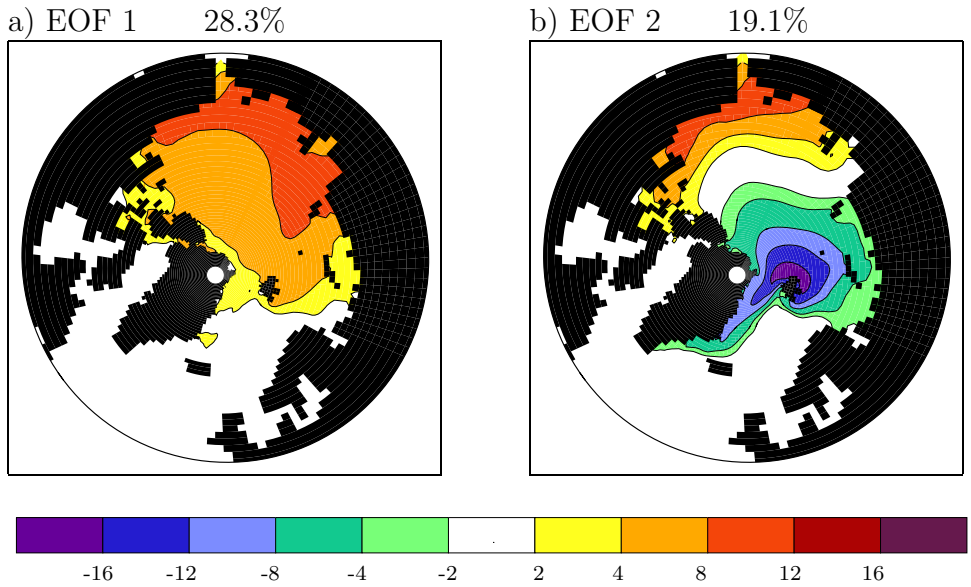

Figure 4.10: EOF 1 and 2 of annual mean sea ice thickness in the control integration.

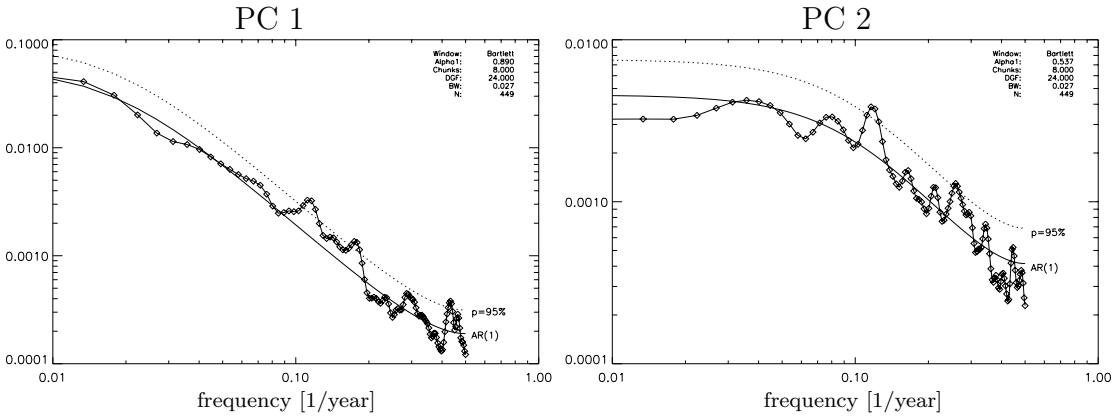

Figure 4.11: Power spectra of the first two PC's of annual mean sea ice thickness in the control integration.

related to the mean Arctic air temperature, averaged from $70°N$ to the North Pole. The correlation coefficient amounts to -0.57. The spectral analysis of the PC (fig. 4.11) indicates that most power is concentrated on long time scales. Although significant peaks occur at about two, three, six and nine years, the variance is very small compared to the multi-decadal time scale.
The second EOF is characterised by a dipole pattern. One pole is situated in the Chukchi Sea and the other is centered around Spitsbergen. In contrast to the first PC, the second PC is mainly determined by interannual to decadal variability. The power spectrum shows the most significant peak at a period of about nine

years. This peak and the EOF pattern fit well to the second EOF of the sea ice transport. Ice transports from the Fram Strait to the Chukchi Sea create the pattern of the second EOF of sea ice thickness. Furthermore, the PC is quite well correlated with the second PC of the SLP while correlation with the Arctic air temperature is much worse.
Apparently, the thermal effect determines ice thickness variations on long time scales while dynamic processes are more important on shorter scales. This is consistent with results of Tremblay and Mysak (1998) who investigated the origin and evolution of sea ice anomalies in the Beaufort-Chukchi Sea.

Table 4.1 provides a summary of means and variations of ice volume in the sub areas of the Arctic Basin. The boundaries of the different areas are shown in fig. 3.9. The mean ice thickness for each region is presented in the first column of the table. It varies between 0.67 m in the Barents Sea and 3.82 m in the East Siberian Sea. The average ice thickness for the entire Arctic Basin reaches 2.72 m. The standard deviation of annual mean values varies between slightly more than 20 cm in the Barents Sea and the Central Arctic and 37 cm in the Laptev Sea. The whole Arctic Basin reaches a standard deviation of 18 cm. Winsor (2001) used observational data from 6 submarine cruises in the 90's to determine the ice thickness variability between the North Pole and the Beaufort Sea. He found year to year variations of up to 80 cm in the Beaufort Sea and up to 40 cm in the area of the North Pole. The standard deviation reaches 7 cm at the North Pole and 17 cm in the Beaufort Sea, which is about half of the model results in this study. However, a comparison is difficult because six years of observations are not enough for proper statistics, particularly under the assumption of decadal and multi-decadal variability in the ice thickness. Yu et al. (2004) analysed results of four submarine cruises through the Arctic between 1958 and 1970 and three cruises between 1993 and 1997. A comparison of the ice thickness during 1958-1970 and 1993-1997 shows a reduction of some centimeters in the Chukchi Sea and more than a meter in the Central Arctic. It is uncertain whether this is due to multi-decadal variability or relates to global warming. Haas (2004) compared ice thickness distributions from drilling and electromagnetic sounding for four different years in the 90's. Their results pointed to a strong interannual variability of sea ice thickness as well.

In the following, the reasons for the year-to-year variations in the ice volume are investigated. For this purpose, the ice volume anomaly is divided in its thermodynamic and its dynamic part. The divergence in the ice transport is calculated for each area and each year (see also fig. 3.9) and is defined as dynamical part of the ice volume change. The thermodynamic part results in the difference of the total ice volume change within one year (from August to August) and the

	mean ice in meter	stddev in meter	corr dt vs dyn	corr dt vs therm	corr dyn vs therm
Barents	0.67	0.21	0.76	0.02	-0.65
Kara	1.56	0.26	0.75	0.32	-0.39
Laptev	3.01	0.37	0.86	0.08	-0.50
East Sib.	3.82	0.30	0.82	0.14	-0.59
Chukchi	3.21	0.30	0.82	-0.02	-0.59
Beaufort	2.88	0.31	0.86	0.25	-0.29
Central Arctic	2.98	0.22	0.82	-0.10	-0.61
Total Arctic	2.72	0.18	0.41	0.58	-0.62

Table 4.1: Mean ice thickness and standard deviation (column 2 and 3) for the Arctic sub areas (see fig. 3.9) and the entire Arctic Basin. Correlation between temporal ice volume change within one year (from August to August) and the dynamic (column 4) and thermodynamic part (column 5) of the change and between dynamic and thermodynamic part (column 6).

dynamic part of the ice volume change:

$$icevol_{therm} = \frac{d}{dt} icevol - icevol_{dyn} \tag{4.2}$$

To estimate the effect of dynamic and thermodynamic processes on the total ice volume change, a correlation analysis between the annual mean values of each part and the ice volume change is carried out (table 4.1, column 4 and 5). The dynamical part is highly correlated with the ice volume change in all sub areas. Correlation coefficients vary between 0.75 in the Kara Sea and 0.86 in the Laptev and Beaufort Seas. In contrary, the correlation between thermodynamic part and ice volume change is predominantly weak in the sub regions of the Arctic Basin. Only in the Kara and the Beaufort Seas a slightly higher correlation of 0.32 and 0.25 is found, respectively. Consequently, the interannual variability of the ice volume in the sub regions of the Arctic Basin is mainly governed by variations in the dynamics of the ice transports. For the entire Arctic Basin the ice volume change is significantly positively correlated with both the dynamic (r=0.41) and the thermodynamic part (r=0.58). This means that the thermodynamic part is slightly more important for the ice volume change. The reason for this is simple: the mean divergence of a totally enclosed area must be zero. The Arctic Basin is quite closed compared to the sub regions. Only variability in the ice exports through Fram Strait, Barents Sea, Bering Strait and the Canadian Archipelago

	Ba	Ka	La	Sib	Chu	Bea	CA
Ba	1/0	0.68/0	0.31/1	0.33/-2	0.32/-4	0.30/-6	0.7/0
Ka		1/0	0.61/0	0.36/-2	0.31/-3	0.27/-5	0.54/0
La			1/0	0.65/0	0.39/-1	0.26/4	0.49/1
Sib				1/0	0.81/0	0.46/-2	0.59/2
Chu					1/0	0.69/0	0.54/3
Bea						1/0	0.44/3
CA							1/0

Table 4.2: Lag correlation among annual mean ice volumes of the sub regions (see fig. 3.9). The highest correlation and the belonging lag is given (correlation/lag in years). Ba=Barents Sea; Ka=Kara Sea; La=Laptev Sea; Sib=East Siberian Sea; Chu= Chukchi Sea; Bea=Beaufort Sea; CA= Central Arctic.

lead to divergent ice volume changes in the Arctic Basin. Hence, the importance of divergent ice transports is small in comparison to the sub regions.
The correlation between the dynamic and thermodynamic part of the ice volume change is summarised in the last column of table 4.1. The correlation is negative in all regions of the Arctic Basin and exceeds -0.5 in all areas except for Kara and Beaufort Seas. A large convergence of ice transport in one area is therefore associated with a negative net freezing rate in the same year. During a convergent ice transport, ice thickness and concentration are increased. As a consequence, less new ice is formed and more ice can be melted in the summer. A considerable part of the annual thermodynamic growth seems to be dependent on the dynamic part. This effect is not as dominant in the Beaufort and Kara Seas.
On longer time scales, the variability of the ice volume is mainly caused by thermodynamic variations. The 20-year running mean of the ice volume in the Arctic Basin is correlated with the 2 m air temperature averaged over the area north of $70°N$ with -0.9.

Table 4.2 summarises a lag correlation analysis among annual mean ice volumes of the different sub regions in the 500-year control integration. The highest correlation and the corresponding time lag is given for each correlation pair. A positive lag means a lead of ice volume in the region in the horizontal and a negative lag a lead of the region in the vertical. Highest correlations occur between neighbouring regions without time lag. The correlation coefficients vary between 0.54 for the correlation between ice volume of the Central Arctic and the Kara Sea and 0.81 for the East Siberian and the Chukchi Seas. The highest

correlations between Central Arctic ice volume and ice volume of the bordering areas of Laptev Sea, East Siberian Sea, Chukchi Sea and Beaufort Sea occur at lags of one (Kara Sea) to three years (Chukchi and Beaufort Seas). Correlations between non-neighbouring regions are highest for a certain time lag. This time lag depends on the distance between the regions. Ice anomalies are propagating clockwise from the Beaufort Sea along the coast to the Laptev Sea and from there into the Central Arctic and along the coast into the Kara and Barents Seas. Thus, anomalies propagate with the mean ice circulation (compare fig. 3.8 a and fig. 3.9). The travel time of an ice anomaly from the Beaufort Sea to the Kara and Barents Sea takes about four to six years.

5 Impact of Fram Strait Ice Export Variability

The sea ice export through Fram Strait has been identified as the main source of ice export out of the Arctic. In this chapter, the 500-year control integration is used to analyse the Fram Strait ice export variability and its impact on the climate in the northern hemisphere.

5.1 Fresh Water Export through Fram Strait

The mean ice export through Fram Strait in the 500-year control integration amounts to 97000 m^3/s. This is in the upper range of observational estimates. Vinje et al. (1998) found a mean ice export of 81300 m^3/s for the time period from 1990 to 1995. Aagaard and Carmack (1989) calculated an ice export of 88500 m^3/s. Estimates for the last 50 years by Vinje (2001b) resulted in an export of 92000 m^3/s. In reconstructions of the ice export by Schmith and Hansen (2003) over the last 181 years the mean reached about 100000 m^3/s. The variability of the ice export in the model is in good agreement with observations as well. In the control integration, annual mean values vary between 40000 and 160000 m^3/s. The standard deviation amounts to 21000 m^3/s.

The total fresh water export through Fram Strait, which consists of the export of ice and the export of liquid fresh water between surface and ground, amounts to 137000 m^3/s for a reference salinity of 34.8 psu. Ice is thus responsible for 70 % of the total fresh water export through Fram Strait. But more important than this is the variability of the fresh water export. The standard deviation of the liquid part reaches 7800 m^3/s, which is small compared to the 21000 m^3/s of the ice export. Furthermore, the total fresh water export is correlated with the ice export with 0.93, while its correlation with the liquid part is rather weak with 0.21.
Figure 5.1 shows the fresh water export through Fram Strait, Denmark Strait and the eastern border of the Labrador Sea ($54 - 60°N, 48°W$) of the upper 100 m. In the Fram Strait it is obviously dominated by the ice export. The annual variability of the liquid part is comparably small. Although this study focus on interannual to decadal time scales, it should be noted that the variability of liquid and solid parts are of the same size on multi-decadal time scales. The ice export through Denmark Strait is about half of the Fram Strait ice export. Both the ice export and the total fresh water export through Denmark Strait are highly correlated with the ice export through Fram Strait (r=0.70 and 0.68, resp.). The liquid part is as large as the solid part but its variability is much smaller. The fresh water transport through the eastern border of the Labrador Sea is governed by the liquid part because most of the ice has melted until it reaches the Labrador Sea. The total amount of fresh water transport amounts to 45000 m^3/s on aver-

age, which is about one third of the total export through Fram Strait. However, the fresh water transport into the Labrador Sea is correlated to both the ice export and the total fresh water export through Fram Strait with 0.59 at a lag of one year. Hence, this study concentrates on the solid Arctic fresh water export.

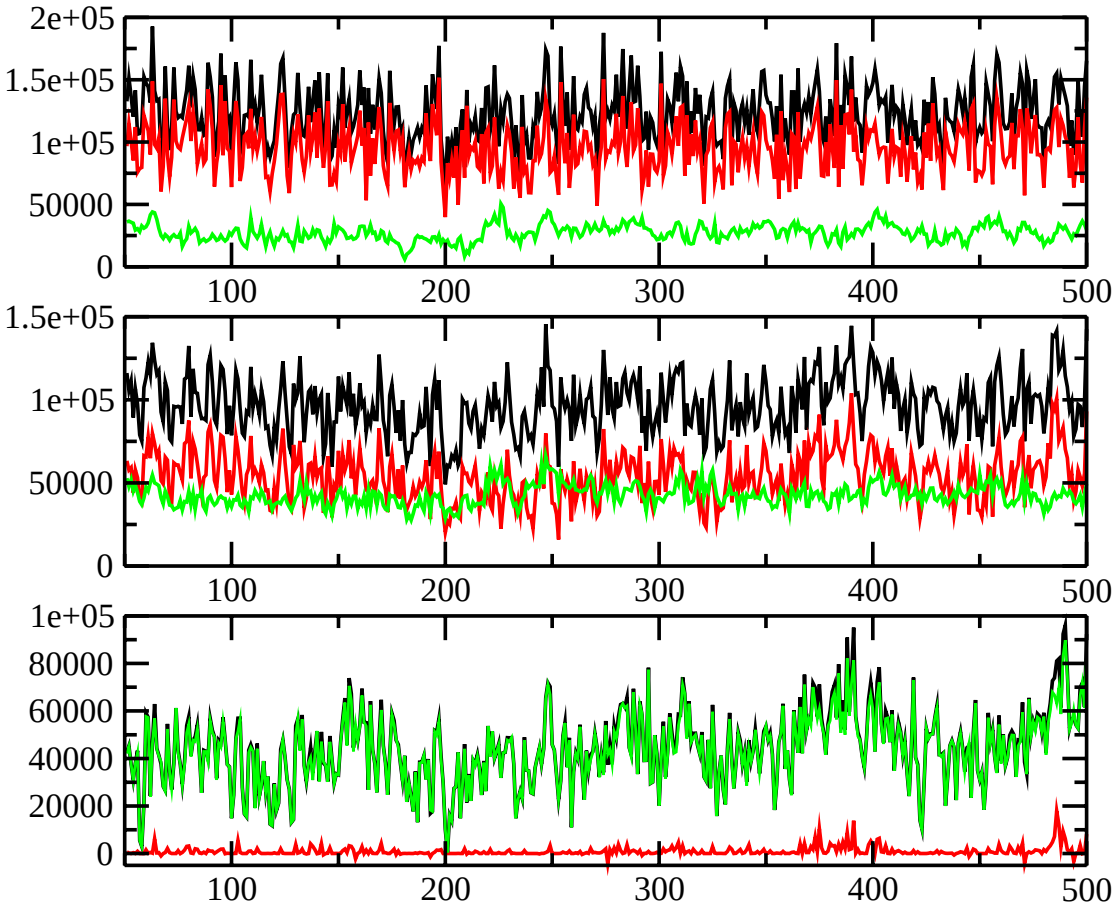

Figure 5.1: Annual mean fresh water transport of the upper 100 m through Fram Strait (top), Denmark Strait (middle) and eastern boarder of the Labrador Sea ($54 - 60°N, 48°W$, bottom) in m^3/s. Black: solid + liquid, red: solid, green: liquid. Reference salinity is 34.8 psu.

The monthly mean ice export through Fram Strait, averaged over the 500-year control integration (fig. 5.2), shows a pronounced seasonal cycle. The maximum occurs in March with an average of 147000 m^3/s and the minimum in August with 35000 m^3/s. This agrees well with observational estimates by Vinje (2001b). He used the observed pressure gradient across Fram Strait to parameterize the ice export for the time period from 1950 to 2000. In average, the parameterized export was highest in March with about 120000 m^3/s and lowest in August with 40000 m^3/s.

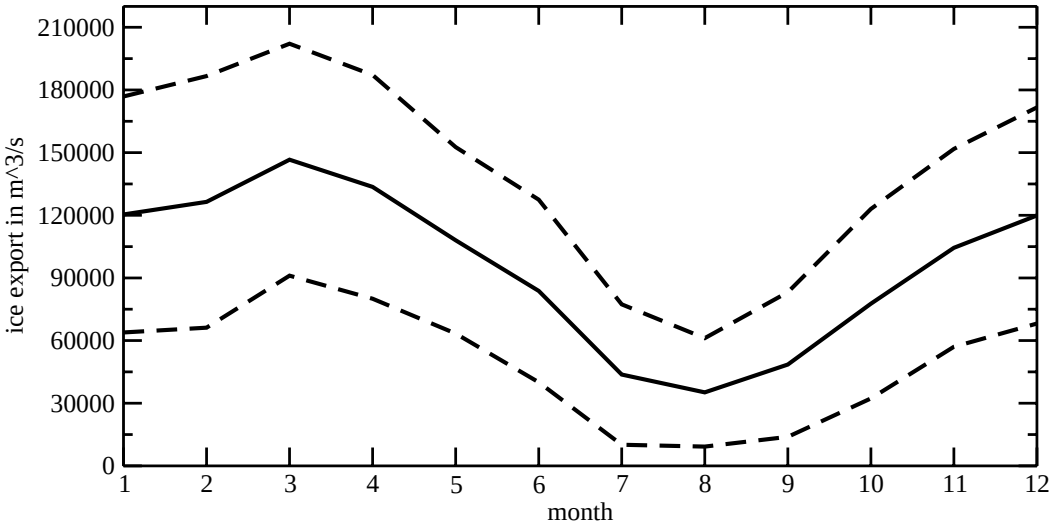

Figure 5.2: Monthly mean ice export and standard deviation in m^3/s, averaged over the 500-year control integration for each month.

Although the ice export in late summer/early autumn is small compared to the winter, it must not be neglected. To prove this, the standard deviation for each month has been calculated. It is in fact largest in late winter/early spring with 50000 to 60000 m^3/s, but in late summer it after all reaches more than half of the winter values and contributes a considerable part to the interannual variability.
The correlation among single seasons is presented in table 5.3. Sequenced seasons are positively correlated with coefficients between 0.15 for spring (MAM) - summer (JJA) and 0.34 for winter (DJF) - spring (MAM). The correlation between non-sequenced seasons is very low. All seasons are highly positively correlated with the annual mean ice export. The correlation is largest in winter but anyhow reaches 0.5 and 0.57 in summer and autumn, respectively.
The same correlation analysis is conducted for ice exports of single months. Sequenced months are significantly positively correlated, whereas highest correlations occur between July-August (r=0.41), August-September (r=0.42) and September-October (r=0.41) ice exports. In this time period, during summer and early autumn, wind variability is much weaker than in winter and the ice export depends greatly on the amount of ice remaining from the previous winter. Significant correlations exceeding r=0.2 can also be found between January-March, February-April, July-September, August-October, September-December and October-December.

	DJF	MAM	JJA	SON
DJF		0.34	0.10	0.04
MAM	-0.04		0.15	0.14
JJA	0.12	0.01		0.31
SON	0.25	0.00	0.11	
Year	0.75	0.64	0.50	0.57

Table 5.3: Correlation between seasonal mean ice exports through Fram Strait. Seasons, written in the horizontal, lead seasons, written in the vertical. The last row indicates the correlation between the annual mean ice export (averaged from September to August) and the single seasons.

5.2 Response of Atmosphere and Ocean

In the following, the impact of ice export variability on atmospheric and oceanic climate is investigated. Composite analyses (see appendix A.3) are applied for several parameters as main tool for this analysis. The cases of high and low ice exports through Fram Strait are investigated separately. High ice exports are defined as ice exports exceeding the mean ice export (from the 500-year control integration) in excess of one standard deviation and vice versa for low ice exports. The ice, exported anomalously through Fram Strait, propagates southwards in the EGC and melts. A part of the fresh water remains in the Greenland Sea but the predominant amount flows into the Labrador Sea. This fresh water anomaly forms a dramatic salinity deficit in the Labrador Sea one to two years later (fig. 5.4, left). The model is able to reproduce the formation of GSA's in the Labrador Sea shown by Häkkinen (1999) and Haak et al. (2003). Apparently, the ice export through Fram Strait is the main factor for these anomalies. Table 5.4 shows that salinity is decreased within one to three years after high ice exports in 35 of 39 cases. Nineteen of these events are leading to major negative salinity anomalies in the Labrador Sea. In the four cases where salinity increases after high ice export events, the fresh water is not reaching the Labrador Sea due to strong anomalous winds. They deflect the ice to the east, south of Fram Strait or at the southern tip of Greenland.
Figure 5.3 shows that the ice transports through the Canadian Archipelago and the Hudson Bay are small in this model with averages of 4800 m^3/s and 6700 m^3/s, respectively. The liquid fresh water input is much higher and of the same size as the input into the Labrador Sea by the EGC. However, the annual variability of the fresh water input through the Canadian Archipelago and the Hudson Bay is rather small. The standard deviations reach 4340 m^3/s and 2850 m^3/s,

respectively, while the standard deviation of the inflow by the EGC amounts to 15600 m^3/s.
Other studies such as Goosse et al. (1997) and Houghton and Visbeck (2002) considered the fresh water flux through the Canadian Archipelago and local processes to be more important for the water properties in the Labrador Sea than assumed in this model. It should be noted that the model resolution is not sufficient to resolve the Canadian Archipelago properly. The ice export through it is probably underestimated. Nevertheless, about 20 % of large negative salinity anomalies could not be explained by previous ice export anomalies through Fram Strait. They occur due to fresh water inflows through the other three boundaries of the Labrador Sea. The local mixing of surface waters with deeper layer waters, which is driven by atmospheric forcing (e.g. high or low NAO-index), plays a role as well. Table 5.5 shows that low ice exports through Fram Strait lead to positive salinity changes in the Labrador Sea.
The fresh water input into the Labrador Sea after large ice export events stabilises the local stratification of the ocean. Deep convection is decreased or even totally suppressed in the Labrador Sea one and two years after high ice exports. This is evidenced by a considerable reduction in the late winter/early spring (Febru-

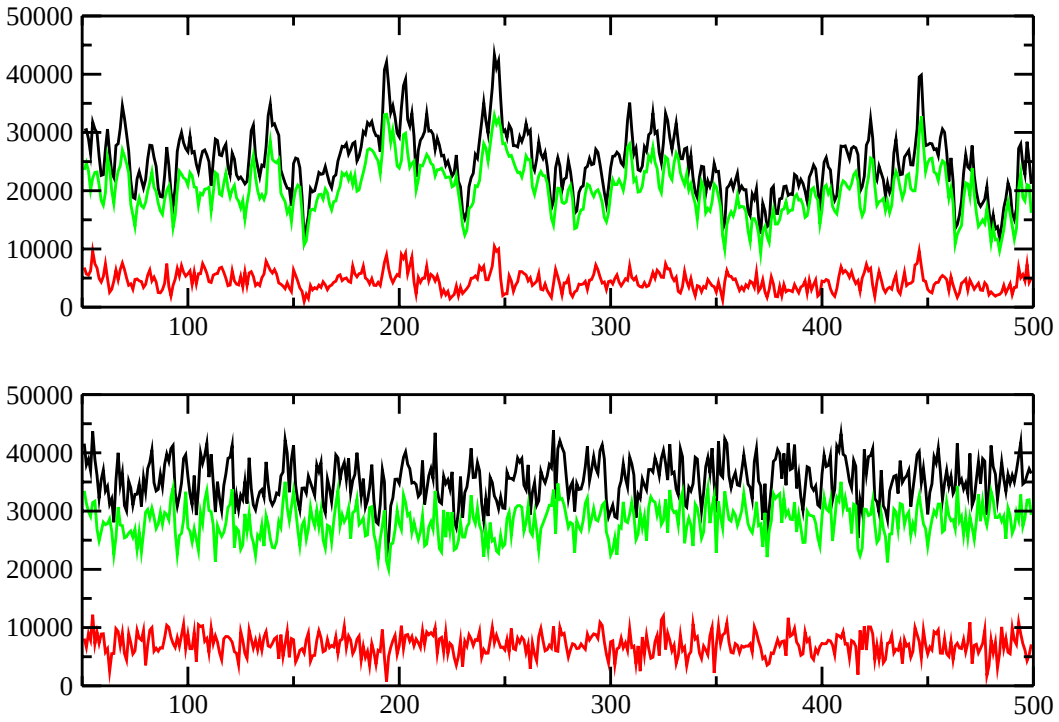

Figure 5.3: The same as figure 5.1, but for the Canadian Archipelago (top) and the Hudson Bay (bottom).

	$\delta S < -1$	$-1 < \delta S < -0.5$	$-0.5 < \delta S < 0$	$\delta S > 0$
number years	19	8	8	4
%	48.7	20.5	20.5	10.3

Table 5.4: Distribution of the maximum year to year decrease in 10m salinity within three years after positive Fram Strait ice export events. 39 years with ice export anomalies exceeding 1.5 standard deviations are used. The salinity is averaged over the central Labrador Sea and δS is given in standard deviations.

	$\delta S > 1$	$0.5 < \delta S < 1$	$0 < \delta S < 0.5$	$\delta S < 0$
number years	13	6	1	3
%	56.5	26.1	4.3	13.1

Table 5.5: Same as Table 5.4 but for positive salinity changes after 23 years with negative ice export anomalies exceeding 1.5 standard deviations.

ary, March, April) mixed layer depth up to 600 meters. Compared to the mean convection depth of 1500 meters, mixed layer depth is reduced by almost half (fig. 5.5, left). In the Greenland Sea, it is decreased by 200 meters. This mainly reflects a change in the position of deep convection. After low ice exports, a deepening in the mixed layer depth and thus an increased convection is obvious in the Labrador Sea. No significant correlation between the salinity in the Labrador Sea and the MOC at $30°N$ of the same and the following years could be found in our model. This agrees well with results of Power et al. (1994) but is contrary to findings of Häkkinen (1999). For longer time scales, the surface salinity of the Labrador Sea and the MOC are highly positively correlated. It takes several years to consume the reservoir of deep water in the Labrador Sea, which is formed during one year with strong deep convection. Consequently, a single year with large or without deep convection has no significant influence on the overturning. If salinity anomalies could persist for more than a few years in the Labrador Sea, there would be a large influence on the entire thermohaline circulation (Jungclaus et al., in press). Mikolajewicz et al. (submitted) show with a regional coupled atmosphere-ocean-sea ice model that this can indeed happen after large ice export anomalies. Mauritzen and Häkkinen (1997) used a fully coupled ocean - sea ice model to perform two runs with different sea ice shear viscosity to change the annual mean ice export through Fram Strait by 800 $km^3/year$. The overturning responded with a reduction of 2 to 3 Sv to the decrease.

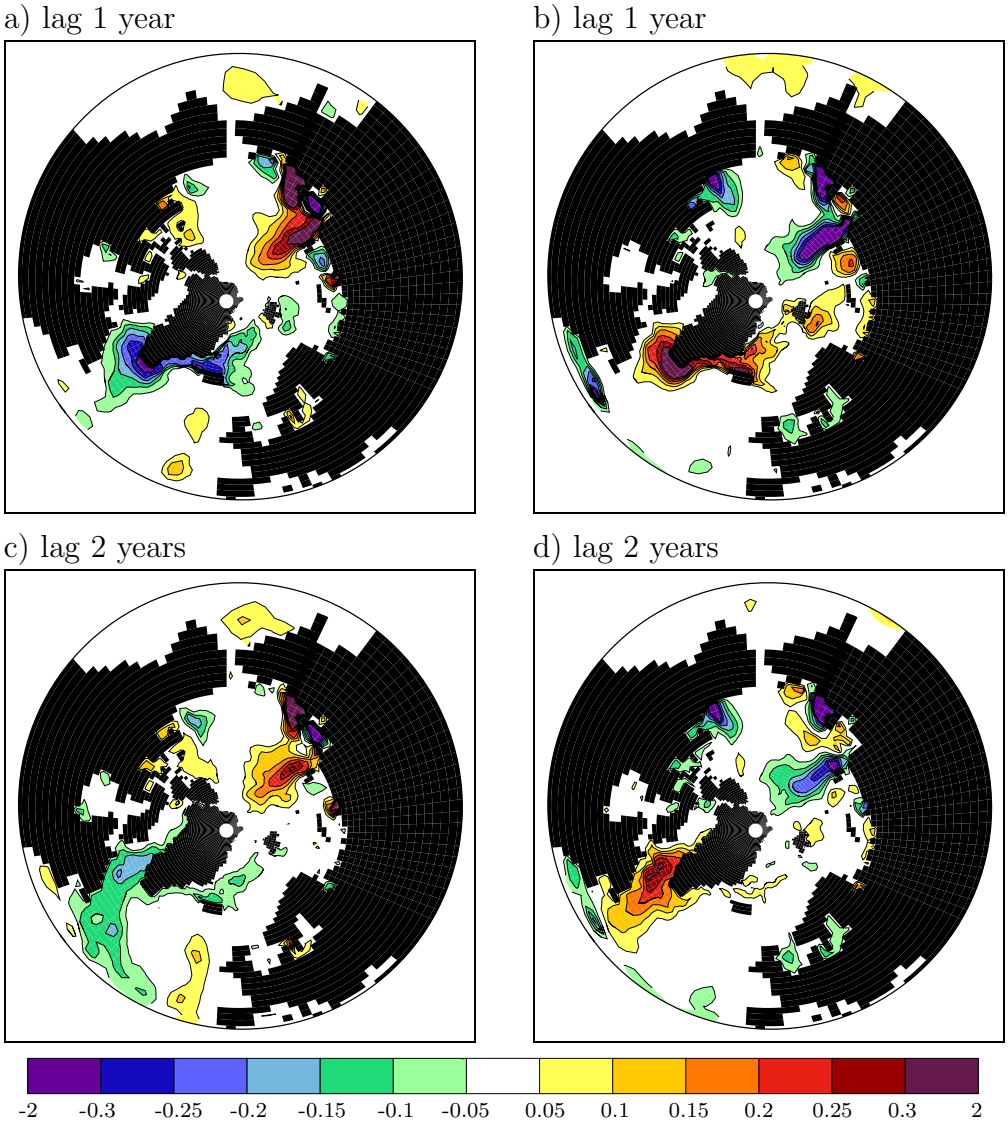

Figure 5.4: Composite analysis of annual mean 10 m salinity anomalies in psu one and two years after high (left) and low (right) ice exports through Fram Strait.

The anomalous sea ice export through Fram Strait affects sea ice concentration in the Greenland Sea (especially in the first year after the ice export) and the Labrador Sea one and two years later (fig. 5.6). The increase of sea ice in the Greenland Sea after high ice export events is due to the direct effect of enhanced ice transport into the Greenland Sea (Walsh and Chapman, 1990; Wang and Ikeda, 2000). Increased ice export is additionally associated with the anomalous advection of cold air from the north into the Greenland Sea. This leads to an intensified sea ice formation in winter and less sea ice melting in summer. Sea ice

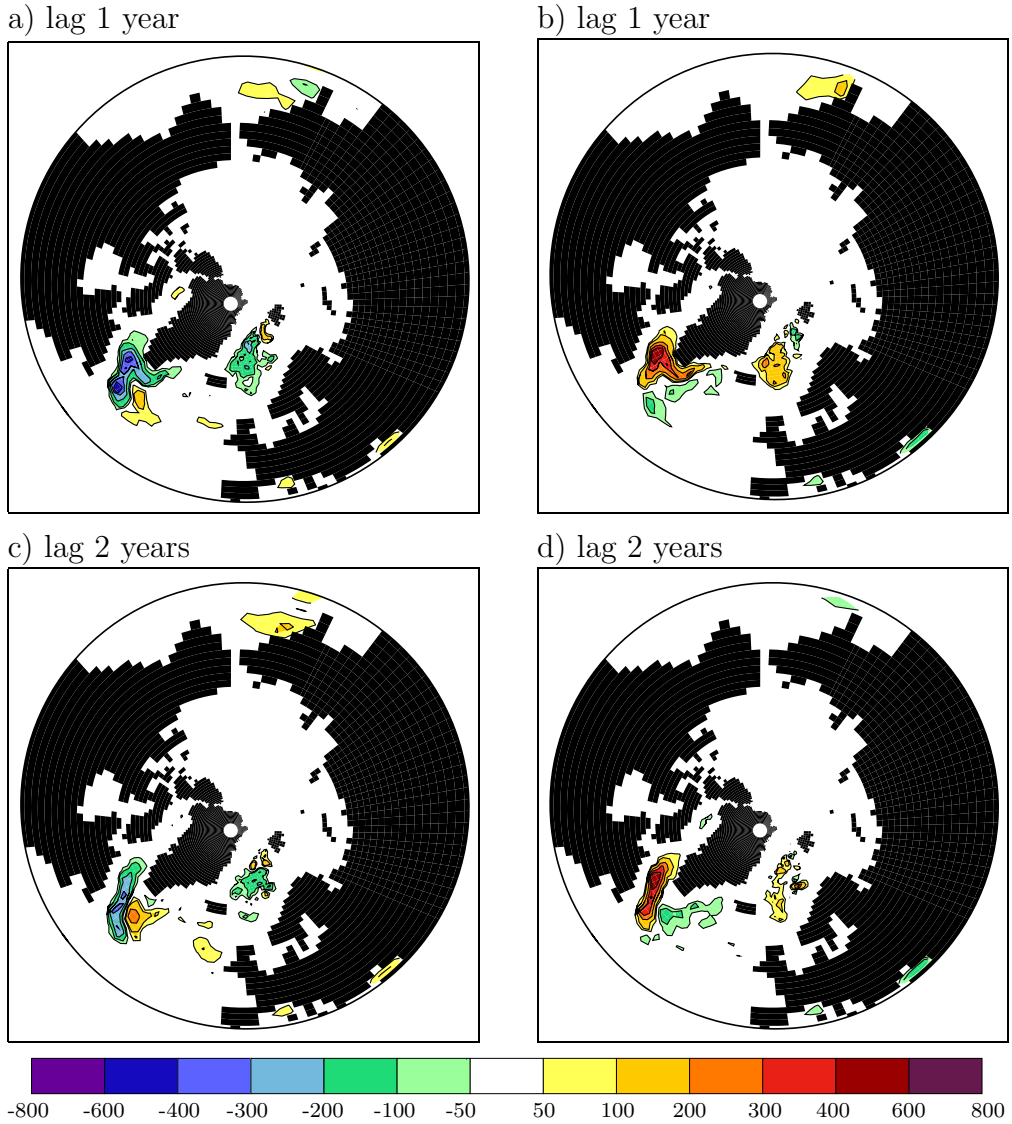

Figure 5.5: Composite analysis of late winter/early spring (February, March, April) mixed layer depth anomalies in m one and two years after high (left) and low (right) ice exports through Fram Strait.

cover is extended in the Labrador Sea as well. The surface waters are colder due to the input of anomalous cold water and decreased convection after large ice export events. The surface can thus freeze more easily. In the first year, sea ice concentration is increased by 10 % both in the Labrador and Greenland Seas. One year later, the ice anomaly is much more pronounced in the Labrador Sea than in the Greenland Sea, because convection in the Labrador Sea is still weak. Therefore, surface waters are still colder and fresher than usual. Deser et al. (2002) found

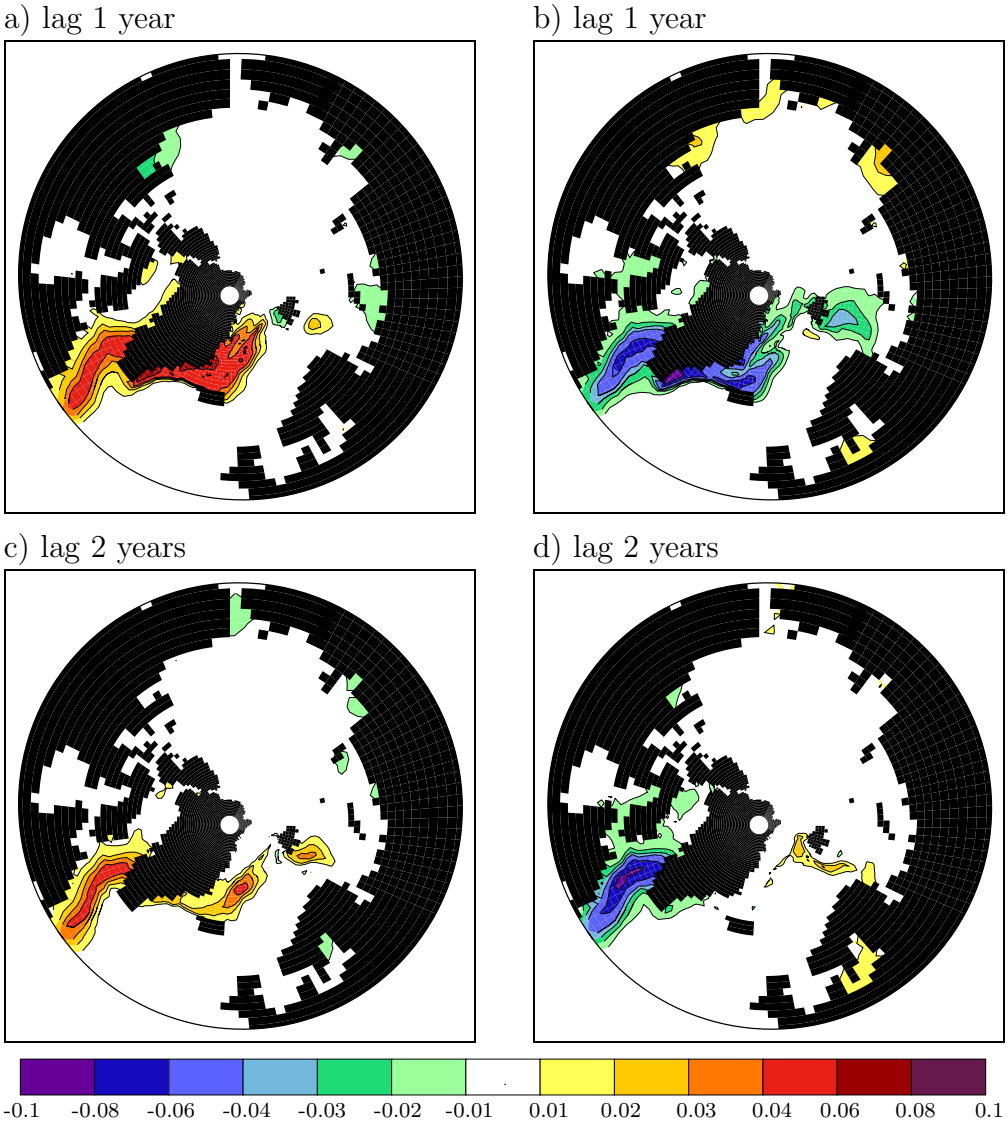

Figure 5.6: Composite analysis of annual mean sea ice concentration anomalies in fraction one and two years after high (left) and low (right) ice exports through Fram Strait.

a good correlation between salinity in the West Greenland Current and sea ice in the Davis Strait, which is in good agreement with results of this study. They determined three periods with especially large and long lasting sea ice anomalies from an EOF analysis of sea ice concentration data from 1953 - 1997: 1972/1973, 1983/1984 and 1990/1991. Additional model simulations by Deser et al. (2002) indicate that these anomalies were accompanied by a northwesterly atmospheric flow in the Davis Strait/Labrador Sea. Similar investigations for annual values of

sea ice concentration from our control run show a correlation of the NAO-index with the sea ice concentration in Davis Strait of 0.38. However, previously to all three sea ice events, high ice exports through Fram Strait had occurred (e.g. Haak et al. (2003)). The ice export and the NAO are well correlated with the sea ice concentration for lags of one and two years. In the next section, it will be shown that the north-westerly wind anomalies in the Labrador Sea, as found by Deser et al. (2002), are formed two years after high ice exports. They are therefore part of the entire process.

Both the decrease in convection and the increase in ice concentration in the model are responsible for a reduced ocean heat release to the atmosphere in the Greenland Sea and particular in the Labrador Sea (fig. 5.7). Here, the turbulent (sensible + latent) heat flux from ocean to atmosphere is reduced by up to 15 W/m^2 for annual means and 30 W/m^2 in late winter (February, March, April, not shown). The ocean heat release over the North Atlantic is slightly increased after large ice exports. The northern North Pacific seems to be affected as well: positive ocean heat release anomalies in the Bering Strait and negative anomalies north of Japan are simulated. The anomalies in the heat flux are mainly due to anomalous advection of cold or warm air masses, except for those in the Labrador and Greenland Seas. The response is again symmetric and low ice exports through Fram Strait lead to a decrease in the ice concentration of similar magnitude. The anomalies in the ocean heat release have consequently the opposite sign.
These heat flux variations have a direct impact on atmospheric climate conditions. Figure 5.8 shows the resulting two meter air temperature anomalies. The reduced ocean heat release to the atmosphere (after large ice export) causes much cooler temperatures in the Labrador and Greenland Seas. Anomalies of up to one Kelvin for annual means and two Kelvin for winter means (December, January, February, not shown) are reached in the Labrador Sea. They are highly significant using a two-sided t-test. Significant anomalies are also obvious in the area of the Caspian Sea and over smaller parts of the North Pacific. They are mainly due to changes in the large scale atmospheric circulation (fig. 5.9).
The largest SLP anomalies can be seen over the North Atlantic and the European Arctic. Two years after large ice exports, a dipole occurs with positive SLP values up to 0.6 hPa over the North Atlantic and negative values up to -0.6 hPa over the Nordic Seas. The SLP anomalies are only locally significant at the 95 % level but extended areas can reach the 90 % significance level. The pattern resembles the positive NAO-index pattern and vice versa both one and two years after low ice exports. The following mechanism is suggested: large ice export leads to an increase in the ice area in the Greenland and Labrador Seas and an enhanced north - south temperature gradient over the North Atlantic. As air and sea temperature anomalies are largest in the Labrador Sea, the north-south temperature gradient is particularly strengthened in the formation area of cyclones

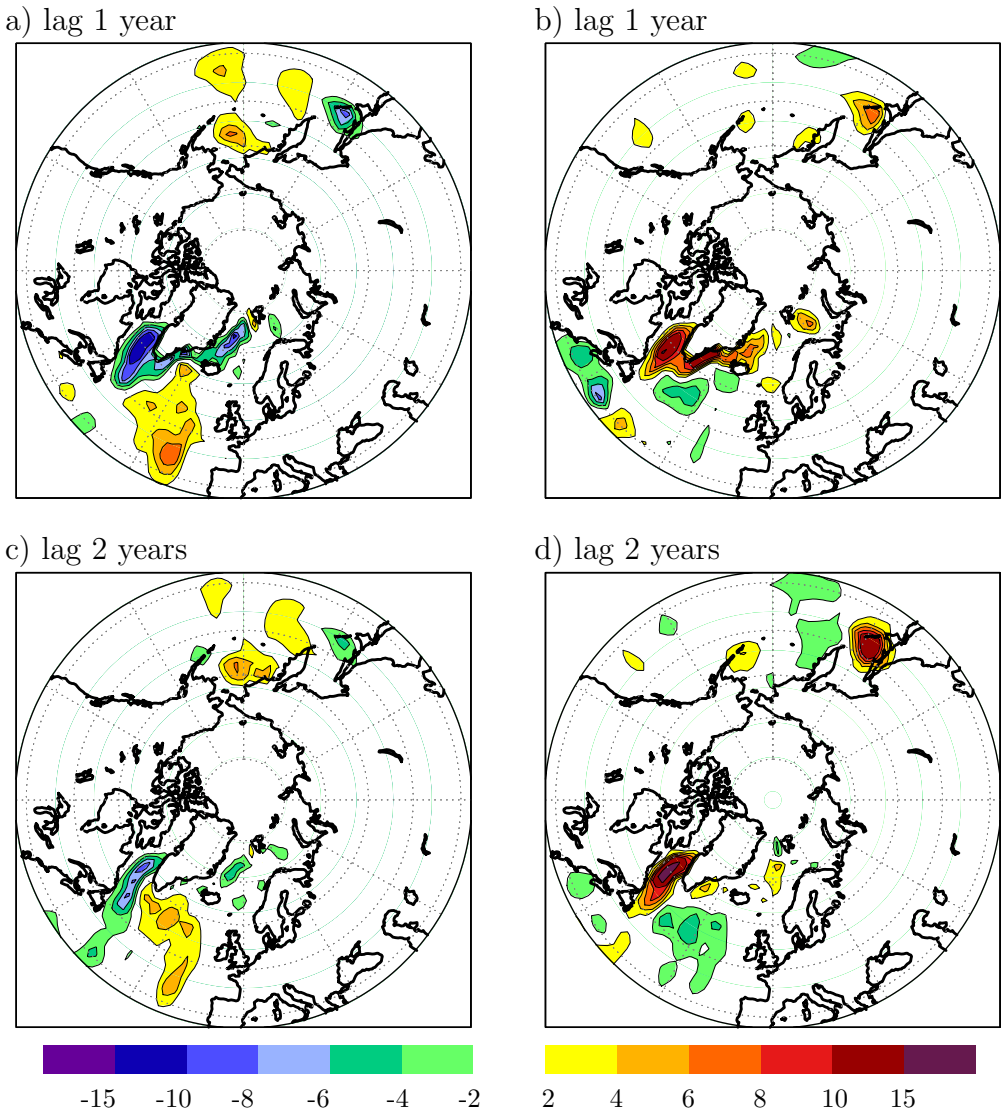

Figure 5.7: Composite analysis of annual mean turbulent (latent + sensible) heat flux anomalies from the ocean to the atmosphere in W/m^2 one and two years after high (left) and low (right) ice exports through Fram Strait.

over the Gulf Stream south of the Labrador Sea. Atmospheric baroclinicity is consequently enhanced, which leads to an increased synoptic activity and a shift in the cyclone track to the north. Murray and Simmonds (1995) investigated the effect of a progressive removal of sea ice in the Arctic on the atmospheric circulation and found a weakening of the Iceland Low and a decrease in pressure over the eastern North Atlantic and southern Europe. Noone et al. (submitted) completely removed Arctic sea ice in all months in sensitivity experiments with

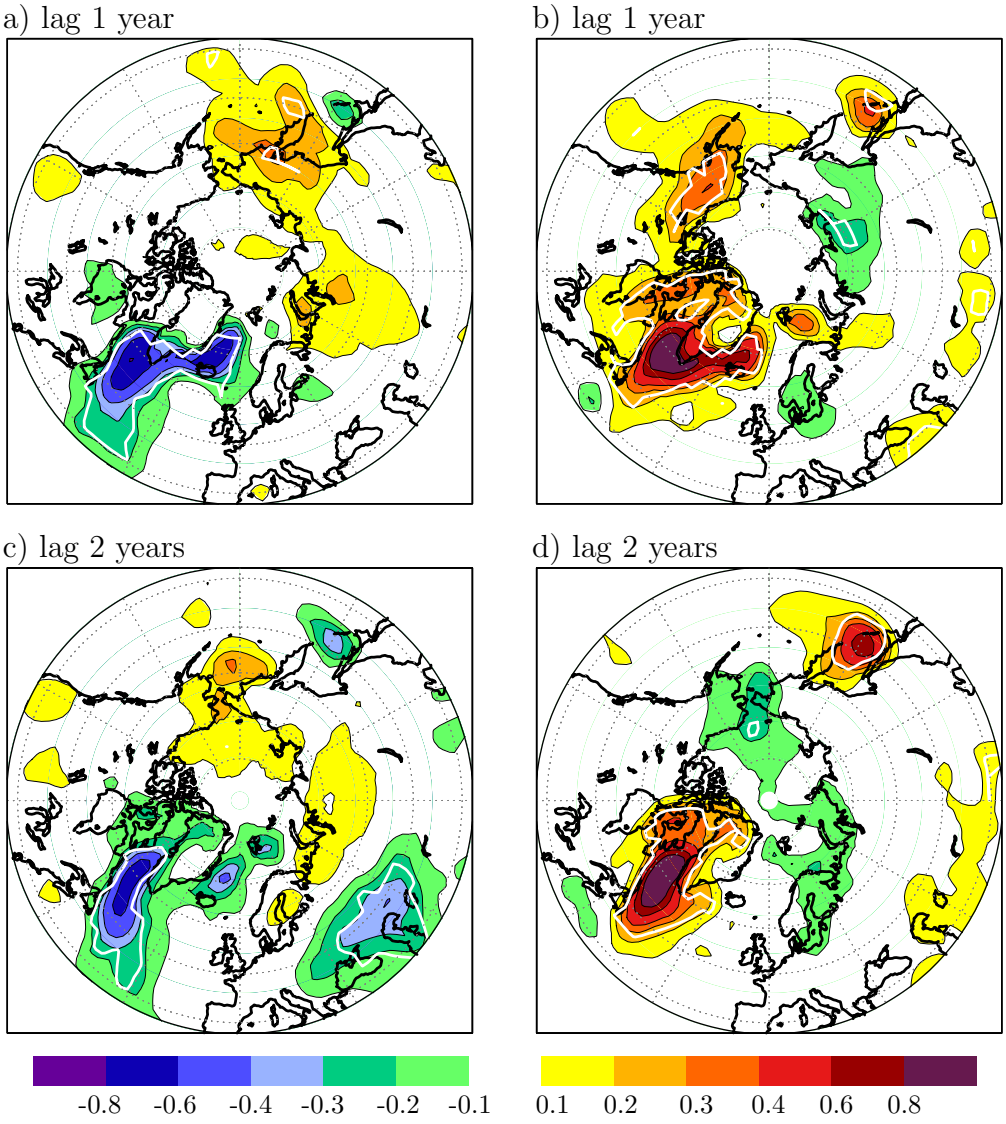

Figure 5.8: Composite analysis of annual mean 2m air temperature anomalies in Kelvin one and two years after high (left) and low (right) ice exports through Fram Strait. The white line indicates the level of 95% significance.

the atmosphere-only model CCM3. The atmospheric response was characterised by a warming of the lower troposphere of 8-12 Kelvin and a negative AO index of -1.8. They suggest that the decreased temperature gradient provides reduced baroclinicity and reduced synoptic scale variability.
Magnusdottir et al. (2004) and Deser et al. (2004) investigated the effects of North Atlantic sea surface temperature and sea ice anomalies on winter circulation in the CCM3 atmospheric circulation model. They used observed 40-year trends in sea

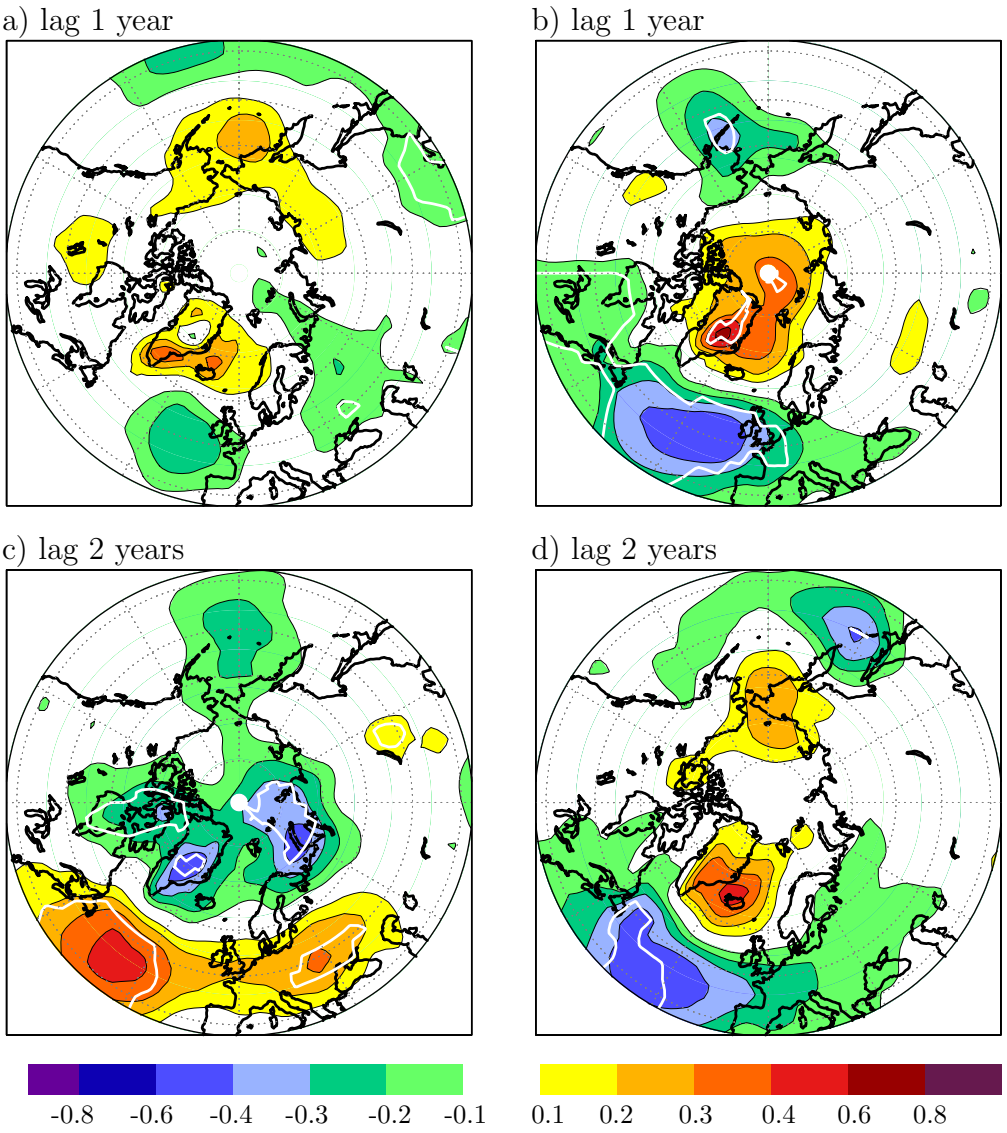

Figure 5.9: Composite analysis of annual mean SLP in hPa one and two years after high (left) and low (right) ice exports through Fram Strait. The white line indicates the level of 90% significance.

ice and SST to derive a realistic spatial pattern of the anomalous forcing. They found that the atmospheric response on sea ice resembled the NAO pattern. A decrease in sea ice in the Greenland and Barents Sea accompanied by an increase in Labrador Sea ice cover led to a negative phase in the NAO. In agreement with the results of Deser et al. (2000), strong changes in the heat fluxes from ocean to atmosphere were linked to variations in ice cover. Similar investigations have been carried out by Alexander et al. (2004). They used the years with largest

and lowest Arctic ice cover from observations during 1979 to 1999 to force an AGCM. Fifty ensemble runs had been carried out to evaluate the impact on the atmosphere in the following winter. The local response showed increased ocean-to-atmosphere heat release and decreased SLP where the ice receded and vice versa where sea ice expanded. The large scale atmospheric response to reduced ice cover east of Greenland resembled the negative phase of the simulated NAO and vice versa.

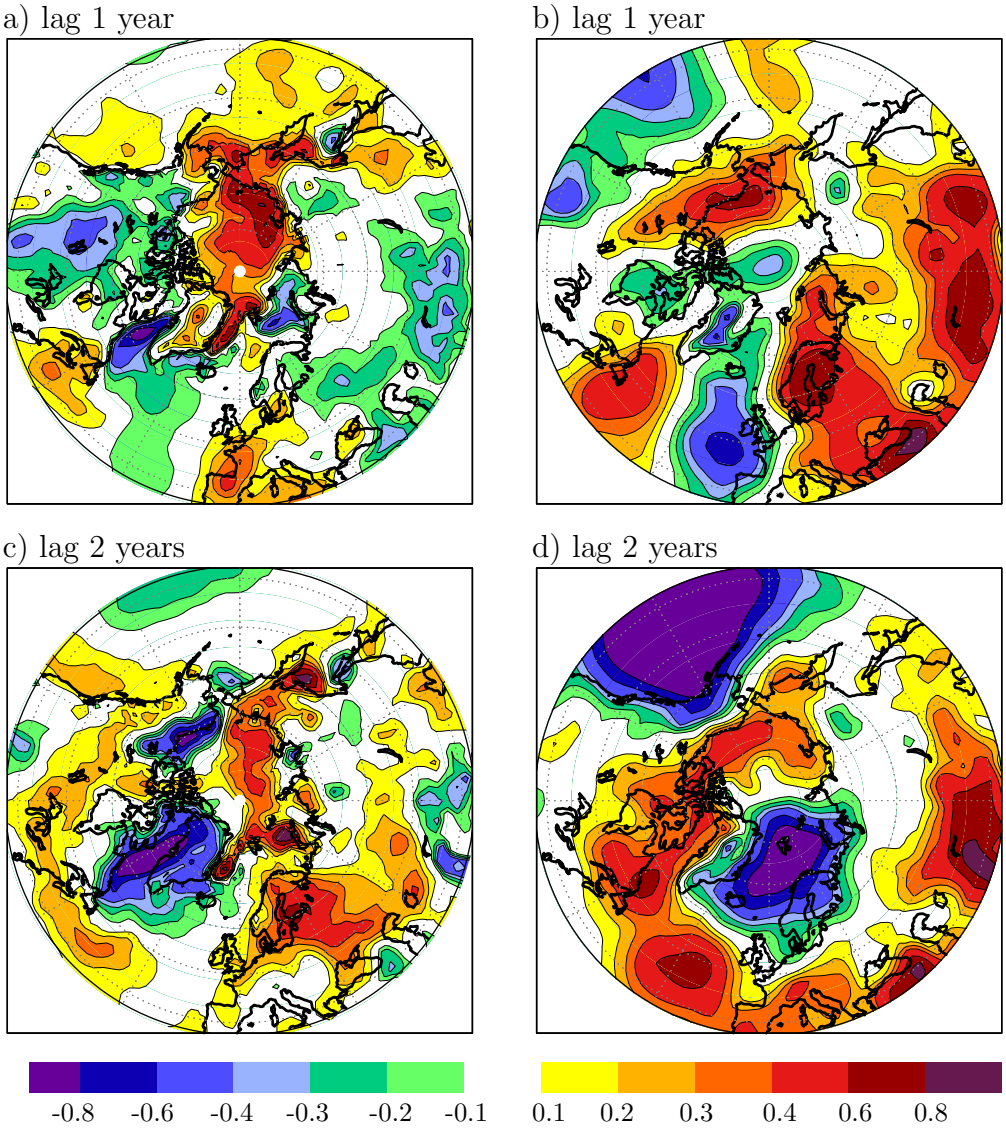

Figure 5.10: Composite analysis for annual mean NCEP 2m air temperature (left, in Kelvin) and SLP (right, in hPa) anomalies one (top) and two years (bottom) after high ice exports through Fram Strait.

To compare the atmospheric response in the model with NCEP/NCAR reanalysis (Kalnay et al., 1996), the Fram Strait ice export from the uncoupled ocean model MPI-OM forced with NCEP reanalysis data has been used (as done in Haak et al. (2003)). The composite analyses for annual mean two meter air temperature and SLP anomalies in the reanalysis are shown in figure 5.10. The fact must be addressed that only five events with large ice export through Fram Strait occurred during the period of reanalysis. Therefore, statistics are poor. Nevertheless, the composite analysis of the air temperature shows negative anomalies in the Labrador Sea of similar magnitude as in the coupled model after large ice exports. In the eastern Arctic and eastern Asia temperatures are increased in both reanalysis and model but the amplitude is much larger in the reanalysis. The reanalysis shows additionally anomalies over Europe and North America in the first and second year, which are not or only partly reproduced in the model simulations.
The SLP-patterns are rather different one year after high ice exports through Fram Strait. One year later when the model simulations show the largest response, the patterns agree quite well. A positive NAO-index is obvious in the reanalysis in the second year as well. In contrast to the model simulation the high pressure anomaly over the North Atlantic and Europe extends further to the east and to the west across the Labrador Sea into the Beaufort, Chukchi and East Siberian Seas. The negative anomaly over the North Pacific is much more pronounced than in the model.

It has been shown above that air temperature variability in the Labrador Sea is strongly dependent on the variability of ice export through Fram Strait and the associated salinity and heat flux anomalies in the Labrador Sea. The correlation of annual mean air temperature and surface salinity is 0.78 (both variables are averaged over a box in the central Labrador Sea $(54 - 60°N, 48 - 56°W)$). This means that slightly more than 60% of the temperature variability can be explained by variations of salinity in the Labrador Sea (fig. 5.11). The advection of air masses also greatly affects temperature. The NAO-index is a good indicator for this: in years with positive NAO-index, anomalous cold air is advected from the Arctic to the Labrador Sea and in the negative NAO-case warm air is advected from the Atlantic. The correlation index between air temperature in the Labrador Sea and the NAO-index is -0.48. Since no correlation between surface salinity in the Labrador Sea and NAO-index is found (r=0.02), it seems there are two different processes operating. Therefore, we compute an index consisting of the difference of the normalised salinity and the normalised NAO-index. The maximum correlation between this index and air temperature in the Labrador Sea is reached when salinity is weighted with 1.3 and the NAO-index with 0.7. The correlation coefficient then amounts to 0.9 and thus about 80 % of the total variance in the temperature is explained.

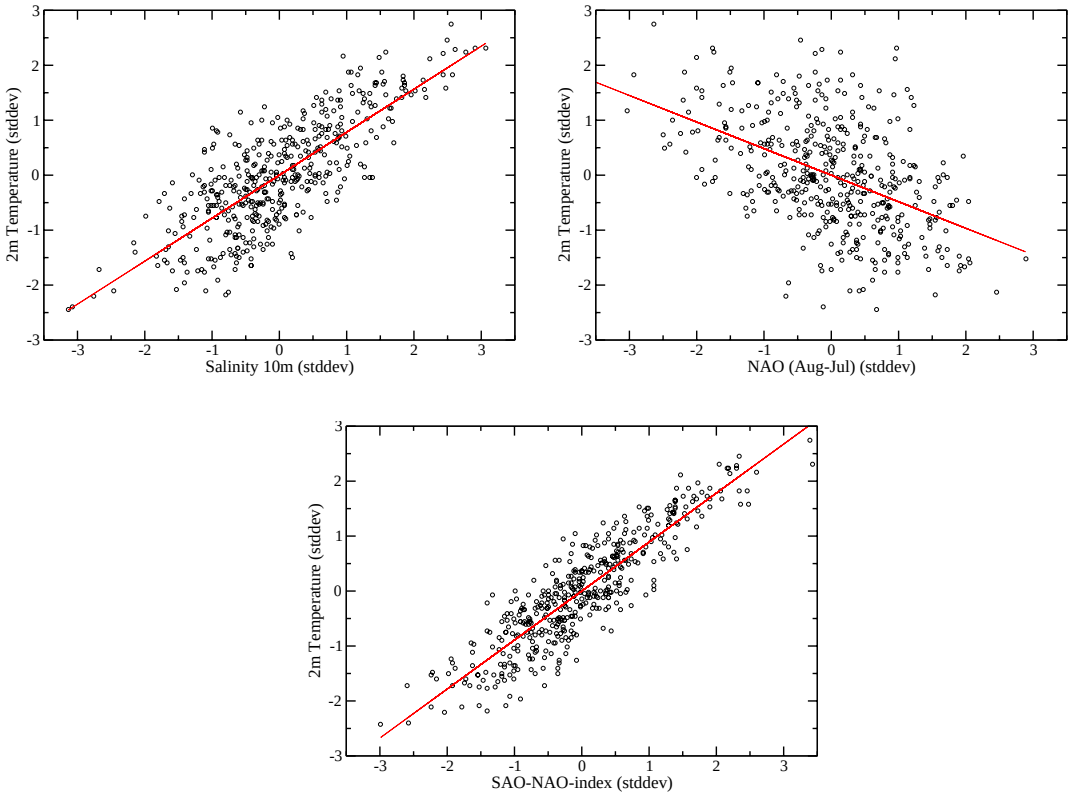

Figure 5.11: Scatterplot of annual mean 10m salinity anomalies and 2m air temperature anomalies in the Labrador Sea (top left), NAO-Index and temperature (top right) and a combined salinity/NAO-Index and temperature (bottom). All units are normalised.

6 Variability of Fram Strait Ice Export

Chapter 5 argues the large impact of the sea ice export variability through Fram Strait on climate conditions in the northern high latitudes. Thus, the mechanisms determing the variability of the ice export are of special interest. A detailed analysis of the interannual to decadal variability is now presented.

A spectral analysis of the modelled ice export (fig. 6.1) indicates pronounced peaks, at time scales of about 3 years, 9 years and 15 years. Time scales of about 10 years and 15 to 20 years are also well documented in other studies. Hilmer and Lemke (2000) used a sea ice model and found a pronounced decadal variability in the Arctic ice volume and Goosse et al. (2002) indicated a mode at a time scale of 15 to 18 years, which might fit to the 15-year peak in the ice export in this study. Venegas and Mysak (2000) analysed a century-long record of sea ice concentration and SLP with a frequency-domain sigular value decomposition. They proposed three different mechanisms for variability of the ice export through Fram Strait: a wind-driven motion of anomalous ice volumes from the East Siberian Sea towards Fram Strait at a time scale of 6 to 7 years, an enhanced ice motion parallel to the TDS at a time scale of 9 to 10 years and a motion of old, thick ice from the offshore northern Canada into the outflow region with a period of 16 to 20 years.

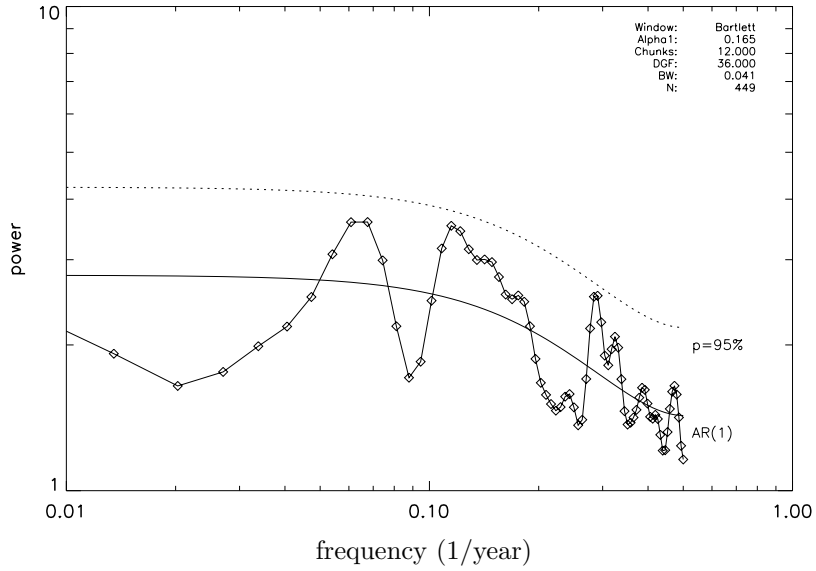

Figure 6.1: Spectral analysis of annual mean Fram Strait ice export.

6.1 Atmospheric Circulation and Ice Export

In chapters 3 and 4, the strong influence of the atmospheric circulation on sea ice distribution and sea ice transport has been demonstrated. The following analyses its impact on the variability of the ice export through Fram Strait.
Figure 6.2 a presents a correlation analysis between annual mean ice export through Fram Strait and SLP anomalies. A high negative correlation exceeding -0.6 is obtained in the area of the Kara Sea. Slightly weaker positive correlations exist over the Canadian Archipelago. This pattern is related to anomalous winds from the coasts of Laptev, East Siberian, Chukchi and Beaufort Seas across the Arctic towards Fram Strait and enhanced northerly windstress in Fram Strait. Consequently, ice is anomalously transported towards Fram Strait in the entire Arctic Basin (fig. 6.2 b). The regression pattern of the ice transport resembles the pattern of the second EOF of the ice transport (fig. 4.8). The associated time series is correlated to the ice export with -0.91 and the power spectra compare very well (see figures 4.9 and 6.1).

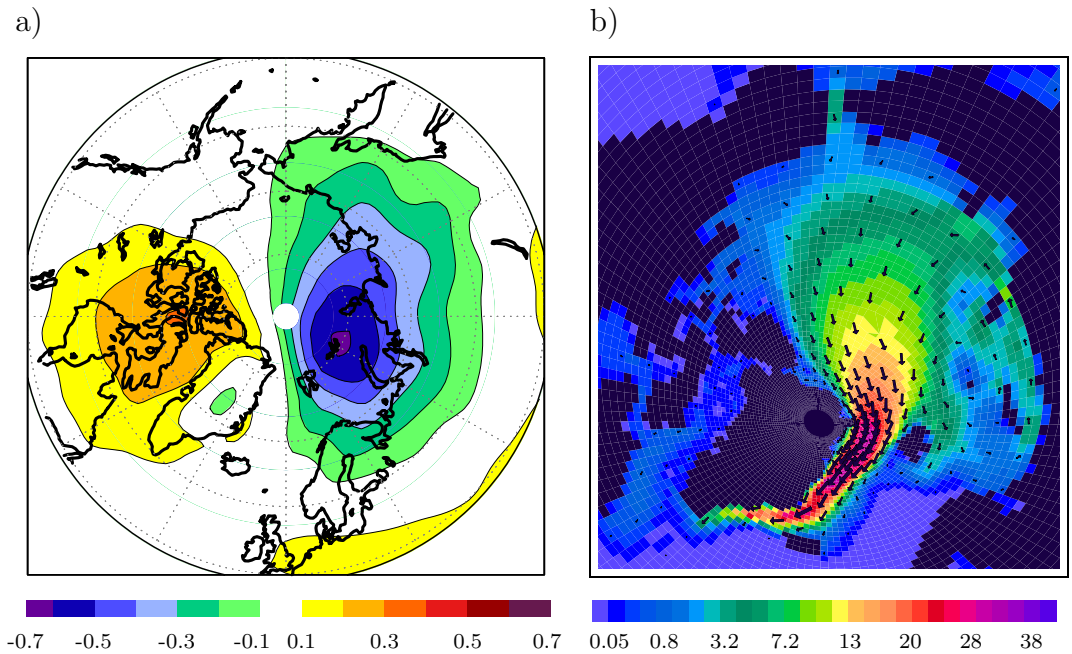

Figure 6.2: a) Correlation pattern between annual mean ice export through Fram Strait and SLP. b) Regression pattern between Fram Strait ice export and sea ice transport in the Arctic in $10^{-3} m^2/s$ per standard deviation ice export.

The correlation between ice export and SLP gradient across Fram Strait reaches 0.86 for annual values. The SLP gradient explains thus about three-fourths of the annual mean ice export variability. This is in good agreement with observationally

based estimates of Kwok and Rothrock (1999) who found an explained variance of 80 %. Anomalous northerly winds lead to an increase of ice export through Fram Strait whereas southerly winds reduce it. Arfeuille et al. (2000) pointed out that the ice thickness in Fram Strait plays an important role as well and that the wind speed in Fram Strait alone is not sufficient to describe the ice export. However, results from this model indicate that a high pressure gradient across Fram Strait is associated with increased ice velocities and anomalous thick ice. The ice is accumulated by the wind north of Fram Strait and Greenland. Thus, the high correlation between ice export and SLP gradient across Fram Strait does not disagree with the results of Arfeuille et al. (2000).
The following sections discuss the impact of large scale atmospheric modes on the variability of the SLP gradient across Fram Strait as well as the ice export itself.

6.1.1 North Atlantic Oscillation

Several studies showed a high positive correlation between the NAO (Hurrel and van Loon (1997); Bojariu and Gimeno (2003)) and the ice export through Fram Strait since 1978. Kwok and Rothrock (1999) analysed satellite data from 1978 to 1998 and found a correlation coefficient of 0.86. Model simulations with a sea ice model of Hilmer and Jung (2000) presented the same results for this time period but without significant correlation between ice export and NAO before 1978. Analysis of a 300-year control run of the atmosphere-ocean-sea ice model ECHAM4/OPYC3 by Jung and Hilmer (2001) showed no significant correlation either. The changing character of the relation between ice export and NAO can be explained by an eastward shift in the extension of the Iceland Low into the Arctic since the late 70's. This shift leads to an increased pressure gradient across Fram Strait in the positive NAO case. Before 1978, the NAO did not affect the SLP gradient across Fram Strait at all. Whether the shift in the NAO is due to anthropogenic climate changes or an usual state of the NAO cannot yet be determined. Ostermeier and Wallace (2003) analysed the trends in the NAO over the 20th century. They found a negative trend from 1920 to 1970 and a strong positive trend since. Several other studies (Moritz et al., 2002; Maslanik et al., 1996; Kwok, 2000) discussed the recent changes in Arctic climate and sea ice motion associated with the NAO and AO. The results of these studies can be summarised as follows: ice concentration has been reduced in the Greenland and Barents Sea and slightly increased in the Labrador Sea. The TDS has weakened and slightly shifted to the Canadian side of the Arctic while the ice export through Fram Strait has increased.
In this model, the NAO has neither influence on the amount of the ice export through Fram Strait nor on the pressure gradient across Fram Strait (fig. 6.3). But the ice export is reduced in the eastern part of Fram Strait and enhanced

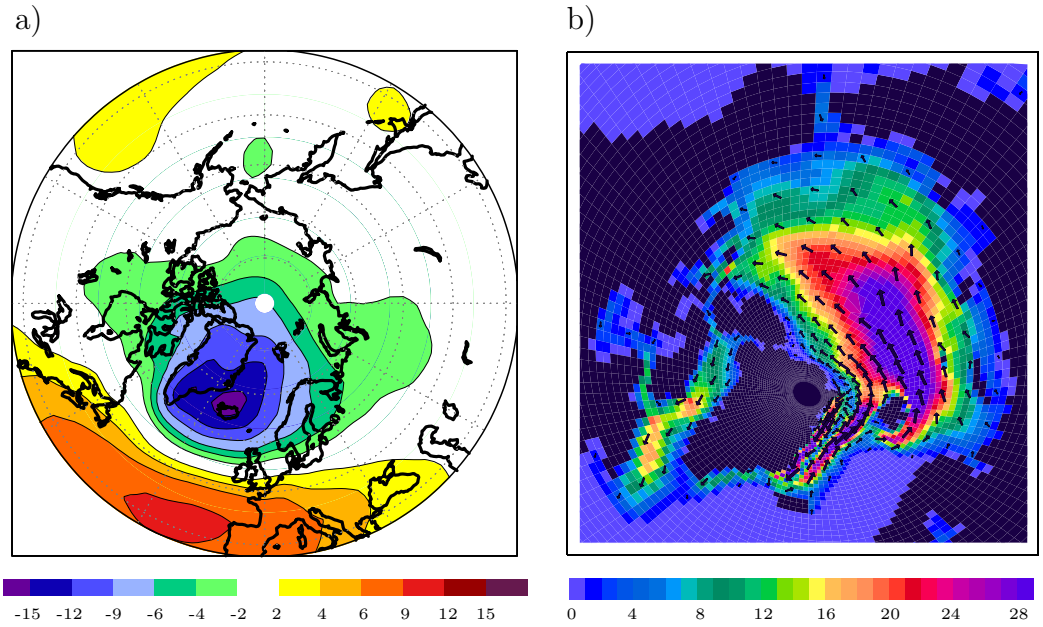

Figure 6.3: a) Difference between high and low NAO sea level pressure (DJF) in hPa. b) same as a) for annual mean ice transports in $10^{-3}m^2/s$.

in the western part during the high NAO case. Nevertheless, the anomalous SLP pattern and the associated wind anomalies lead to strong anomalous ice transports from the Barents Sea across the North Pole to the Beaufort Sea. Ice transport to the south is enhanced in Baffin Bay and Labrador Sea.
To discuss the temporal relationship between NAO-index and sea ice export through Fram Strait, running 30-year intervals of the 500-year control run have been analysed. In the entire 500 years, no 30-year period with a high correlation between ice export or SLP gradient and NAO could be found. This confirms the presumption of Jung and Hilmer (2001) that the recent state of the NAO is rather unusual and may be a response to anthropogenic forcing. One has to keep in mind that the model represents climate conditions from the end of the 70's and may not be able to reproduce an eastward shift in the NAO.

6.1.2 Stratospheric Polar Vortex

Several studies have recently discussed the effect of the stratospheric circulation on tropospheric climate. Christiansen (2001) as well as Graversen and Christiansen (2003) showed that zonal wind anomalies from the stratosphere propagate downward to the troposphere in about 10 to 15 days. Thompson et al. (2002) and Baldwin et al. (2003) proposed an increased skill from the stratospheric circulation to predict northern hemisphere tropospheric conditions on this time

scale. Charlton et al. (2003) used a statistical model and found in contrary to Thompson et al. (2002) only a very small increase of statistical predictability for the troposphere using the stratosphere as predictor. In a further study with a high resolution weather prediction model, Charlton et al. (2004) showed that the initial conditions in the lower stratosphere are of importance for the prediction. Norton (2002) performed sensitivity experiments with an atmospheric general circulation model and altered the mean state and variability of the stratosphere. The winter time SLP responded with a lag of 10 to 25 days with a pattern which is similar to the one of the AO.
The impact of the stratospheric polar vortex on the ice transport in the Arctic and especially the ice export through Fram Strait in the ECHAM5/MPI-OM is discussed in the following. In this study, the polar vortex has been defined, according to Castanheira and Graf (2003), as the zonal mean zonal wind speed in 50 hPa height and 65 degrees north.

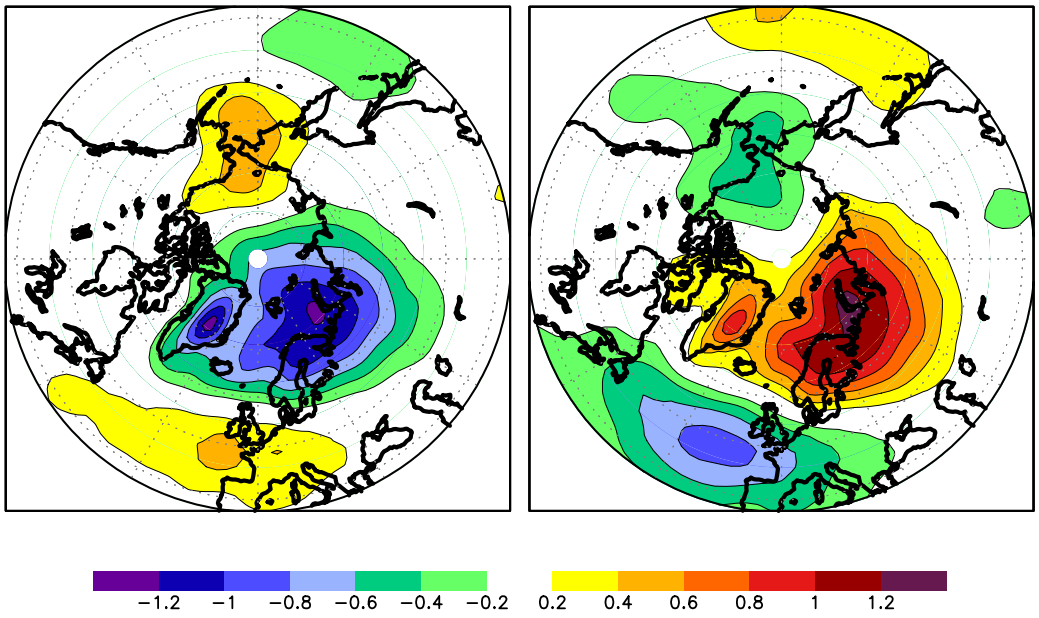

Figure 6.4: Composite analysis of annual mean SLP anomalies in hPa for strong (left) and weak (right) vortex regimes.

In contrast to the NAO, the annual mean stratospheric polar vortex is significantly positively correlated (r=0.34) with the annual mean ice export through Fram Strait in the control integration.
Figure 6.4 displays annual mean SLP anomalies for strong and weak stratospheric polar vortex regimes (exceeding the mean +/- 1 standard deviation). During strong regimes, negative pressure anomalies of slightly more than 1 hPa occur centered over the Barents Sea. Weaker positive anomalies appear over the North Atlantic, western Europe and the Bering Strait. The pattern is almost symmetric

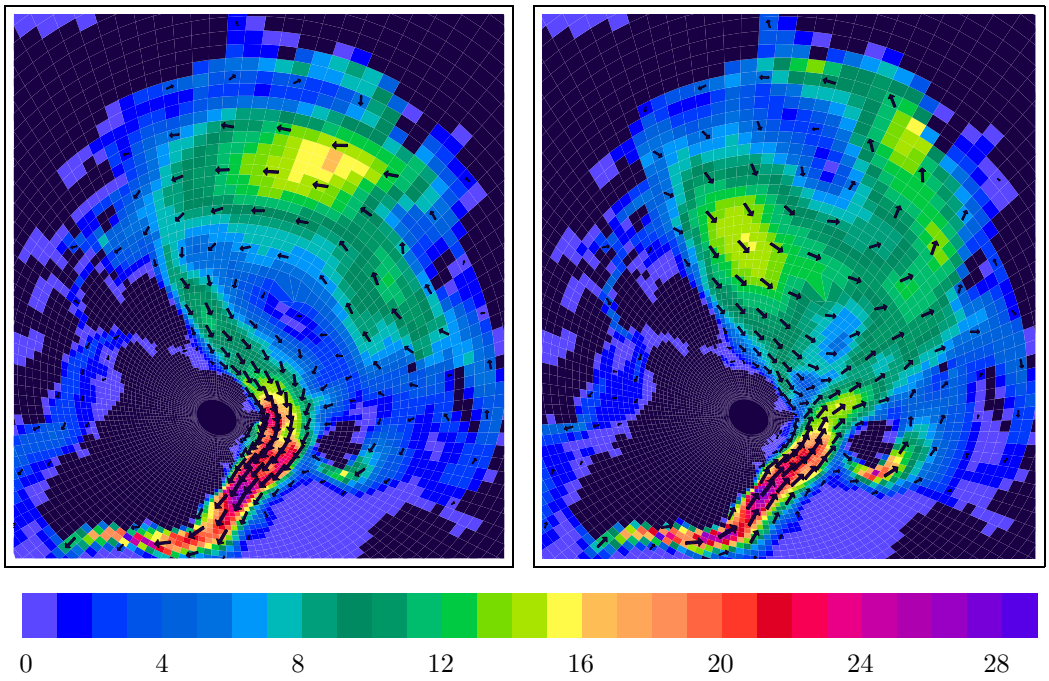

Figure 6.5: Composite analysis of annual mean sea ice transport anomalies in $10^{-3}m^2/s$ for strong (left) and weak (right) stratospheric polar vortex regimes.

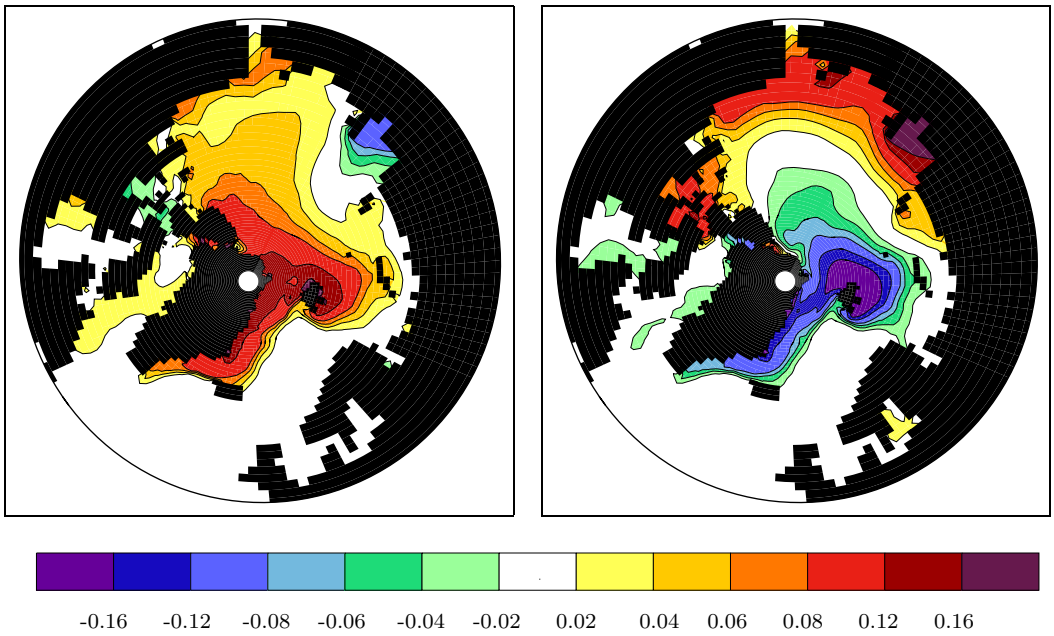

Figure 6.6: Composite analysis of annual mean sea ice thickness anomalies in m for strong (left) and weak (right) vortex regimes.

for weak vortex regimes. This SLP pattern compares well to results of the sensitivity experiments of Norton (2002). The maximum pressure anomaly in the ECHAM5/MPI-OM model is slightly shifted towards the Barents Sea. The fact that annual mean values are used in this study while Norton focused on winter means must be addressed.
The SLP anomalies, associated with a strong polar vortex, lead to an increased SLP gradient across Fram Strait and stronger northerly winds. The ice export through Fram Strait is consequently enhanced and vice versa during weak vortex regimes (fig. 6.5). The anomalous ice transport within the Arctic Basin is not symmetric during strong and weak regimes. It is characterised by an anti clockwise transport from the European Arctic along the Siberian coast to the Beaufort Sea and further to the north coast of Greenland and Fram Strait during strong vortexes. During weak regimes, the TDS is weakened and anomalous transports take place from the Beaufort Sea in a semi-circle towards the coasts of Siberian and Chukchi Seas. These circulation patterns determine the anomalous distribution of ice thickness (fig. 6.6). Thicker ice than usual occurs in the Nordic Seas as well as north of Greenland and Fram Strait while ice is thinner in the Laptev Sea during strong regimes. A weak vortex is characterised by a dipole with positive ice thickness anomalies, extending along the coast from the Kara Sea to the Canadian Archipelago, and negative anomalies in the Greenland/Barents Seas and north of Fram Strait and Greenland.

6.1.3 Atmospheric Planetary Waves

Large scale atmospheric planetary waves in the northern hemisphere are mainly caused by the topography and land-sea distribution. A summary of the current knowledge of the formation and impact of planetary waves is presented by O'Hanlon (2002). Cavalieri and Häkkinen (2001) investigated the relationship between atmospheric planetary waves and Arctic climate variability. They performed a zonal Fourier analysis over a monthly averaged 50-year SLP-record from 1946 to 1995 for different latitude bands. They showed that the phase of the first wave for the latitude band from 70 to $80°N$ in January is well correlated with the ice export through Fram Strait. The first wave is determined by the Siberian High and the Iceland Low. A ridge of the Siberian High that extends into the East Siberian and Chukchi Seas and a trough of the Iceland Low into the Arctic form the maximum and minimum of the first wave. A shift in the positions of the pressure systems to the east is associated with reduced pressure in the Barents and Kara Seas. Thus, the pressure gradient across Fram Strait is increased. In contrast to the NAO, the high correlation between ice export and the first wave in January held for the entire 50-year period. Cavalieri (2002) attributes this consistency to the sensitivity of the first wave phase to the presence of secondary

low pressure systems in the Barents Sea that serve to drive Arctic sea ice southward through Fram Strait.

In this study, the relationship suggested by Cavalieri and Häkkinen (2001) has been analysed in the 500-year control integration. Coinciding with the results of Cavalieri and Häkkinen (2001), the ice export through Fram Strait is highly correlated with the phase of the first SLP wave for the latitude band from 70 to 80°N. This relation holds for the entire year. Highest correlations occur in winter (r=0.6 in February) while the correlation in June and July is quite weak (r=0.2 resp. 0.15). For annual mean values a correlation coefficent of 0.59 could be found.
In spite of the high correlation between phase and ice export, usage of the phase as index has some disadvantages. In months with a small amplitude, the first wave explains only a minor part of the SLP variability. Then the phase is of minor importance. Figure 6.7 shows that large anomalies in the phase are associated with a small amplitude. Furthermore, it is difficult to qualify large shifts in the phase as positive or negative because phase anomalies of nearly $-180°$ or 180° both describe the same SLP pattern. A shift in the phase exceeding 90° is not further increasing the SLP gradient across Fram Strait and the ice export is not enhanced anymore. To vanquish these difficulties, a new index containing both the phase and the amplitude of the wave is introduced here:

$$WI1 = A * sin(\phi^{'}) \tag{6.1}$$

This index is called wave index 1 (WI1). A is the amplitude of the first wave and $\phi^{'}$ the phase anomaly. Use of $sin(\phi^{'})$ instead of the phase anomaly has two effects: WI1 is decreased if the phase anomaly exceeds 90° and the function is continuously differentiable at the location $\phi^{'} = 180°$. $sin(\phi^{'})$ is weighted with the amplitude to reduce the noise of years with small explained variances of the first SLP wave.
The WI1 is slightly better correlated with the ice export through Fram Strait than the phase. Table 6.6 displays the correlation between monthly mean WI1 and monthly mean ice exports through Fram Strait. The correlation is generally high between September and May with a maximum of 0.7 in February. In the summer months, correlation is significant but does not exceed 0.35. For comparison, the relation between WI1 and SLP gradient across Fram Strait is shown. One can clearly see that this correlation is reduced in summer as well.
Figure 6.8 shows the SLP pattern for the cases of large positive and negative WI1 (exceeding the mean +/- 1 standard deviation) for winter means. The pattern during positive WI1 is characterised by negative anomalies up to -6 hPa at the Siberian coast with center in the Kara Sea and much weaker positive anomalies of about 2 hPa in the western Arctic and in western Europe. During the negative case of WI1, the pattern is quite symmetric. The positive anomaly over the Kara

	Jan	Feb	Mar	Apr	May	Jun	Jul	Aug	Sep	Oct	Nov	Dec
FI	0.66	0.70	0.61	0.66	0.59	0.34	0.26	0.35	0.49	0.54	0.56	0.59
FG	0.73	0.73	0.69	0.67	0.59	0.31	0.31	0.53	0.66	0.67	0.60	0.61

Table 6.6: Correlation between monthly means of WI1 and Fram Strait ice export (FI) and SLP gradient across Fram Strait (FG).

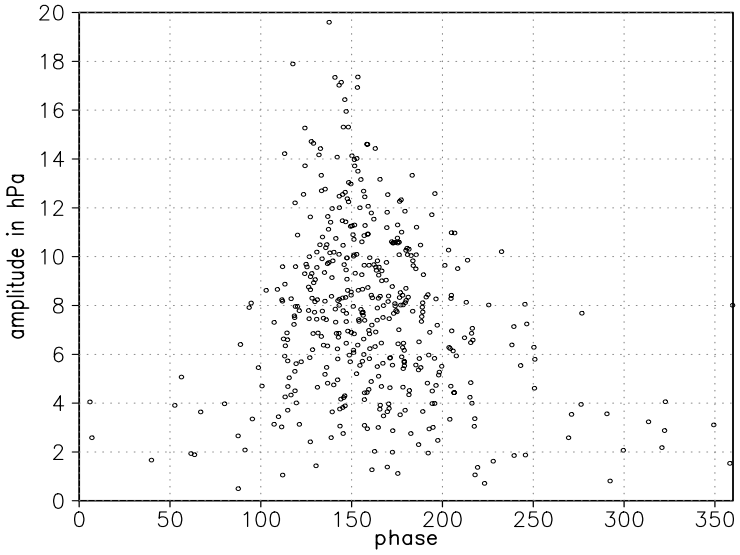

Figure 6.7: Scatterplot between phase (in degrees) and amplitude (in hPa) of the first wave for winter (DJF) SLP in $70 - 80°N$.

Sea extends slightly further into the Chukchi Sea and the anomaly over the western Arctic is slightly shifted towards the Canadian Archipelago compared to the positive case. The anomaly over Europe is not as pronounced during a negative WI1. Obviously, the WI1 is mainly governed by SLP variations in the Kara Sea. This results in a steepened SLP gradient across Fram Strait during a positive WI1 and vice versa. Dorn et al. (2000) depicted from model simulations with a regional coupled model that a warm and cold Arctic winter climate is connected with two distinct circulation states of the Arctic atmosphere. Cold Januaries are characterised by the extension of the Iceland Low into Barents and Kara Sea while warm Januaries are linked to a more pronounced Siberian High. These two states fit well to the positive and negative WI1 pattern.
The associated large SLP anomalies affect the ice transport in the entire Arctic. Figure 6.9 displays the composite analysis of annual mean ice transport for positive and negative WI1 (mean +/- 1 standard deviation). During a positive WI1, anomalous ice transport occurs from the Siberian coast over the Central Arctic

	Ba	Ka	La	Sib	Chu	Bea	CA	AB
WI1	-0.45	0.20	0.67	0.61	0.60	0.24	-0.75	0.57

Table 6.7: Correlation between DJF ice transport divergence in the Arctic regions and WI1 (Ba=Barents Sea, Ka=Kara Sea, La=Laptev Sea, Sib=East Siberian Sea, Chu=Chukchi Sea, Bea=Beaufort Sea, CA=Central Arctic, AB=Arctic Basin).

towards Fram Strait and Barents Sea. During negative WI1, ice is anomalously transported from Fram Strait to the Siberian coast and cyclonic in the Beaufort Gyre. Both the Gyre and the TDS are thus weakened. The ice transport anomalies reach their maximum with more than $5 * 10^{-2} m^2/s$ in Fram Strait and the EGC.
The composite pattern for SLP and ice transport compares well to the correlation and regression patterns between ice export through Fram Strait and SLP and ice transport, respectively (fig. 6.2). The ice transport anomalies due to the variability in WI1 are associated with variations in the ice transport divergence (table 6.7). During positive WI1, anomalous divergent ice transports occur from the Laptev Sea to the Chukchi Sea. Convergences can be seen in the Barents Sea and particularly in the Central Arctic. The entire Arctic shows an ice volume lost because of the large ice export through Fram Strait.

The probability distribution of annual mean ice exports through Fram Strait for highly anomalous WI1 (fig. 6.10) provides evidence that almost all extreme export events in the 500-year control run are related to WI1. The distribution for the cases of large positive and negative WI1 show a distinct shift towards corresponding positive and negative ice export anomalies.

It has been demonstrated above that the state of the WI1 is mainly characterised by SLP in the Kara Sea. The persistence and the source of these SLP anomalies are analysed in the following.
A correlation analysis among single months of WI1 shows no or only a very weak correlation. The highest correlation coefficient of 0.15 is obtained between WI1 of January and February. For further investigations, daily winter (DJF) SLP values in the Kara Sea are compared for months with high positive and negative WI1. Two features are particularly striking: the SLP for positive WI1 in the Kara Sea is generally lower than for negative WI1 and the variability is larger. A sequence of short, relatively large negative anomalies occurs during positive WI1. Contrary, high SLP can persist for a time of one to two weeks in the Kara Sea during a negative WI1. The standard deviation of daily SLP in the Kara Sea

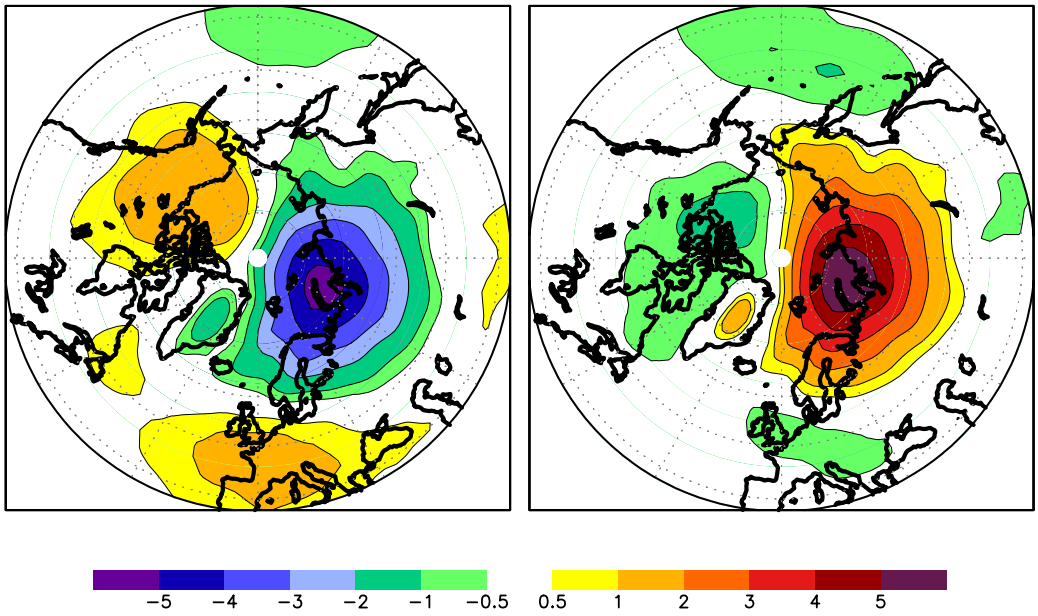

Figure 6.8: Composite analysis of SLP anomalies (DJF) in hPa for the cases of large positive (left) and negative (right) winter WI1.

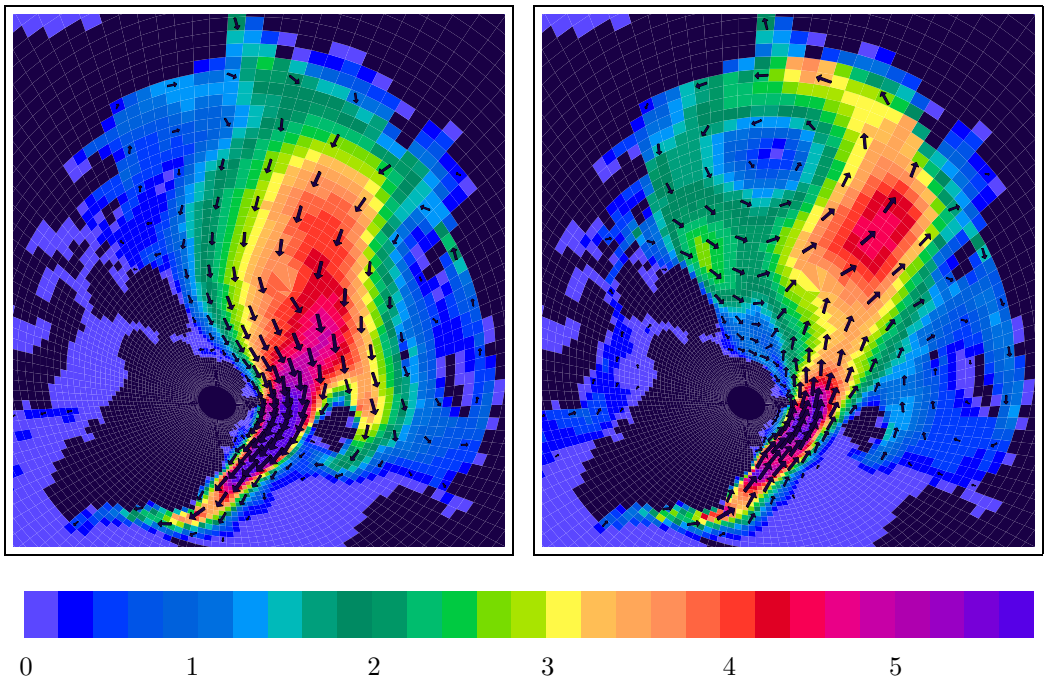

Figure 6.9: Composite analysis of annual mean sea ice transport anomalies in $10^{-2}m^2/s$ for the cases of large positive (left) and negative (right) annual WI1.

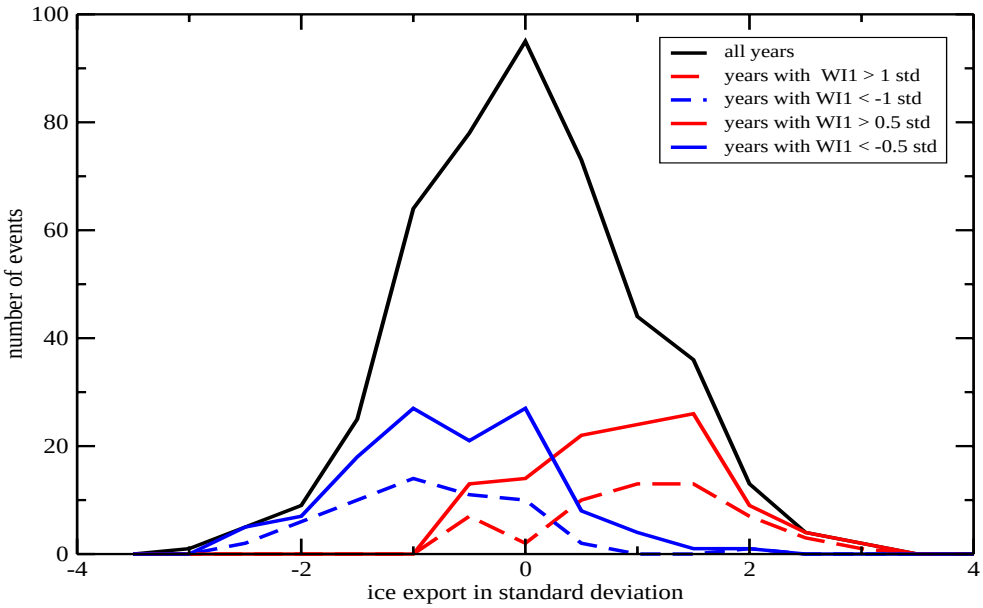

Figure 6.10: Probability distribution of the annual mean ice export through Fram Strait for the cases of positive (red) and negative (blue) annual WI1 exceeding the mean +/- 0.5 (dashed) and +/- 1 (solid) standard deviation. The black line shows the distribution for all years.

reaches 12.5 hPa for the high positive and 10.7 for the high negative WI1 case. During a positive WI1, more cyclones are active in the Barents and Kara Seas while in the negative case, longer periods with stable anticyclonic regimes occur. Storm tracks are calculated from daily winter SLP data to determine the source of the cyclones. They can be defined in several different ways. Gulev et al. (2001) used a cyclone tracking technique while others (e.g. Harnik and Chang (2003); Rogers (1997)) prefer variance statistics of the pressure field. In this study, the standard deviation of the two to six days bandpass filtered daily SLP data is defined as storm track. A composite analysis of these storm tracks for winter means of the WI1 (fig. 6.11) shows distinct changes between the phases of WI1. During positive WI1, the storm track over the North Atlantic is extended far into the Barents Sea and the Kara Sea, whereas it is much more zonal during negative WI1. Then the standard deviation of the bandpass filtered daily SLP in the Barents and Kara Seas is small with 3 hPa. Furthermore, the standard deviation in the formation area of the North Atlantic low pressure systems over northeastern North America is slightly increased in the positive WI1 case. In contrary, the storm track over the North Pacific is intensified in the low WI1 case.

One can conclude that an intensification of the North Atlantic storm track and especially a deflection to the north are the main reasons for a positive WI1. Thus,

the cyclones propagate mainly from the North Atlantic into the Barents and Kara Sea and are not formed locally. This is in good agreement to the results of Cavalieri (2002). As the Fram Strait is located on the west side of the storm track, an enhanced pressure gradient across it and anomalous northerly winds are the consequence. This implies that single cyclones are of great importance for the ice export through Fram Strait, which fits well to observations of cyclones in the Fram Strait by Brümmer et al. (2001, 2003). Serreze and Barry (1988) analysed the synoptic activity in the Arctic Basin and found the largest activity in the European sector of the Arctic for the winter season. Most of the cyclones emigrated from the North Atlantic into the Arctic Basin, which is consistent with the assumption of this study. Furthermore, Serreze (1994) analysed the development and decay of Arctic cyclones. He identified the Iceland, Greenland and Norwegian Seas as regions with largest cyclogenesis while cyclolysis dominates in the Arctic Basin. Rogers and Mosley-Thompson (1995) showed that anomalous cyclone activity in the Kara and Barents Seas is highly correlated with the Siberian air temperature. It has much more influence on the temperature than large scale features such as the NAO or the Siberian High.

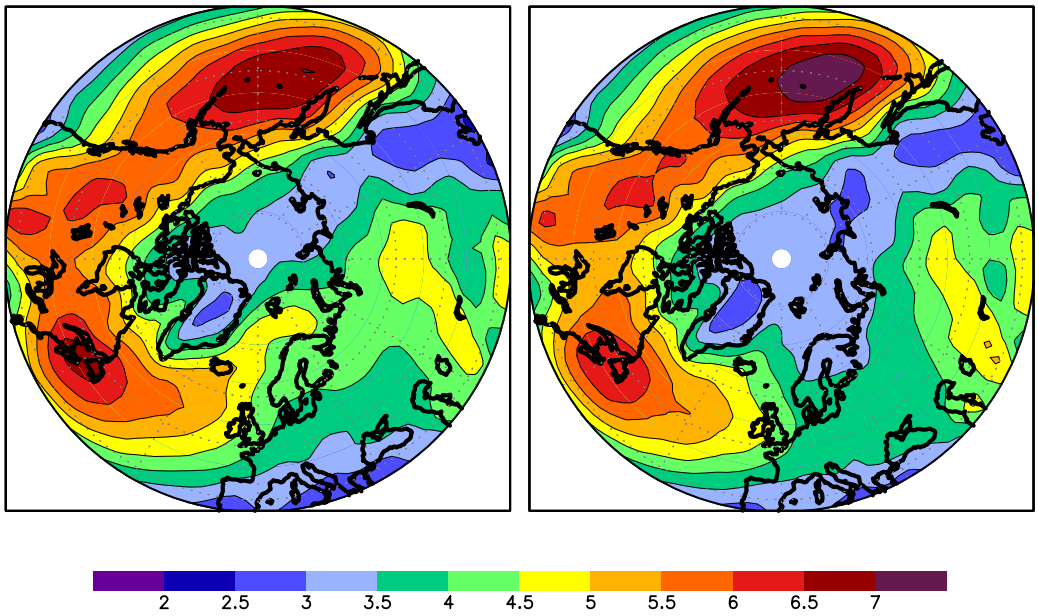

Figure 6.11: Composite analysis of the standard deviation of the bandpass filtered (2-6 days periods) winter (DJF) SLP in hPa for the cases of large positive (left) and negative (right) annual WI1.

During a negative WI1 the Siberian High extends further into the Kara and Barents Seas and the storm track is more zonal. It remains unclear whether it can extend further to the north due to a weaker, more zonal storm track or if a strong

Siberian High blocks the cyclones. One possible mechanism affecting the Siberian High are early fall snow anomalies over Siberia. Cohen et al. (2000) showed that they do indeed influence SLP in the northern hemisphere and especially had impact on the AO in the following winter. Gong et al. (2003) affirmed these results with model experiments but found a much weaker amplitude in SLP anomalies. However, no significant correlation could be found between autumn snow cover over Siberia and the winter time SLP or the storm track in the control integration of this model. The impact on the atmospheric circulation is very weak even after extreme snow cover anomalies.
Midlatitude atmospheric blocking (D'Andrea et al., 1998) which deflects the low pressure systems to the north could be another possibility for the shift in the storm tracks.

6.2 Ice Thickness Anomalies and Ice Export

In the previous sections, the strong influence of the atmospheric circulation on the interannual variability of Fram Strait ice export has been demonstrated. However, several studies pointed out that sea ice thickness anomalies have a considerable impact on the export through Fram Strait as well (e.g. Koeberle et al. (1999); Arfeuille et al. (2000)). Koeberle and Gerdes (2003) used an ocean - sea ice model to show that ice thickness anomalies play an equally important role for the ice export through Fram Strait.
In chapter 6.1, it has been argued that a strong SLP gradient across Fram Strait is also associated with anomalous thick ice. To further analyse the relation between ice thickness anomalies in the Arctic and Fram Strait ice export, a lag regression analysis has been performed (fig. 6.12). Five years before high ice exports, positive ice thickness anomalies are formed at the coasts of Chukchi and East Siberian Sea (fig. 6.12 a). In agreement with results of Tremblay and Mysak (1998), these anomalies are caused by a convergent ice transport due to an anomalous wind field and associated with a negative ice export through Fram Strait. In the next two years, the positive ice thickness anomaly slowly propagates clockwise along the Siberian coast (fig. 6.12 b) and crosses the Arctic to reach Fram Strait leading the ice export by one year (fig. 6.12 c). High ice exports themselves are associated with large anomalous ice transports all over the Arctic towards Fram Strait (fig. 6.2 b) caused by the anomalous atmospheric forcing described above (fig. 6.2 a). A negative ice thickness anomaly occurs at the Siberian coast as a consequence. It propagates across the Arctic to Fram Strait in the next years, which leads to a decreased ice export (fig. 6.12 e and f) four years later. A further year later, the ice export is still reduced and ice thickness at the Siberian coast is again increased. The entire cycle takes about nine years and matches the peak in the power spectrum of the ice export at the same time scale (fig. 6.1).

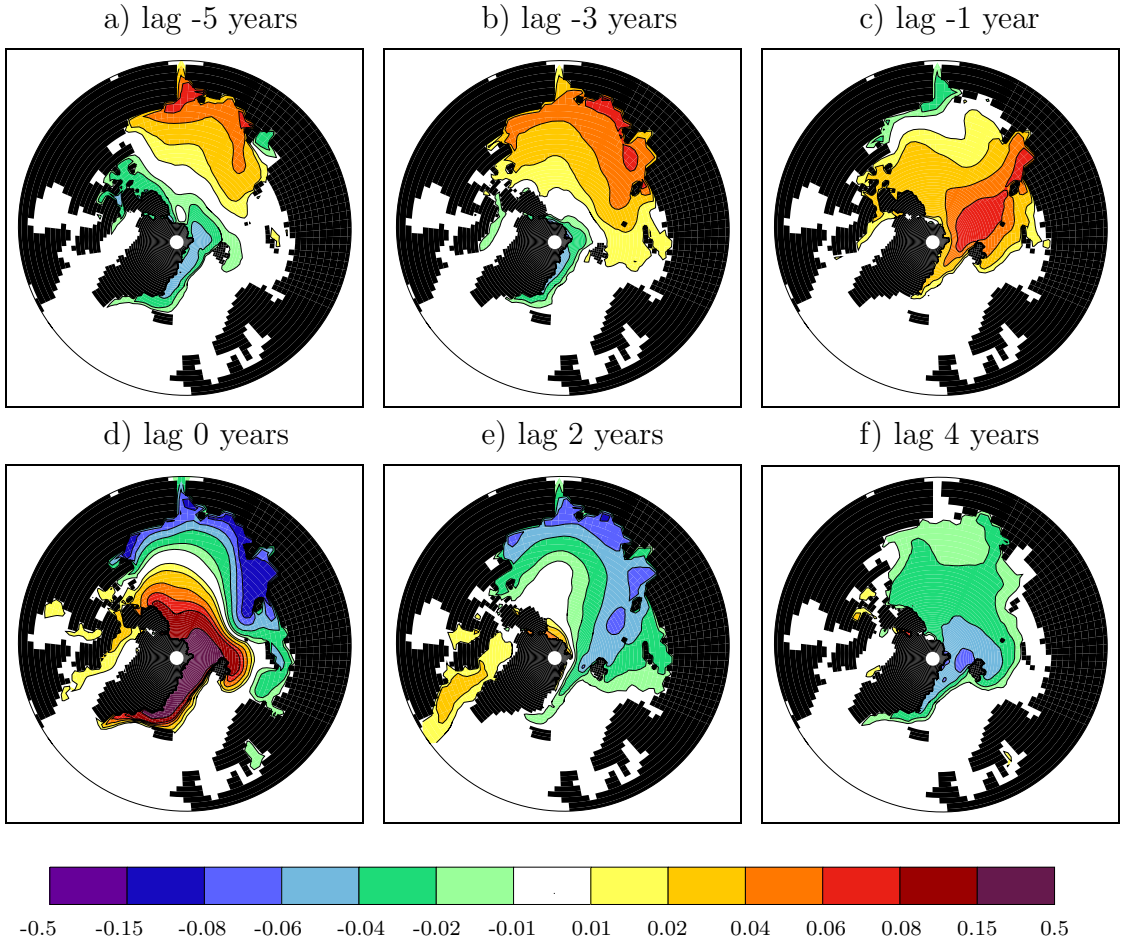

Figure 6.12: Regression coefficient between annual mean ice exports through Fram Strait and ice thickness anomalies in m per standard deviation ice export. a) ice export lags 5 years, b) ice export lags 3 years, c) ice export lags 1 year, d) lag 0, e) ice export leads 2 years f) ice export leads 4 years.

In order to determine how the propagation of ice thickness anomalies towards Fram Strait fits to the temporal and spatial variability of ice thickness in the Arctic Basin, a lag EOF-analysis of ice thickness in this region has been carried out. A 40-year Hanning high pass filter has been applied to focus on interannual to decadal variability. The Hanning filter belongs to the cosine-filters and is defined as: $W(k+1) = 0.5 \cdot (1 - cos(2 \cdot \pi \cdot k/(n-1))$, k=0,1,...,n-1.
The EOF-analysis has been calculated for winter centred annual mean ice thicknesses of the 500-year control run for lags from one to eight years. The resulting EOF-pattern describes the temporal evolution of ice thickness anomalies in the Arctic Basin.

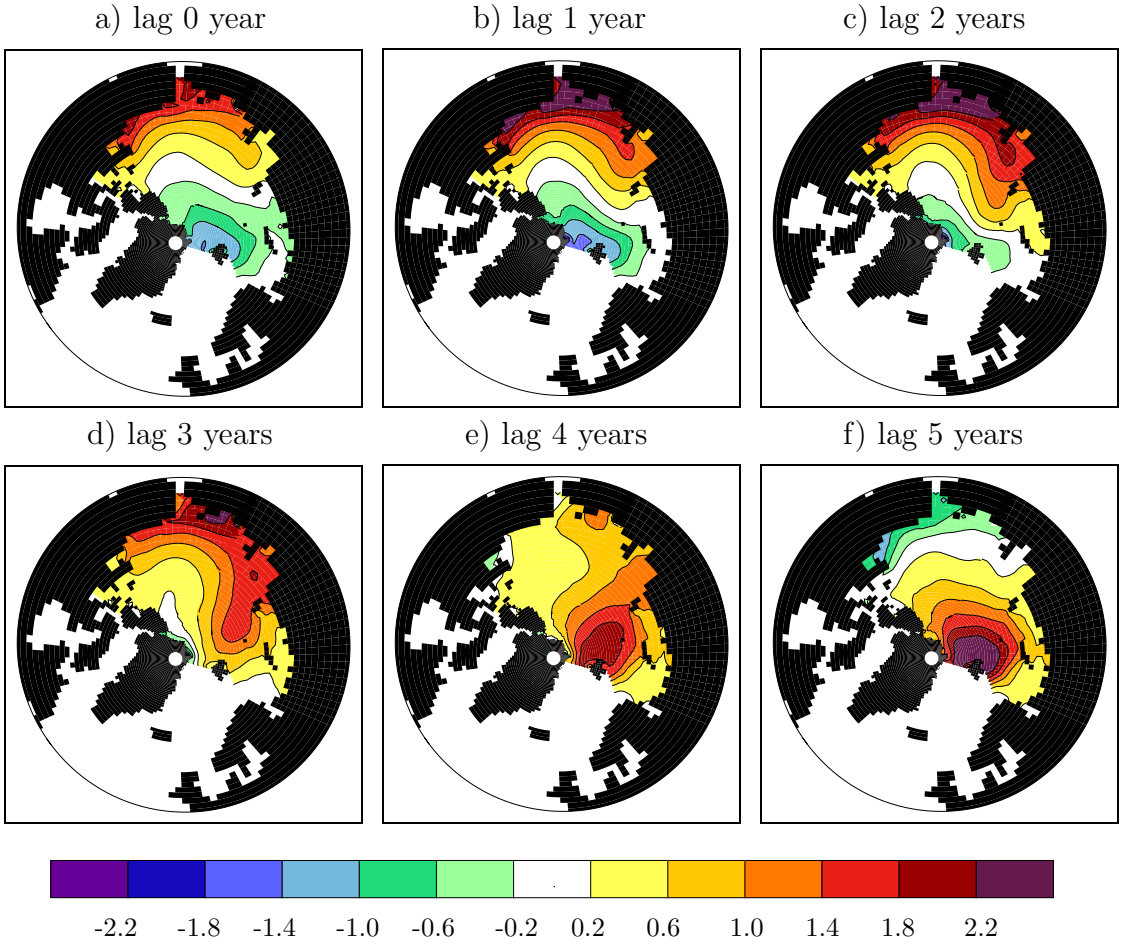

Figure 6.13: 1. EOF of a lag EOF analysis (0-8 years lag) of annual mean sea ice thickness in cm per standard deviation of the PC. Shown are lags from 0 to 5 years. A 40-year Hanning high pass filter has been used.

The first EOF (fig. 6.13) explains about 10 % of the total sea ice thickness variance. At the time T=0, a positive anomaly extends from the Beaufort Sea along the coast to the Laptev Sea and a negative anomaly occurs in the area of Fram Strait. In the following years, the positive anomaly spreads over larger parts of the Arctic while the center slowly propagates along the Siberian coast to the west. At lags of three and four years, almost the entire Arctic Basin shows positive values. The maximum crosses the Arctic quite fast in the TDS and reaches Spitsbergen and Fram Strait. One year later, maximum variations occur in the area of Fram Strait and Spitsbergen while negative anomalies are formed at the opposite side of the Arctic between Beaufort and Laptev Sea. Now a phase difference of about 180 degrees to the lag 0 - pattern can be seen. In the following years, the negative

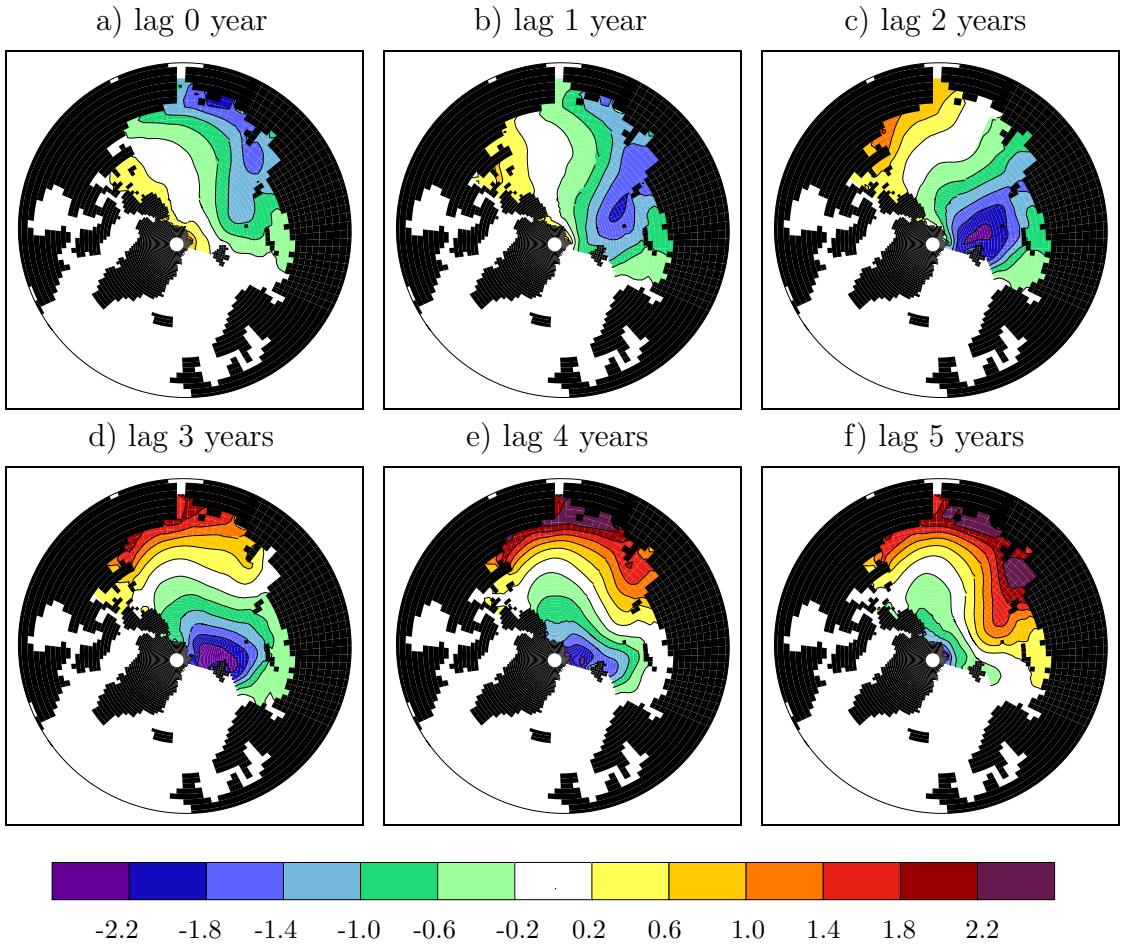

Figure 6.14: 2. EOF of a lag EOF analysis (0-8 years lag) of annual mean sea ice thickness in cm per standard deviation of the PC. Shown are lags from 0 to 5 years. A 40-year Hanning high pass filter has been used.

anomaly at the Siberian coast spreads and takes its way across the Arctic and reaches Fram Strait after 4 to 5 more years. Thus, the oscillation period of the first EOF accounts to about 10 years.
The second EOF (fig. 6.14), which explains 9 % of the total ice thickness variability, describes a mode similar to the first EOF. At a lag of zero, largest negative values extend along the coast from Chukchi Sea to Laptev Sea and further into the Central Arctic. Slightly weaker positive anomalies can be seen from Fram Strait to Beaufort Sea. During the following years, the negative anomaly propagates across the Arctic to Fram Strait. The positive anomaly strengthens and rotates clockwise to the Siberian coast before it passes the Arctic towards Fram Strait. The time scale of this mode is also about 10 years.

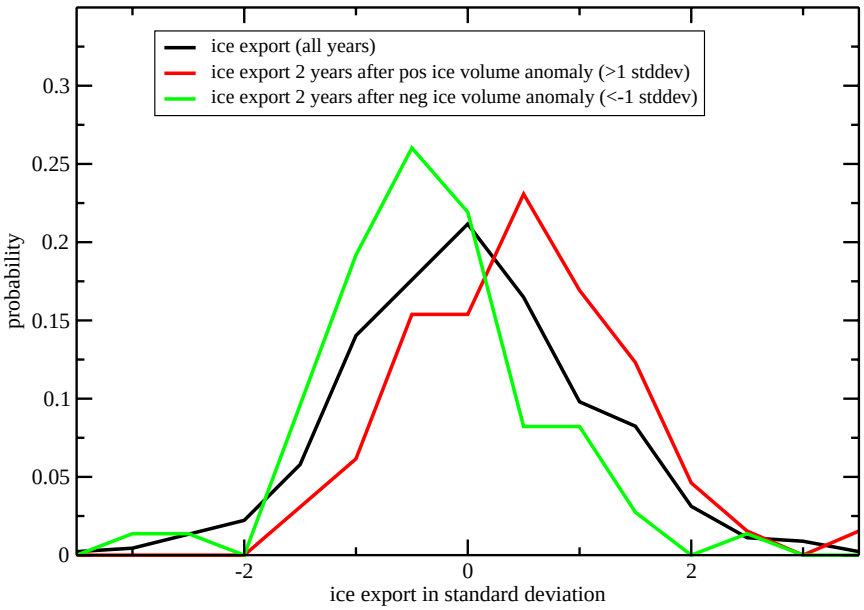

Figure 6.15: Probability distribution of annual mean Fram Strait ice export 2 years after positive (red) and negative ice volume anomalies (green) (exceeding one standard deviation) in the Laptev Sea. In black the mean ice export distribution for all years is given.

Both the first and the second EOF describe a mode that is characterised by a formation of an ice thickness anomaly in the area between Beaufort Sea and the Siberian coast, a clockwise propagation through the Arctic and a strong weakening after reaching Fram Strait. However, while the entire anomaly seems to be exported through Fram Strait in the first EOF, a part of this recirculates in the Arctic Basin in the second EOF. The first and second EOF are apparently not independent. This is proved by a cross spectrum analysis (not shown). The power spectra of the first two PC's are nearly identical, particularly for time periods shorter than 20 years. For these time periods the coherence is very high and the phase difference accounts to about 90 degrees. Furthermore, a lag correlation shows a high negative correlation at lags of -2 and -3 years and a high positive correlation at lags of 2 and 3 years, which fits well to the phase difference of 90 degrees.
A comparison of the results from the EOF analysis with the lag regression analysis between ice export through Fram Strait and sea ice thickness (fig. 6.12) indicates a high agreement between the process described by the first and second EOF and the lag regression analysis. Both patterns and time scales compare well. In chapter 6.3 the relation between this sea ice mode and atmospheric variations are analysed in more detail.

The mode presented above provides skill for predictability of the ice export through Fram Strait. Apparently, large ice exports are characterised by previous ice volume anomalies at the Siberian coast and vice versa. Statistical analyses show the largest predictability for the ice export through Fram Strait if ice thickness is increased two years before in the Laptev Sea. Figure 6.15 displays the probability distribution of the annual mean ice export two years after 69 positive and 71 negative ice volume anomalies (exceeding the mean +/- 1 standard deviation) in the Laptev Sea. After positive anomalies a considerable shift in the mean ice export towards positive values can be seen and vice versa. The skewness of the distribution is negative after thick ice and positive after previous thin ice in the Laptev Sea. Thus, the probability for negative ice export events is highly decreased while probability for extreme positive events increases only slightly after thick ice in the Laptev Sea. The statistical analysis shows additionally that probability for increased ice exports is only slightly enhanced at the first and third year after preceding positive ice volume anomalies. In contrast decreased ice exports are as probable in the first, second and third year after negative ice volume anomalies. The travel time of negative ice signals is apparently more variable than that of positive anomalies.
Ice thickness in the Laptev Sea before extreme ice exports through Fram Strait, which exceed the mean + 2 standard deviations, have been analysed: in four of five cases, ice volume has increased by more than one standard deviation two years before. All four extreme negative exports have been led by largely reduced ice thicknesses in the Laptev Sea. The formation of ice thickness anomalies at the coasts of Laptev and East Siberian Sea can be regarded as preconditioning for extreme ice export through Fram Strait.

6.3 Decadal Sea Ice Mode

The propagation of sea ice anomalies through the Arctic on a decadal time scale has been described in the previous section. Furthermore, evidence has been shown for the large impact of the atmospheric circulation on the ice drift.
A combined lag EOF analysis for annual values of SLP and sea ice thickness north of $50°N$ is performed to further analyse the relation between sea ice and atmospheric circulation. A 40-year Hanning high pass filter is used to suppress the multi-decadal variability in the ice thickness. SLP and ice thickness data are normalised by division of the value at each grid point through the standard deviation, spatially averaged over the area north of $50°N$. In order to compare the results to the lag EOF of sea ice thickness, this analysis is also calculated for lags from 0 to 8 years.
The leading EOF of the combined analysis which explains about 10 % of the variance of SLP and sea ice thickness is shown in figure 6.16. At the time T=0, the SLP field is characterised by a region of strong positive values, which extends

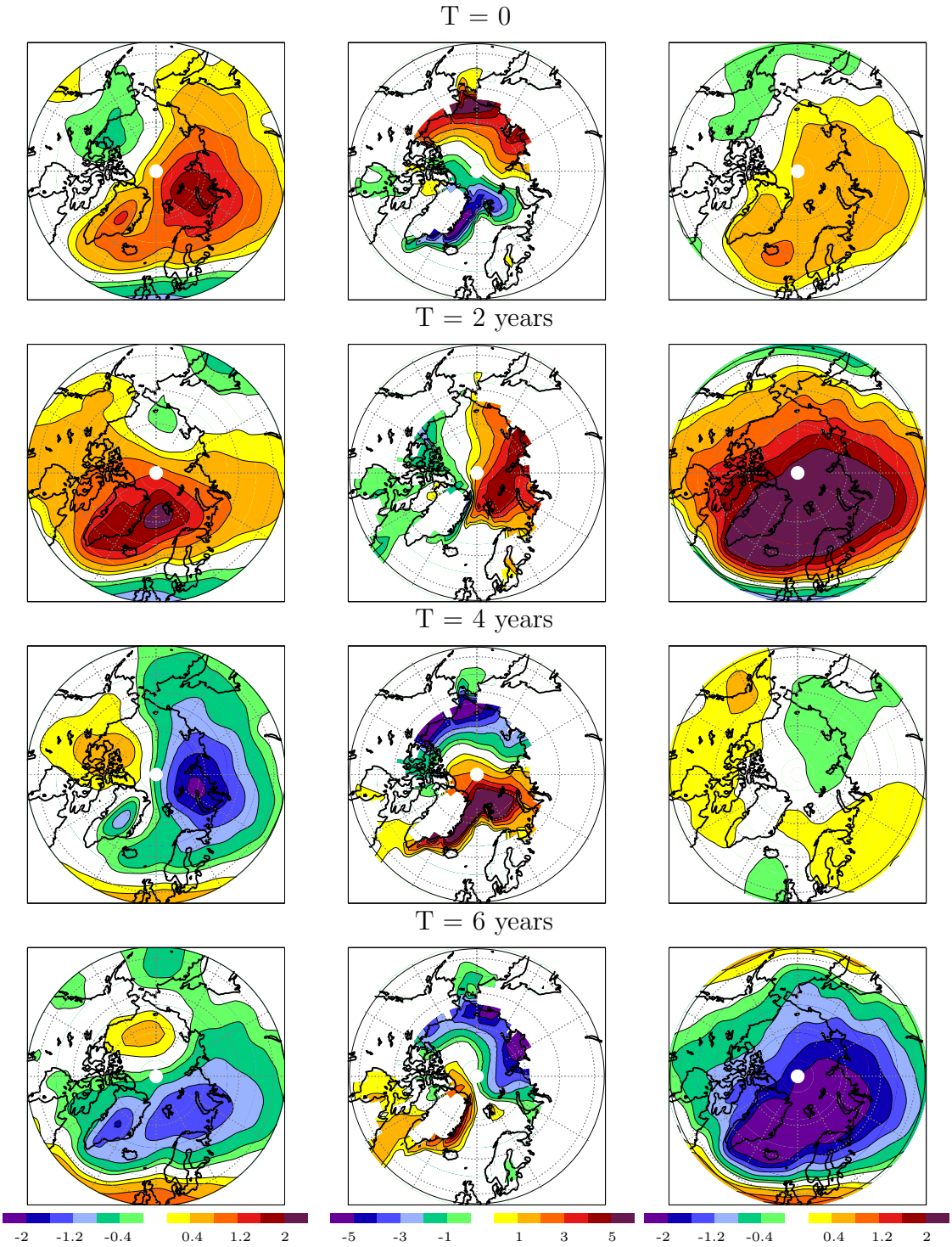

Figure 6.16: Left and middle: 1. EOF of a combined lag-EOF of SLP (left) and sea ice thickness (middle) with lags from 0 to 8 years. A 40-year Hanning high pass filter has been used. Right: The same for SLP-only.

over the entire European and eastern Arctic. The center is situated over the Barents and Kara Seas. A much smaller dipole occurs in the western Arctic. The related ice thickness field shows negative anomalies (for positive PC's) in the Barents and Greenland Seas and positive anomalies from the Beaufort Sea along the coast to the Laptev Sea. This situation fits well to the negative case of the WI1 and associated low ice exports through Fram Strait. Two years later, the SLP pattern has been rotated clockwise by about 90° and largest positive values can now be seen east of Greenland. The negative anomaly is located in the Siberian Sea and has further weakened. The ice pattern shows a similar rotation. Positive values occur from the Laptev Sea across the eastern Arctic towards Fram Strait. The large negative values in the Greenland Sea have disappeared but negative ice anomalies have occured in the Labrador Sea and in the Canadian Archipelago. Only a very small part of the ice can propagate from the Greenland Sea around the southern tip of Greenland into the Labrador Sea without melting. One can assume that new ice anomalies have been formed there. The anomalous SLP pattern leads to south-easterly winds and thus advection of warm air into this region. Furthermore, convection processes, associated with the previous low ice export, also reduce the ice in Labrador Sea (see chapter 5).
After four years, the SLP pattern is almost opposite to the initial distribution. The small negative anomaly at the East Siberian coast has strongly strengthened and its center has moved to the Laptev Sea. The large positive anomalies at a lag of two years have rotated by nearly 90° and substantially weakened. This situation resembles the positive case of WI1 and is associated with high ice exports through Fram Strait. Thus, positive values appear in Greenland and Barents Seas while negative anomalies occur from the Beaufort Sea to the East Siberian Sea. The rotational process continues in the following two years.
A rotation of about 180° takes slightly more than four years for both parameters. The whole cycle fits well to the peak at about 9 years in the spectrum of Fram Strait ice export and the sea ice oscillation in the Arctic Basin. The sea ice thickness part of the combined EOF is nearly identically to the patterns of the first and second EOF of the sea ice thickness-only lag EOF analysis (fig. 6.13 and 6.14). The first PC of the combined EOF is highly correlated with the first and second PC of the sea ice thickness EOF for lags of minus and plus one year. The correlation to the PC's of the lag-EOF of SLP-only is much weaker (fig. 6.16 right). The first PC's of both EOF's are correlated with 0.39. The first lag EOF of SLP explains only about 8 % of the total variance. Thus, it can clearly be suggested that the combined variance of SLP and sea ice thickness on a decadal time scale is mainly dominated by sea ice thickness variability. Obviously, there is no strong atmospheric mode in the Arctic on a decadal time scale. The atmospheric pattern of the first combined EOF can be interpreted as the stochastic pattern which is most appropriate to strengthen the sea ice mode. Once an ice thickness anomaly has been formed at the coast of the Chukchi or

East Siberian Sea, the atmosphere can amplify it but can also weaken or even suppress the ice mode. This does not rule-out that the sea ice mode in certain stages modifies the atmospheric circulation in a way that tends to maintain the mode. For lags of two and six years the SLP pattern of the combined EOF is quite similar to the pattern of the SLP-only EOF. These atmospheric conditions occur two years after low and high ice exports (lag 0 and lag of 4 years) and as argued in chapter 5 are due to changes in the meridional temperature gradient across the Gulf Stream.
A comparison of this EOF analysis with a complex combined EOF analysis of 40-year winter SLP and annual mean sea ice concentration data north of 45°N by Mysak and Venegas (1998) shows quite a high agreement concerning the sea ice. They also found a rotation of sea ice cover anomalies around the Arctic at a time scale of about 10 years. In contrary to sea ice, the SLP variations only partly agree. Mysak and Venegas (1998) suggest a standing oscillation in SLP in the Arctic related to the state of the NAO/AO. Similar SLP patterns occur in fig. 6.16 at lags of two and six years but not as standing oscillation but as part of a rotation around the Arctic. One has to keep in mind that Mysak and Venegas (1998) used winter SLP data while annual mean SLP are applied in this study.

7 Sensitivity Studies

One important mode of high latitude climate variability on interannual to decadal time scales has been identified in the control integration. Key processes of this mode are the formation of ice thickness anomalies at the Siberian coast, anomalous ice export through Fram Strait and the subsequent interactions between ocean and atmosphere in the Labrador Sea.
In order to further analyse the processes in these three key regions and their impact on climatic conditions in high latitudes, three sets of sensitivity experiments have been performed. In the first experiment (EXP1), ice anomalies are implemented at the Siberian coast. In the second experiment (EXP2), an ice volume anomaly in the East Greenland Current south of Fram Strait is used to prescribe extreme ice export events through Fram Strait. The third experiment (EXP3) describes the impact of fresh water anomalies in the Labrador Sea on oceanic and atmospheric conditions. Figure 7.1 presents the regions that are perturbed by sea ice and fresh water anomalies in the experiments, respectively. This chapter discusses the results of the model simulations.

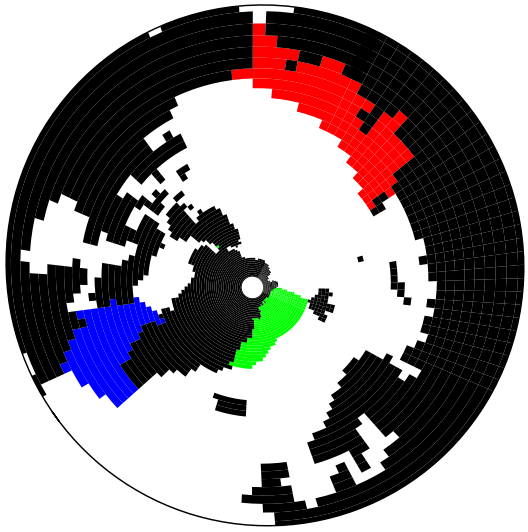

Figure 7.1: Experiment regions: Areas perturbed by sea ice and fresh water anomalies are shown, respectively. Red: EXP1, green: EXP2, blue: EXP3.

7.1 Ice Anomaly at the Siberian Coast

The Siberian coast is a main source region for the formation of ice volume anomalies. To analyse the propagation of such signals across the Arctic and their interactions with the atmosphere, ice volume anomalies of 2000 km^3 are prescribed

at the Siberian coast in model experiments (see fig. 7.1). Twenty runs are performed, starting from 1st Mai of twenty different years. This assures that the initial conditions are not relevant for the ensemble mean. The ice volume anomaly is produced by increasing the ice thickness by 1 m in an area along the Siberian coast and 0.5 m in a transfer region (two grid points) to the Central Arctic relative to the initial conditions.

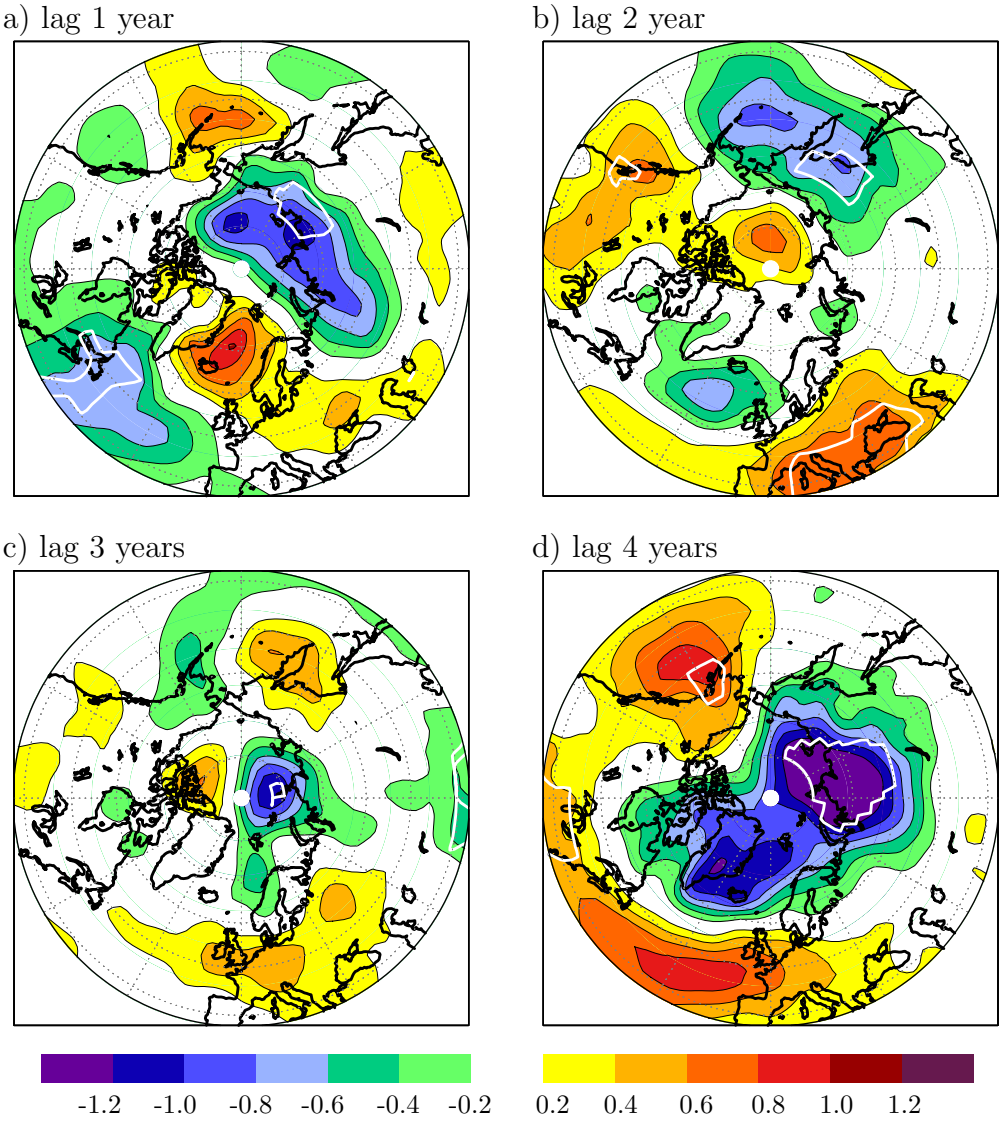

Figure 7.2: Annual mean SLP anomalies in hPa one to four years after addition of the ice thickness anomaly at the Siberian coast. Mean of the 20 ensemble runs. The white line indicates the level of 95% significance.

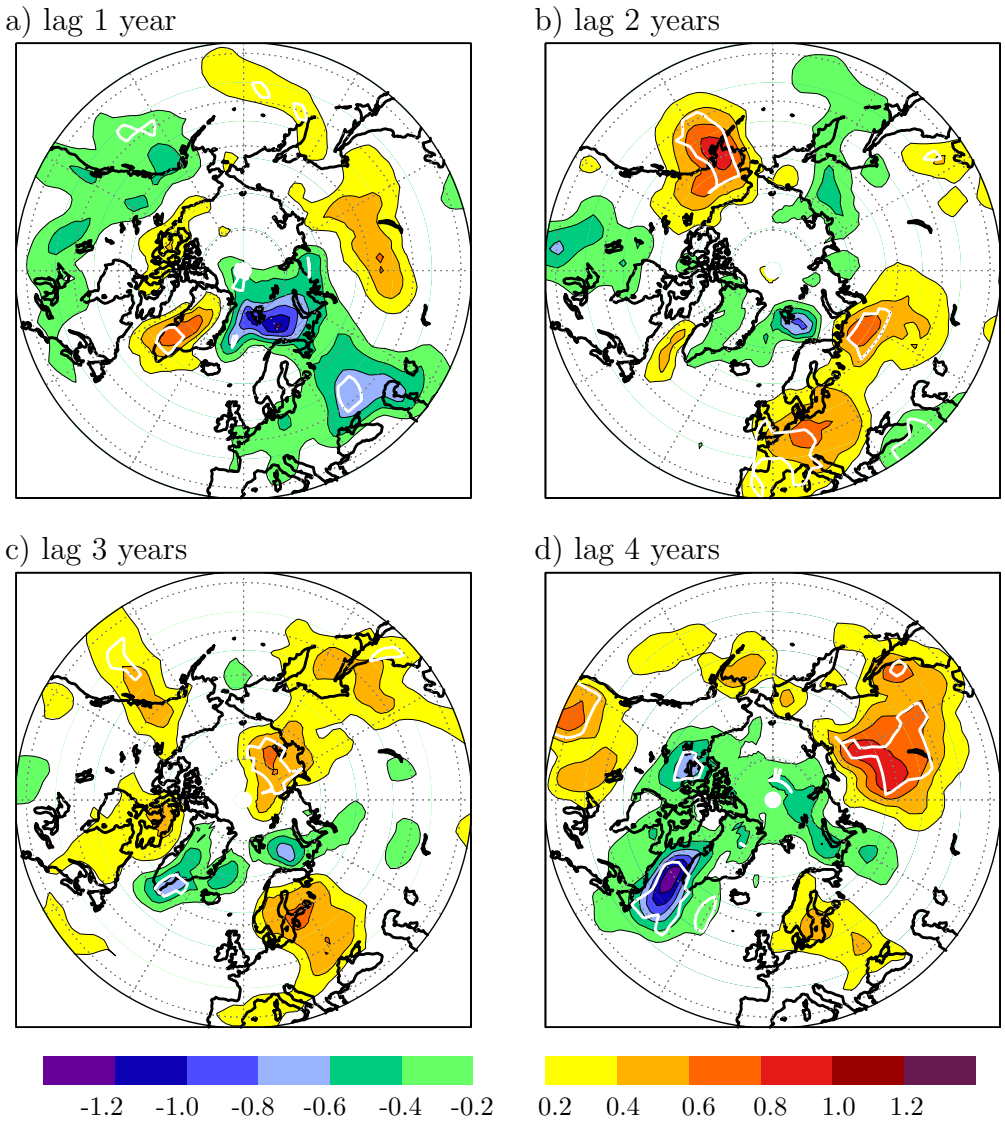

Figure 7.3: Annual mean two meter air temperature anomalies in Kelvin one to four years after addition of the ice thickness anomaly at the Siberian coast. Mean of the 20 ensemble runs. The white line indicates the level of 95% significance.

Results of the ensemble mean are now discussed. A lag of one year is defined as the mean from August in the year in which the experiment starts to July of the following year. Figure 7.2 shows the SLP response to the ice anomaly for lags of one to four years. The response describes the mean difference between the 20 experiment runs and the associated 20 control runs.
After one year, a large negative anomaly of more than -1 hPa, which is partly significant at the 95 % significance level, occurs along the Siberian coast. SLP is also

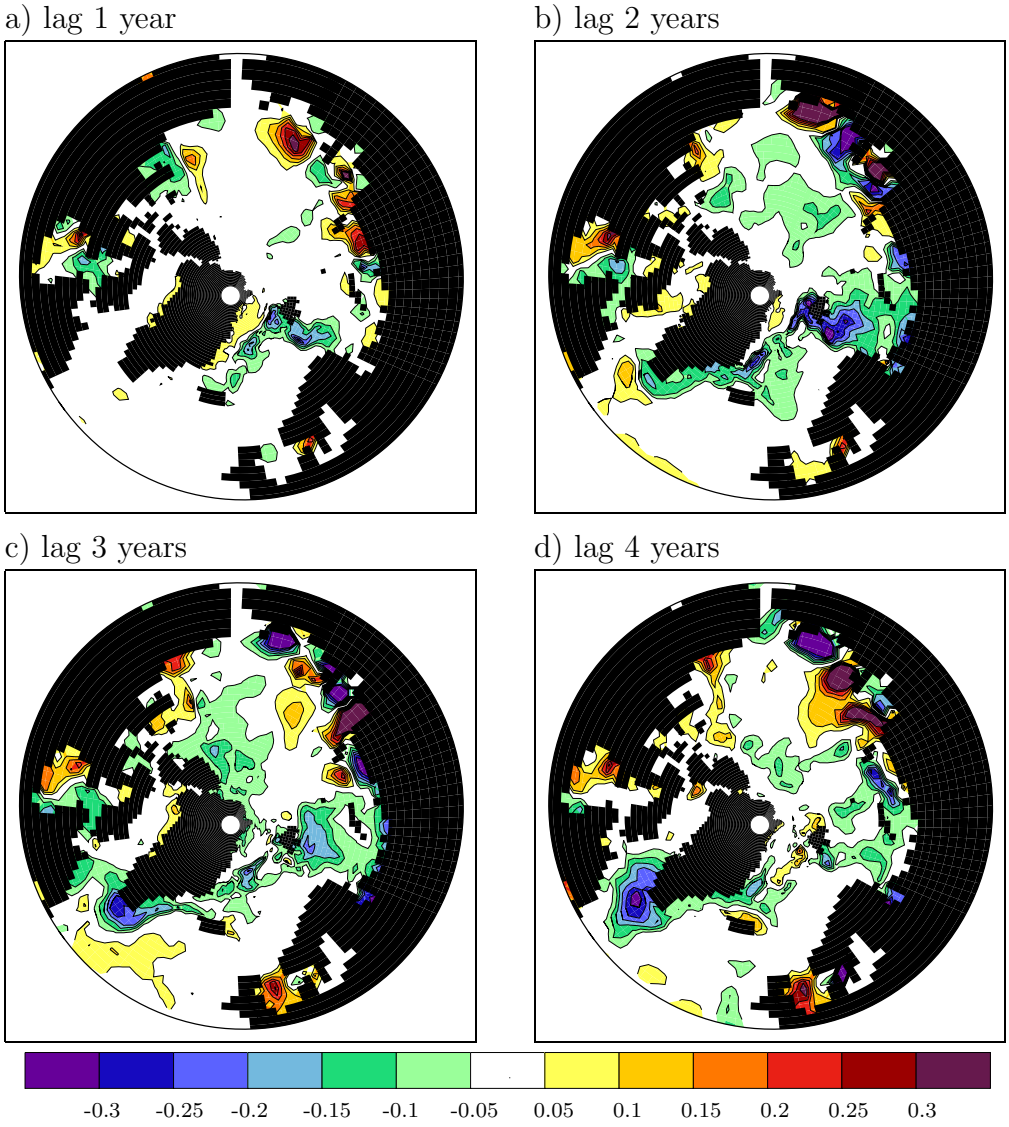

Figure 7.4: Annual mean 10 m salinity anomalies (in psu) one to four years after addition of the ice thickness anomaly at the Siberian coast. Mean of the 20 ensemble runs.

significantly reduced over the southern Labrador Sea and the western North Atlantic Ocean. In the Greenland Sea, SLP is increased by 1 hPa. This anomalous SLP pattern influences the ice transport and thus the ice thickness distribution (fig. 7.5). In addition to the propagation of the prescribed ice thickness anomaly with the mean circulation, ice is anomalously advected from the western Arctic towards Barents Sea and through Fram Strait into the Greenland Sea. Thus, ice thickness is increased in these areas, which leads to an intensified melting during

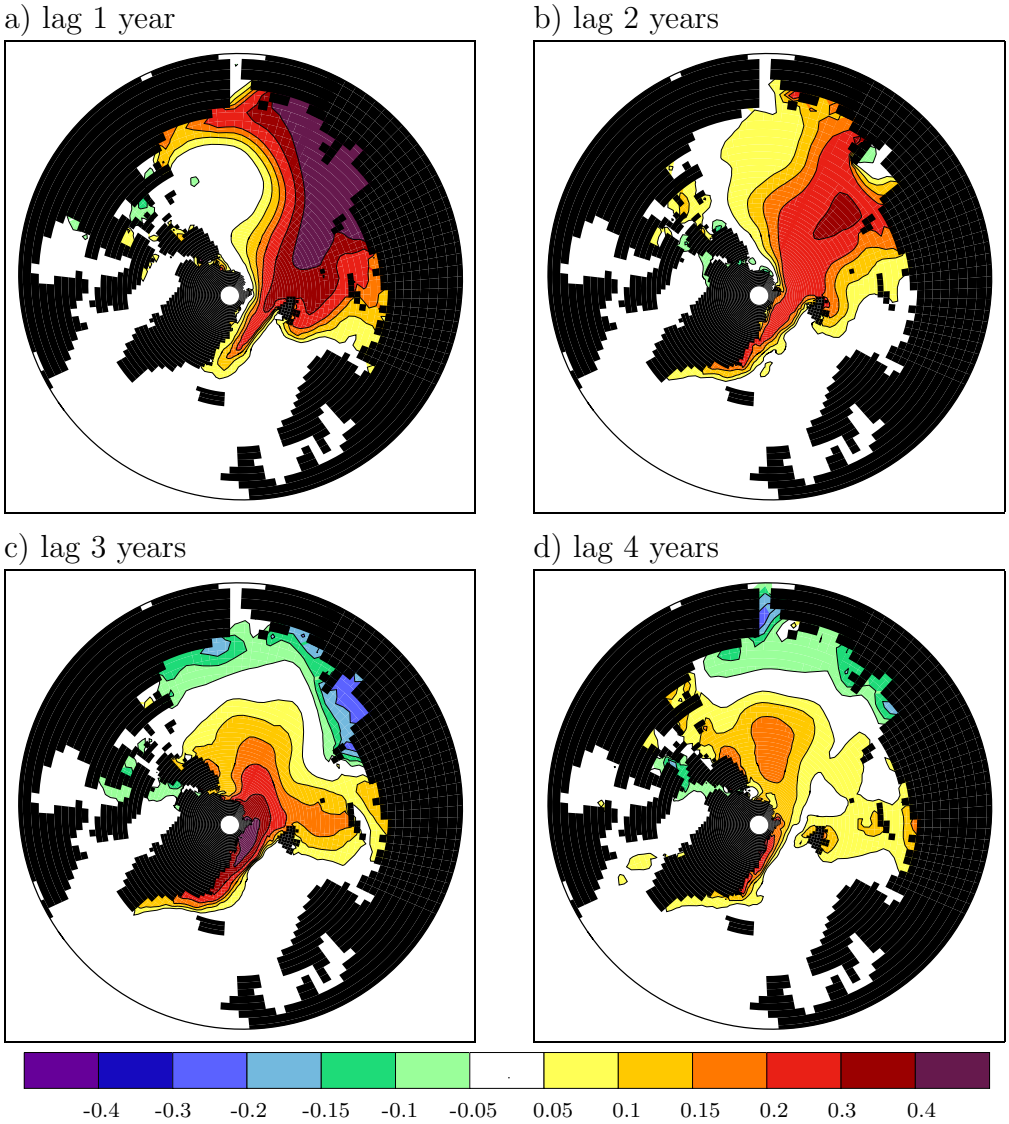

Figure 7.5: Annual mean sea ice thickness anomalies (in m) one to four years after addition of the ice thickness anomaly at the Siberian coast. Mean of the 20 ensemble runs.

summer and a slightly reduced surface salinity (fig. 7.4). Large positive salinity anomalies occur at the Siberian coast.
The impact on air temperature is shown in figure 7.3. Much cooler temperatures are obvious in the Barents Sea due to increased ice cover. They are also reduced over eastern Europe and parts of North America. Warmer temperatures occur in central Asia. These anomalies are only partly significant at the 95 % significance level and are mainly due to the anomalous wind field.

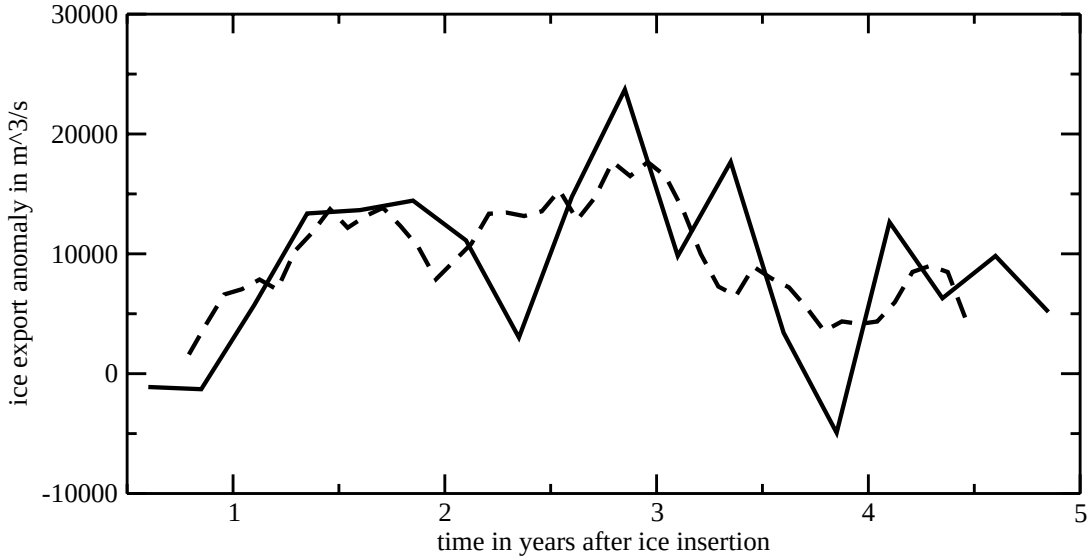

Figure 7.6: Anomalies of seasonal mean ice exports (in m^3/s) through the Fram Strait (solid) and 12 month running mean (dashed). Shown are the ensemble means of the first five years. The time axis starts with the summer season (JJA) in the year with the prescribed ice anomaly.

At a lag of two years, the negative SLP anomaly over the Siberian coast has weakened and shifted to the southeast. A positive pressure anomaly appears in the Central Arctic, in North America and particularly over southern Europe. The high SLP over southern Europe advects warm air from the Atlantic to the middle of Europe and northwestern Siberia. Advection of warm air from the Pacific leads to warmer temperatures over southern Alaska. The sea ice anomaly spreads over most parts of the Arctic while the amplitude becomes smaller. The center is situated in the eastern Central Arctic and the anomaly starts to loosen from the coast of the Laptev Sea. Ice thickness in Fram Strait keeps above the mean. Salinity in Barents Sea and at the ice border of Greenland Sea remains lower than usual.
One year later, significantly reduced SLP over the Kara and Laptev Seas strengthens the TDS, which leads to advection of the ice thickness anomaly into the Barents Sea and through Fram Strait into the Greenland Sea. In Fram Strait and Greenland Sea, the ice thickness is increased by up to 40 cm. Furthermore, the SLP distribution is associated with offshore winds at the Siberian coast. A negative ice thickness anomaly is consequently formed along the Siberian coast. This situation coincides well with the sea ice distribution during high ice exports through Fram Strait, as shown in the regression analysis between ice export and sea ice thickness (fig. 6.12) and in the lag EOF analysis of ice thickness (fig. 6.13 and 6.14). The SLP pattern which leads to the sea ice distribution at a lag

of three years is a response to the prescribed sea ice thickness anomaly at the Siberian coast. This suggest that the sea ice mode summarised in chapter 6.3. provides a weak feedback on the atmospheric circulation.
At a lag of four years, SLP is highly reduced in large parts of the Nordic Seas and the Arctic Basins. One maximum occurs at the coast of Kara and Laptev Seas and a second in the Greenland Sea and eastern Greenland. Increased SLP occurs in a semi-circle from western Europe over the North Atlantic and Canada to the northeastern Pacific. This coincides well to the situation two years after high ice exports (figure 5.9).
Salinity anomalies at lags of 3 and 4 years indicate the propagation of fresh water to the Labrador Sea, which is due to the enhanced ice export through Fram Strait. Convection weakens in the Labrador Sea and air temperatures are colder (fig. 7.3). A detailed description of this process has been given in chapter 5.
Figure 7.6 presents the ensemble mean of seasonal and 12-months running mean ice exports through Fram Strait. The largest positive anomalies occur from spring of the second year through winter of the third year as well as from summer of the third year through spring of the fourth year. The 12-months running mean ice export shows increased sea ice export over the entire 5-year period with largest exports three years after the prescribed ice volume anomaly at the Siberian coast. The sum of the anomalous ice export of the first five years amounts to 1260 km^3. This means that 63 % of the inserted ice volume leaves the Arctic through Fram Strait within 5 years. Because the ice export over the Barents Shelf into the North Atlantic is enhanced as well, one can conclude that the Arctic reaches its balance mainly by dynamical reduction of sea ice and subsequent melting in the northern North Atlantic.

7.2 Ice Anomaly in Fram Strait

In order to analyse the isolated impact of the ice/fresh water signal associated with high ice exports through Fram Strait, the effect of large ice exports is prescribed in EXP2. Additionally, it should be shown that the anomalies in the Labrador Sea after anomalous ice exports are largely independent from certain starting conditions in atmosphere and ocean. As initial conditions, twenty different years from the 500-year control run with about normal winter ice exports through Fram Strait are used. Each run starts at the beginning of May with a single anomalous ice volume input of 3000 km^3 into the EGC, south of Fram Strait (fig. 7.1). The amount of ice has been chosen according to the anomalous ice volume export through Fram Strait before the GSA in 70/71. Each simulation is run for five years.

Figure 7.7 shows seasonal mean (DJF, MAM, JJA, SON) surface (10 m) salinity and two meter air temperature anomalies in the central Labrador Sea in the first

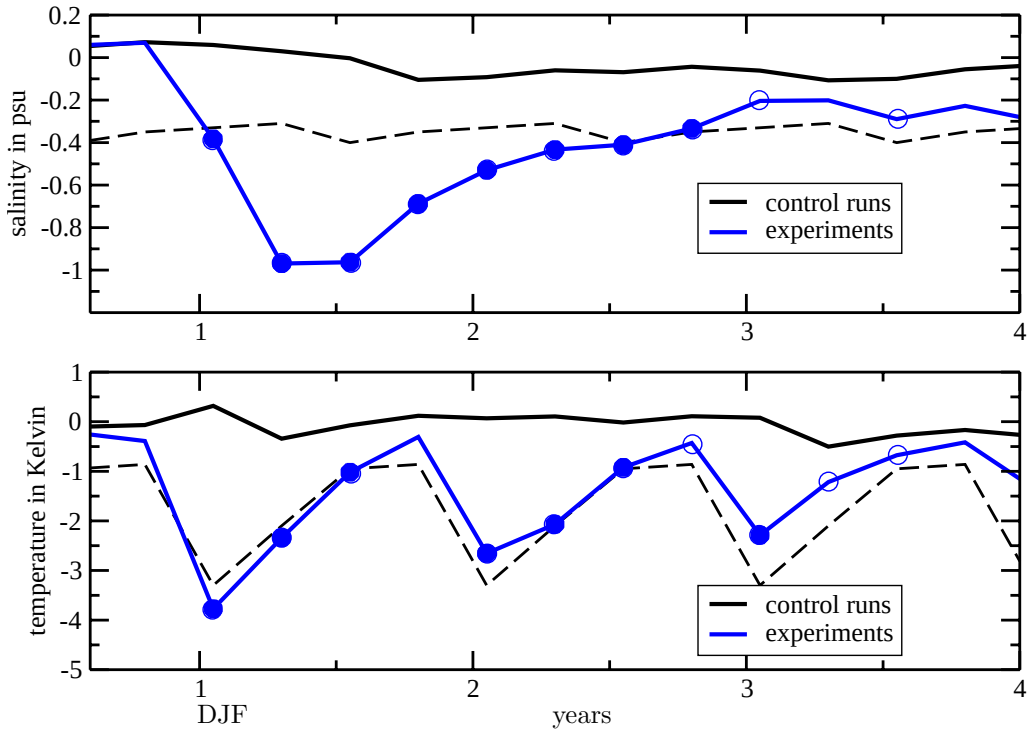

Figure 7.7: Seasonal mean 10m salinity (top, in psu) and 2m air temperature (bottom, in Kelvin) anomalies in the Labrador Sea. Means of the 20 experiment runs (blue) and the associated control runs (black). The dashed black line indicates minus one standard deviation of the 500-year control run. A blue cycle (filled blue cycle) indicates a significance at the 95 % (99 %) level. The time axis starts with the summer season (JJA) in the year with the prescribed ice anomaly.

four years after the prescribed ice export. Temperature and salinity are averaged over an area bounded by 54-60°N and 48-56°W. The anomalies describe the mean differences between the seasonal values of the 20 experiment runs and the 500-year control run just as for the associated 20 control runs. The standard deviations were calculated from the 500-year control integration as a quantity for the magnitude of the anomalies. The added ice melts while propagating southwards and reaches the Labrador Sea after approximately one year. Surface salinity (fig. 7.7, top) is reduced and reaches its minimum one and a half years from the export event. The salinity anomaly has a magnitude of more than two standard deviations. A two-sided student t-test shows that it is statistically highly significant. It takes four years until salinity is recovered. Observations of the GSA in the early 70's of the Ocean Weather Ship Bravo show similar surface salinity anomalies in the central Labrador Sea (e.g. Dickson et al. (1988); Lazier (1995)). The observations confirm that it took about four to five years to reinstall normal conditions.

But the propagation time of the fresh water anomaly from the Fram Strait to the Labrador Sea was about one year longer than usual in these model simulations. In idealised simulations of the GSA in a coupled ocean - sea ice model by Häkkinen (1999), surface salinity was decreased by -1 psu in the Labrador Sea in the second and third year after the ice export. This led to SST anomalies of up to -2.5 Kelvin.

In contrast to the salinity, the modelled temperature anomalies (fig. 7.7 bottom) show a pronounced seasonal cycle. Largest values occur in winter with up to four Kelvin in the first winter. Nevertheless, the temperature anomalies are highly significant in spring and summer as well. They are smallest during autumn and the significance is slightly weaker. Again, it takes four years to reinstall normal temperature conditions in the Labrador Sea.

The spatial distribution of annual mean values of sea ice thickness, surface salinity, 2m air temperature and SLP for lags of one to three years are shown in figures 7.8 to 7.11. One year after the prescribed ice export, ice thickness is largely increased along the east coast of Greenland. Additionally, a positive anomaly in the eastern Arctic and parts of the Barents Sea can be seen. A negative ice thickness anomaly is formed in the Chukchi Sea. A large amount of the ice inserted south of Fram Strait has already been melted and leads to a dramatic salinity deficit south of Denmark Strait and in the Labrador Sea. After two years, almost the entire prescribed ice volume has been melted. The associated salinity anomaly is centered in the Labrador Sea and extends southeastwards into the North Atlantic. It propagates zonally across the North Atlantic in the following year, while it weakens in the Labrador Sea. As described in chapter 5, the salinity deficit in the Labrador Sea leads to reduced oceanic convection. As a consequence, surface waters are colder and ice cover in the Labrador Sea is increased. The ocean heat release is reduced, which has a considerable impact on atmospheric conditions as well.
The spatial distribution of air temperature anomalies in the first three years after the simulated ice export shows by far the largest values in the area of the Labrador Sea (fig. 7.10). However, temperature is also significantly reduced in some other regions. Positive anomalies extend from the Ural Mountains to the Ochotsk Sea after one and three years. In contrast to the first and third year, advection of warm air to Siberia is reduced two years after the ice export. This might explain the lack of positive temperature anomaly in year two, but its existence in the years one and three. Positive anomalies statistically not significant at the 95 % level are apparent over parts of Europe after two and three years. A decrease in temperature occurs over the Gulf of Alaska and north of the Caspian and Black Seas after one year and over the Bering Sea and the Canadian Archipelago after two and three years. The temperature anomalies are mainly caused by changes in the wind field except for the one in the Labrador Sea. The associated variations of

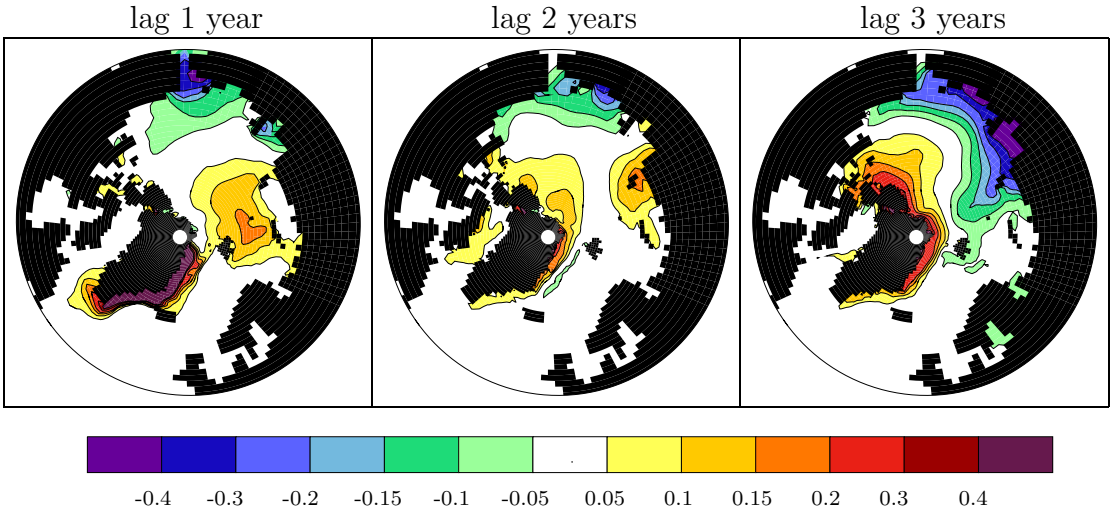

Figure 7.8: Annual mean sea ice thickness anomalies (in m) one to three years after the prescribed ice export through Fram Strait. Mean of the 20 ensemble runs.

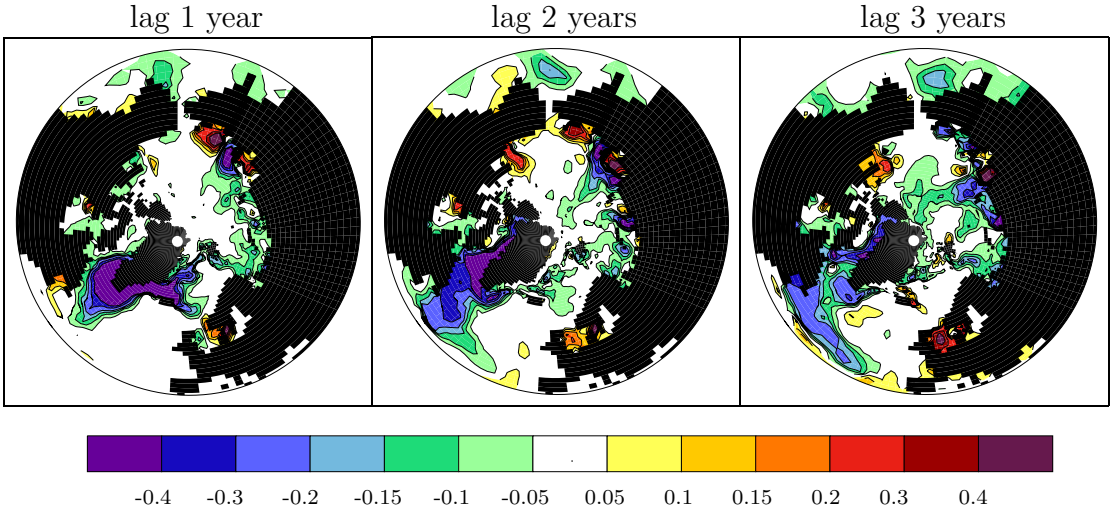

Figure 7.9: Annual mean 10 m salinity anomalies (in psu) one to three years after the prescribed ice export. Mean of the 20 ensemble runs.

the SLP-field are shown in figure 7.11. There are only small areas with significant changes one year after the ice export. Lower SLP than usual can be seen at the Siberian coast and east of Japan while SLP is increased over the Bering Sea. In the years with lag two and three, a positive pressure anomaly extends from the Labrador Sea across the Atlantic to the southwest of Europe. SLP is reduced further north over Scandinavia and the Nordic Seas. Thus, the SLP pattern

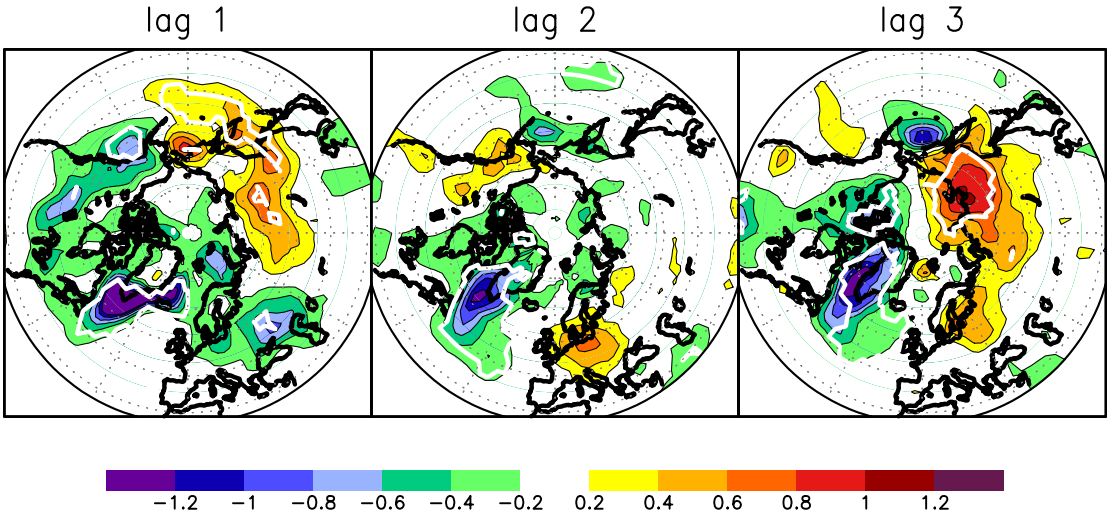

Figure 7.10: Annual mean 2m air temperature anomalies (in Kelvin) one to three years after the prescribed ice export. Mean of the 20 ensemble runs. The white line indicates the level of 95% significance.

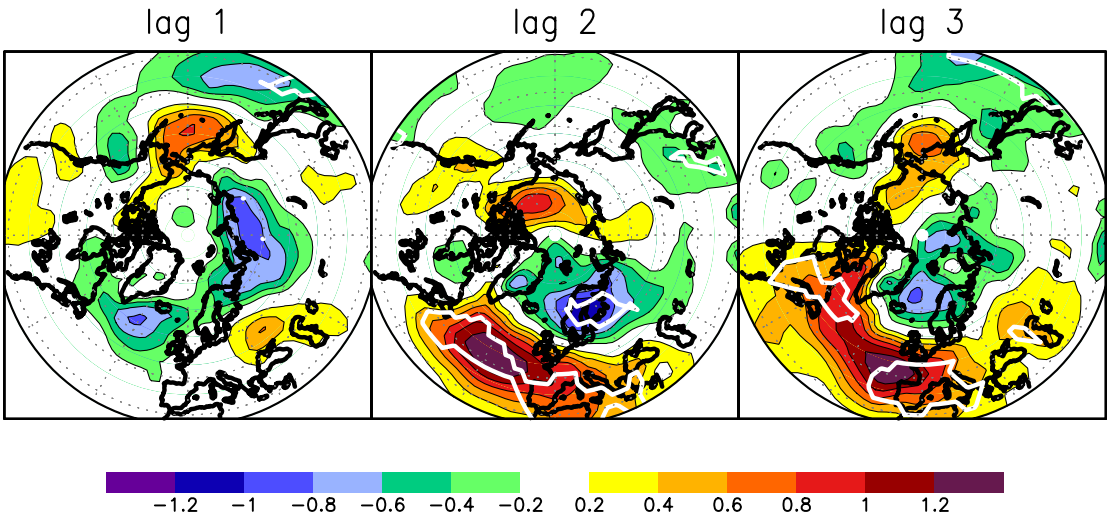

Figure 7.11: Annual mean SLP anomalies (in hPa) one to three years after the prescribed ice export. Mean of the 20 ensemble runs. The white line indicates the level of 95% significance.

is similar to the positive phase of the NAO. These results correspond to those obtained from both the control run and the run with NCEP-reanalysis.
Two and three years after the prescribed ice export, a pressure gradient across the Arctic with low pressure over the Nordic Seas and anomalous high pressure over the Chukchi Sea is formed. This amplifies the TDS which implies that more

ice is transported from the Siberian coast across the Arctic towards Greenland and Fram Strait. The negative ice thickness anomaly in the Chukchi Sea (fig. 7.8, left) strengthens and extends along the East Siberian coast to the Laptev Sea and into the eastern Central Arctic. Furthermore, increased sea ice thickness appears in the Greenland Sea, north of Greenland and the Canadian Archipelago. This leads to an enhanced ice export through Fram Strait in the model experiments after three years (fig. 7.12). The anomaly amounts to 0.5 standard deviation, which is significant at the 90 % significance level. The positive feedback from the inserted ice on the ice export in this model experiment matches well the three-year peak in the spectral analysis of the ice export in the control run. However, the control integration shows negative ice thickness anomalies three years after large ice exports as part of the decadal sea ice mode. One has to consider that the decadal mode is not permanently active. A wavelet analysis (not shown) of the ice export indicates that the three-year cycle shows only up then. Furthermore, it must be addressed that this experiment has not prescribed the negative ice anomaly at the Siberian coast associated with large ice exports. This may have an influence on the atmosphere as well. Thus, one cannot expect exactly the same response in the control run and the experiment.

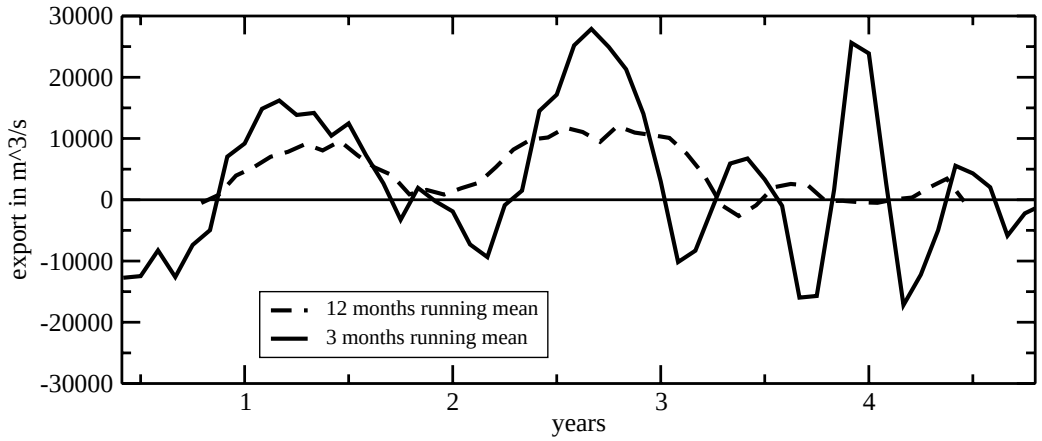

Figure 7.12: Fram Strait ice export (in m^3/s) in the first years after the prescribed ice anomaly. Mean of the 20 ensemble runs. The time axis starts with the summer season in the year with the prescribed ice anomaly.

7.3 Fresh Water Anomaly in the Labrador Sea

In the Labrador Sea, the atmospheric response is very sensitive to oceanic changes. To further investigate this sensitivity, a fresh water anomaly of 2000 km^3 in the Labrador Sea is prescribed in EXP3. Additionally, the argumentation above that the changes in convection and ocean heat release in the Labrador Sea are responsible for a considerable part of the large scale atmospheric response should be proved. The fresh water is added into the Labrador Sea by reducing the salinity of the upper three layers by 1, 0.5 and 0.25 psu in the area of EXP3 (fig. 7.1). Twenty runs are realised with initial conditions from 30th November of 20 different years. In all runs, initial salinity conditions are about normal in the Labrador Sea. The date has been chosen in order to cover the entire convection period in the Labrador Sea. Each simulation is run for 25 months.

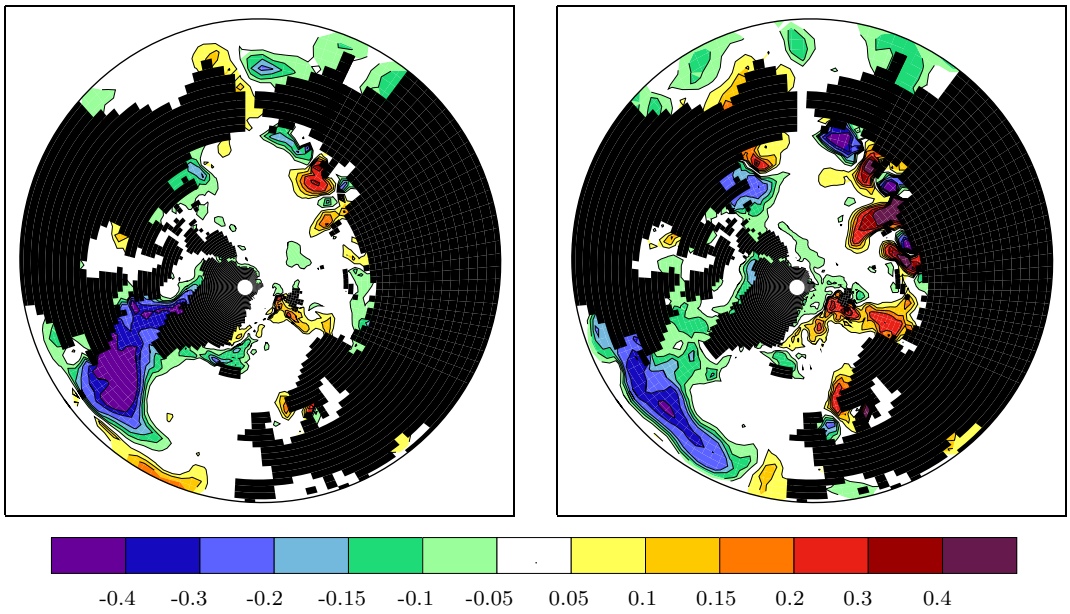

Figure 7.13: Annual mean 10 m salinity anomalies (in psu) in the first (left) and second (right) year after addition of the fresh water anomaly in the Labrador Sea. Mean of the 20 ensemble runs.

Figure 7.13 shows the propagation of the salinity anomaly in the first two years after the fresh water pulse. The annual mean has been calculated by averaging from January to December in this experiment. In the first year, the salinity anomaly spreads quite fast to the south and further to the east in the second year. Then the center of the anomaly extends zonally from the coast of Newfoundland across the Atlantic to the Azores. Salinity in the Labrador Sea remains below average. The salinity anomaly does not stay as long in the Labrador Sea as in the

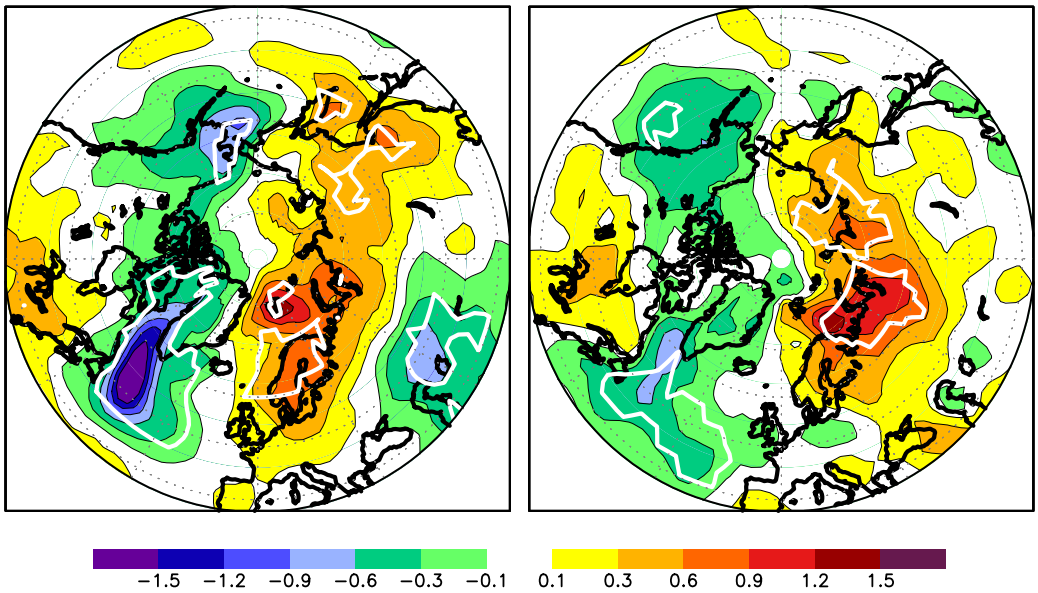

Figure 7.14: Annual mean 2m air temperature anomalies (in Kelvin) in the first (left) and second year (right) after addition of the fresh water anomaly in the Labrador Sea. Mean of the 20 ensemble runs. The white line indicates the level of 95% significance.

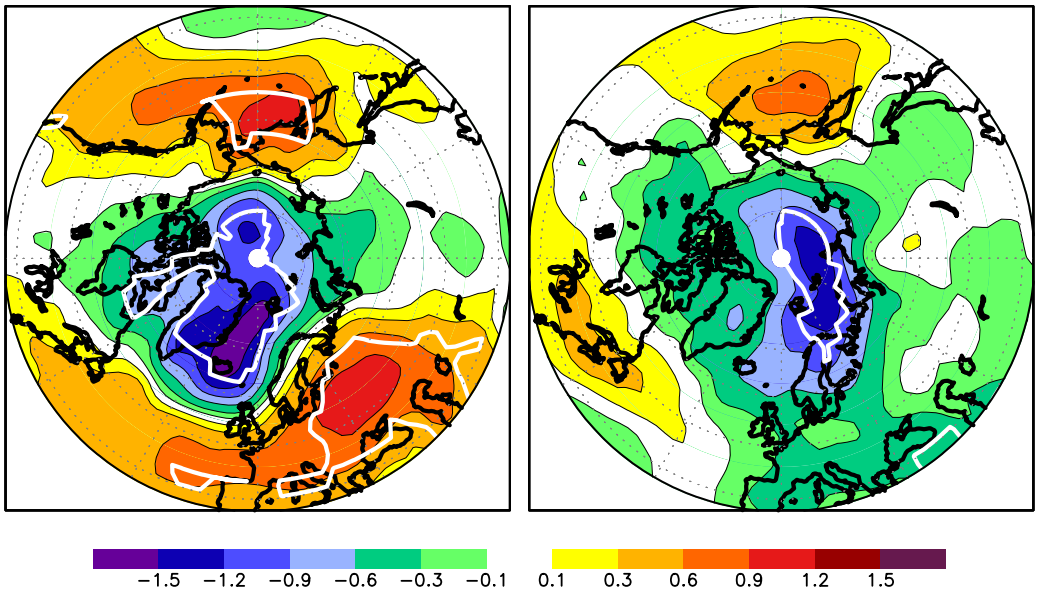

Figure 7.15: Annual mean SLP anomalies (in hPa) in the first (left) and second year (right) after addition of the fresh water anomaly in the Labrador Sea. Mean of the 20 ensemble runs. The white line indicates the level of 95% significance.

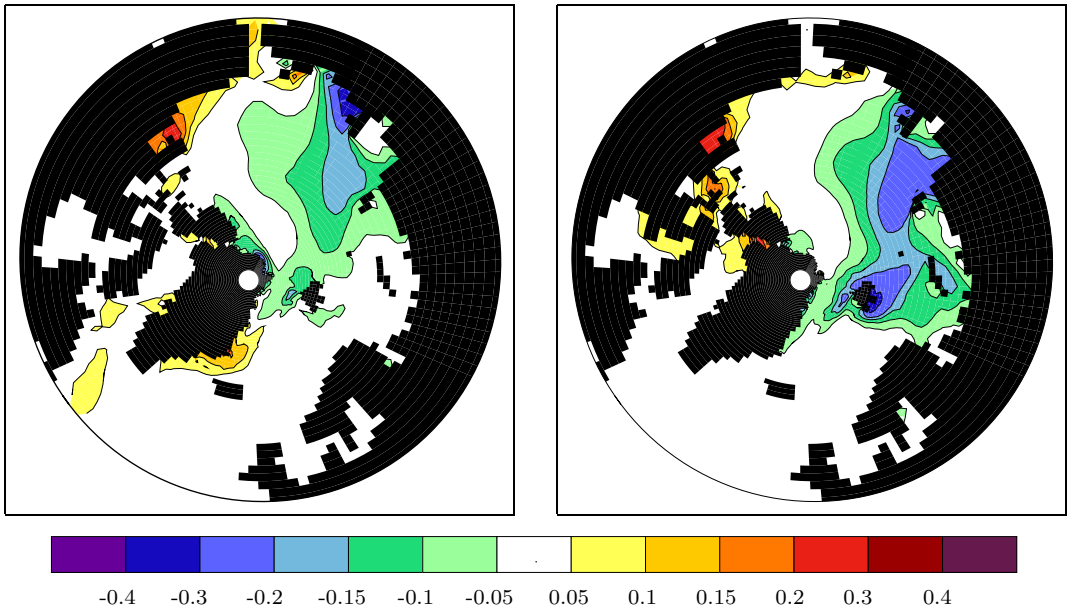

Figure 7.16: Annual mean sea ice thickness anomalies (in m) in the first (left) and second year (right) after addition of the fresh water anomaly in the Labrador Sea. Mean of the 20 ensemble runs.

other experiments and the control run. The reason is that only one strong fresh water impulse is given into the Labrador Sea in this experiment while inflow into the Labrador Sea spans over a certain time period in the other experiments. Nevertheless, temperature is decreased by up to 1.5 Kelvin in the Labrador Sea in the first year after the fresh water impulse (fig. 7.14). Other negative anomalies occur over Bering Strait and east of the Caspian Sea. The largest positive anomaly can be seen in the Barents Sea with more than 1.2 Kelvin. It is also warmer than usual in Scandinavia and most parts of northern Asia. In the second year, the distribution is similar but the negative anomaly in the Labrador Sea has weakened and no below normal temperatures occur at the Caspian Sea. The temperature variations can again be linked to the SLP response to the fresh water impulse (fig. 7.15). In the first year, SLP is significantly reduced by up to -1.5 hPa over the Nordic Seas and parts of the Arctic Basin. SLP increases by slightly more than 1 hPa over Europe and the Bering Sea. The anomalous SLP gradient between Europe and the Nordic Seas advects warm air from the Atlantic Ocean to Scandinavia, Barents Sea and western Siberia. The cold temperatures at the Caspian Sea can be explained by the advection of cold air from the north at the east side of the European high. Higher pressure over the Bering Sea than normal leads to anomalous advection of warm air masses from the Pacific to the eastern part of Asia. In combination with unusually low SLP over the Arctic, cold air is transported to the Bering Strait. In the second year, the negative anomaly

over the Nordic Seas and the Arctic Basin has slightly shifted with its center to the Kara Sea, while the positive SLP anomaly over Europe has disappeared. So decreased temperatures do not occur at the Caspian Sea any longer.

Results of the control integration and EXP2 have shown that a sea ice/fresh water signal reaches the Labrador Sea one to two years after it has passed Fram Strait. Therefore, one has to compare the results of the first year in this experiment with results for a lag of 2 years after large export events in the control run and EXP2, and a lag of 4 years in EXP1. The atmospheric response to the fresh water input in this experiment shows the main features of the atmospheric response in the control run and EXP1 and EXP2. There are differences in detail, but the negative SLP-anomaly over the Nordic Seas and parts of the European Arctic is well reproduced. The anomalous high pressure over the North Atlantic and parts of Europe can be seen as well, although the center in EXP3 is shifted towards Central and Eastern Europe. The increased SLP over the Bering Strait and the North Pacific are also partly captured in EXP1 (fourth year after prescribed ice anomaly at the Siberian coast) and EXP2. However, the composite analysis of SLP after high ice exports in the control run does not show the SLP anomaly over the North Pacific. This indicates that other processes than the ice export must have some impact on the atmospheric circulation. A possible source is the negative sea ice thickness anomaly at the Siberian coast that occurs during high ice exports through Fram Strait.

As air temperature is highly dependent on the atmospheric circulation, temperature anomalies in the different experiments show similarities as well. Thus, one can conclude that an important part of the atmospheric response to Fram Strait ice export variations is indeed due to the fresh water input into the Labrador Sea and the associated processes of decreased convection, enhanced sea ice cover and reduced ocean heat release.
Sea ice thickness also responds to the fresh water anomaly in the Labrador Sea (fig. 7.16). In the first year, a negative anomaly is formed at the coast of Laptev and Kara Seas and extends far into the eastern Central Arctic. This is caused by anomalous winds which lead to an ice transport from this area to the Chukchi and Beaufort Sea. Ice thickness is increased there. Slightly thicker ice can also be found at the east coast of Greenland and in the Labrador Sea. In the second year, the negative ice thickness anomaly in the Laptev Sea spreads across the Arctic towards Barents Sea and Fram Strait. This coincides with results of the control run and EXP2: the SLP response to the fresh water input into Labrador Sea is responsible for the formation of thinner ice than normal at the Siberian coast, which subsequently propagates across the Arctic towards Fram Strait.

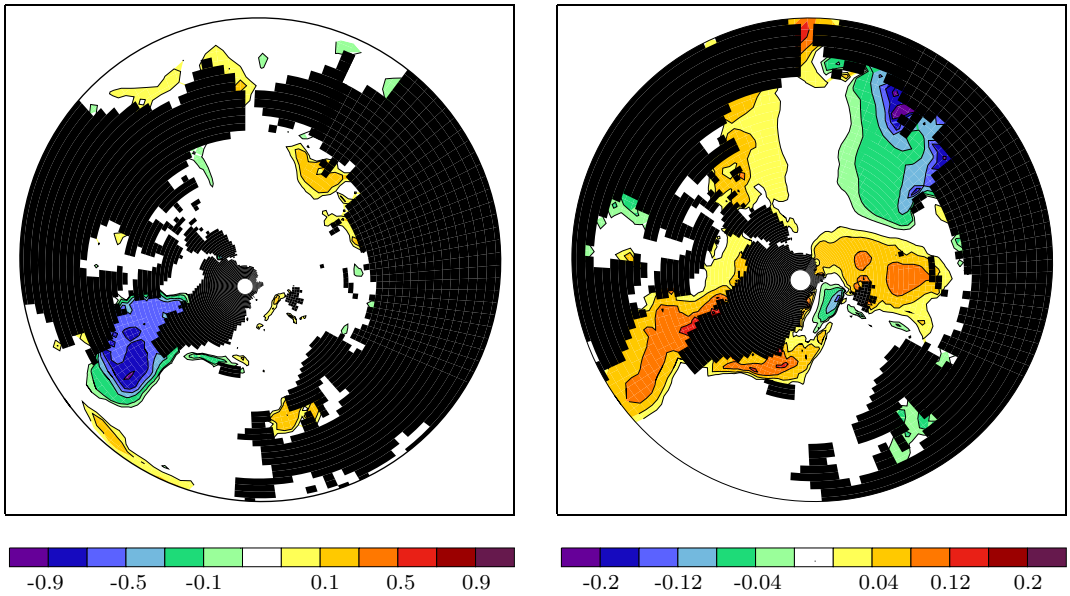

Figure 7.17: Salinity anomaly (left, in psu) and sea ice thickness anomaly (right, in m) in the first winter season (DJF) after addition of the fresh water anomaly in the Labrador Sea. Mean of the 20 ensemble runs.

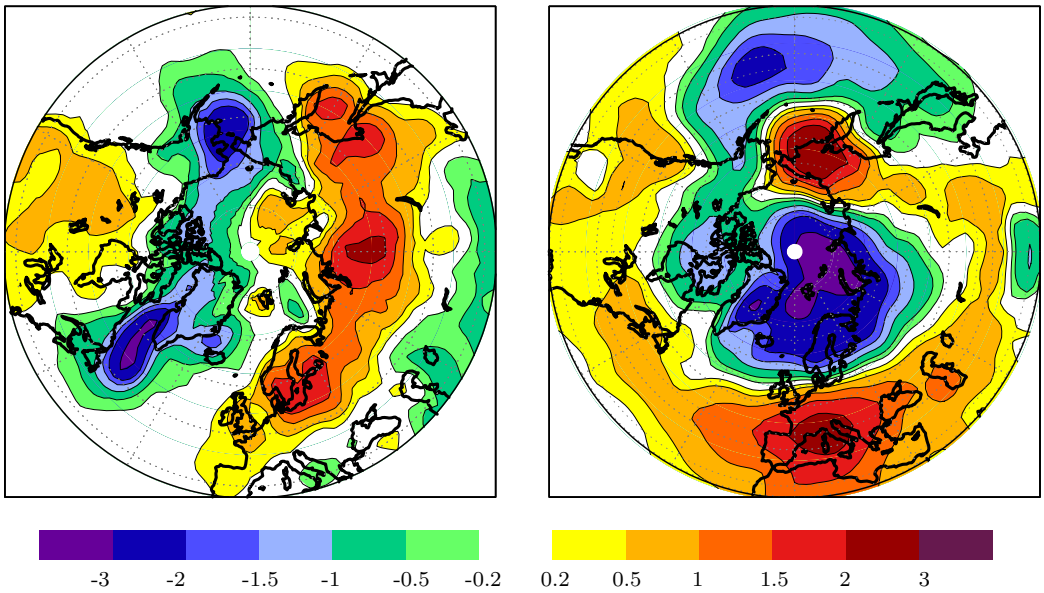

Figure 7.18: 2m temperature anomaly (left, in Kelvin) and SLP anomaly (right, in hPa) in the first winter season (DJF) after addition of the fresh water anomaly in the Labrador Sea. Mean of the 20 ensemble runs.

To determine the climate response to the fresh water input on shorter time scales, the first three months (DJF) thereafter are analysed. The salinity (fig. 7.17, left) is characterised by the prescribed negative signal in the Labrador Sea. However, the anomaly has already spread to the north and south and slightly weakened. Enhanced salinity occurs also in the Laptev Sea and in the North Sea. The ice thickness increases by up to 12 cm in the Labrador Sea (fig. 7.17, right). The fresh water anomaly reduces convection maintaining a colder and fresher surface which can freeze more easily. Ice in Barents Sea and Denmark Strait is thicker as well while ice thickness in the Laptev and East Siberian Seas is reduced by up to 20 cm. Already in the first months after the prescribed anomaly, the typical SLP pattern can be seen (fig. 7.18, right). A sequence of SLP anomalies occurs with positive centers over central and southern Europe as well as over northeastern Asia and Bering Strait. Negative anomalies occur over the Nordic Seas, Scandinavia and the European Arctic as well as over the northern Pacific. The SLP distribution over the North Atlantic/European sector shows similarities with both the NAO pattern and the SENA pattern (southern Europe - northern Atlantic pattern) while the Pacific sector is dominated by the Bering Sea pattern. A detailed description of the leading SLP pattern in the northern hemisphere is presented by Rogers (1990). The air temperature (fig. 7.18 a)) is increased from Scandinavia over Asia to Kamschatka by up to 3 Kelvin. Parts of North America are warmer than usual as well. Colder temperatures can be seen in the Bering Sea and at the Caspian Sea with a reduction of -3 Kelvin and -1 Kelvin, respectively. The largest deviation occurs over the Labrador Sea with more than -3 Kelvin and is only to a small fraction of advective nature.

7.3.1 Atmospheric Response to GSA's in an AGCM

A sensitivity experiment with the atmosphere model ECHAM5 has been carried out to determine the uncoupled atmospheric response to GSA's. A daily climatology from the 500-year control run of the coupled model of sea surface temperature, sea ice concentration and thickness is used to perform a 20-year control run of the atmosphere model. Additionally, a 20-year experiment run has been performed. The daily climatology of the three forcing parameters has been replaced in the Labrador Sea (area of EXP3 including 4 grid points to the south and east), Davis Strait and Baffin Bay by daily sea surface temperature, sea ice concentration and thickness associated to negative salinity anomalies in the Labrador Sea exceeding minus one standard deviation. Since the ocean is prescribed by climatology, the SLP response to the GSA-signal includes no feedbacks between ocean and atmosphere (fig. 7.19).
The pattern is characterised by positive SLP anomalies over the North Pacific Ocean and over Scandinavia and a negative anomaly centred over Greenland, which extends across the Arctic to Siberia. Obviously, this SLP distribution

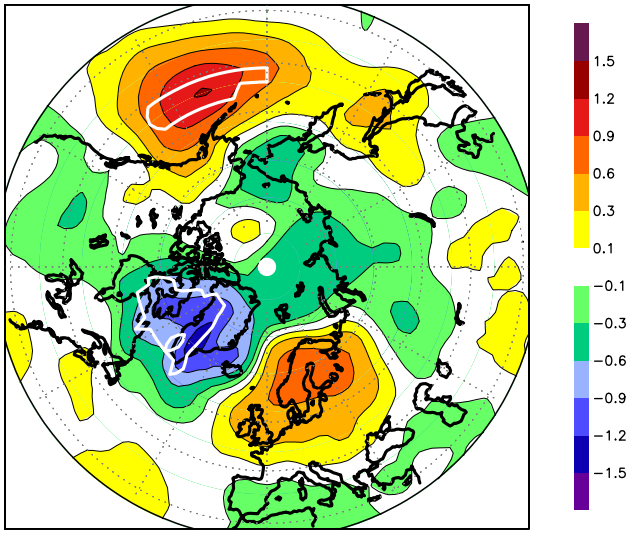

Figure 7.19: Mean SLP difference in hPa of the 20-year GSA-forced run and the 20-year, climatology-forced, control run. The white line indicates the level of 95% significance.

is very similar to the one in EXP3 one year after the prescribed fresh water input into the Labrador Sea (fig. 7.15, left). Both the negative anomaly over Greenland and the positive anomaly over Scandinavia are slightly shifted to the west in the atmosphere-only experiment. Moreover, the increased SLP over the North Atlantic is not reproduced. Apart from this, the atmospheric SLP response in this experiment covers large parts of the coupled response to the GSA-forcing in EXP3.

8 Predictability of Labrador Sea Climate

In the sensitivity studies, it has been demonstrated that the isolated effect of the ice/fresh water signal after extreme ice exports through Fram Strait accounts for a considerable fraction of climate variability in the Labrador Sea. In this chapter, we will explore the potential use of Fram Strait sea ice export as predictor for Labrador Sea climate. The predictability is analysed for seasonal and annual mean values of 10 m salinity and 2 m air temperature in the 500-year control integration.

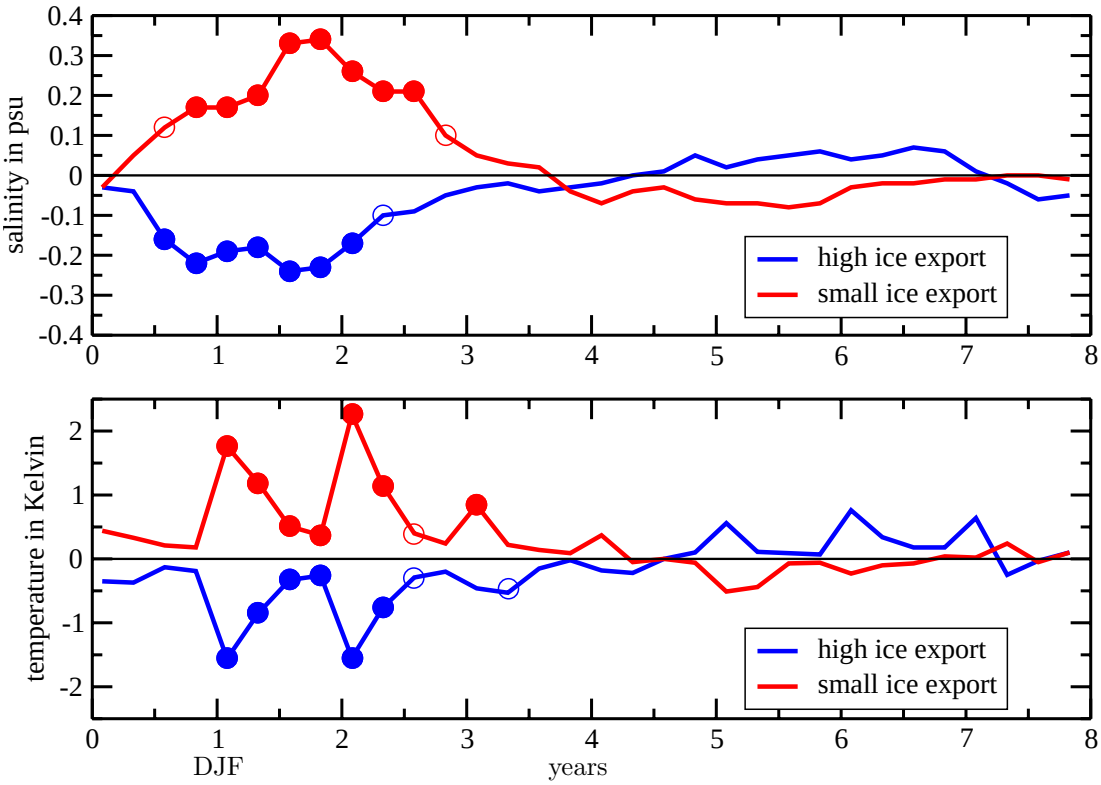

Figure 8.1: Seasonal means of 10m salinity (top, in psu) and 2m air temperature (bottom, in Kelvin) anomalies in the Labrador Sea in the first 8 years after high and low annual (August - July) ice exports through Fram Strait (mean +/- 1 standard deviation). The time axis starts with the winter season in the year of the ice export event. A cycle (filled cycle) indicates a significance at the 95 % (99 %) level.

Figure 8.1 shows seasonal averaged anomalies of the surface salinity and the 2m air temperature in the central Labrador Sea (54-60°N) in the first eight years after high and low ice exports through Fram Strait. 68 years (winter centred)

with high ice exports (exceeding the mean + 1 standard deviation) and 70 years with low ice exports (exceeding the mean - 1 standard deviation) are used. The time axis starts with the winter season in the year of the ice export event. A negative salinity anomaly occurs in the Labrador Sea half a year after high ice export events, which is fast compared to the normal propagation time from Fram Strait to the Labrador Sea in this model. The difference in travel time can be explained by enhanced exports in the year before the ice export event. Although the autocorrelation of the ice export through Fram Strait is small for a lag of one year (r=0.2), slightly more ice is transported through Fram Strait in the preceding and following year.
The salinity anomaly in the Labrador Sea intensifies in the next seasons and reaches -0.25 psu one year later. This anomaly is highly significant. It weakens thereafter and is no longer significant in the fourth year. A decadal variability of the ice export through Fram Strait has been identified in chapter 6. Thus, ice exports are small four to five years after positive anomalies, which lead to higher than normal salinity in the Labrador Sea in the fifth and sixth years.
Obviously, the fresh water signal needs slightly longer to reach the Labrador Sea after low than after large ice exports. Those are associated with northerly winds that accelerate the propagation of the fresh water signal to the south. Contrary anomalous southerly winds, associated with low exports, slow down the EGC. The salinity anomaly reaches its maximum with 0.35 one and a half to two years from low ice exports, and decreases afterwards. In the fourth through sixth years, salinity is lower than the mean due to increased ice exports.

The temperature is significantly colder in the second and third year after high and warmer after low ice exports. The largest anomalies occur in the winter seasons of the second and third year with -1.7 Kelvin and 2.3 Kelvin, respectively. Although they are much weaker in the other seasons, they are still highly significant because their standard deviations are also smaller. As well as salinity, temperature anomalies change sign after five years due to decreased ice exports. The anomalies reach up to 0.8 Kelvin in the winter seasons of year five and six. However, the significance does not exceed the 90 % significance level.

Apparently, the response of Labrador Sea climate to ice export anomalies is largest at a lag of one to two and a half years. Table 8.8 shows the statistical probability for annual mean salinity anomalies (winter centred) one and two years after high and low ice exports in the 500-year control integration. The cases of positive salinity anomalies ($S > 0$), anomalies larger than one standard deviation ($S > 1$), negative anomalies ($S < 0$) and anomalies exceeding minus one standard deviation ($S < -1$) are analysed. The mean distribution for all years of the control run is given for comparison. The probability for reduced salinity in the central Labrador Sea ($54 - 60°$N, $48 - 56°$W) after large ice ex-

	ice $> 1std$ lag 1 year	ice $> 1std$ lag 2 years	ice $< -1std$ lag 1 year	ice $< -1std$ lag 2 years	distr. all years
$S > 1$	4.4 (3.8)	4.4 (10.1)	35.3 (28.5)	37.1 (22.7)	12.0
$S > 0$	20.6 (23.4)	25.0 (32.3)	71.4 (76.8)	82.9 (61.4)	47.7
$S < 0$	79.4 (76.4)	75.0 (67.7)	28.6 (23.2)	17.1 (38.6)	52.3
$S < -1$	27.9 (22.6)	25.0 (19.3)	2.9 (3.3)	4.3 (6.8)	12.2

Table 8.8: Probability (in %) for positive and negative annual salinity anomalies (in standard deviations) in the Labrador Sea one and two years after large and low ice export events through Fram Strait. 68 years with large ice exports and 70 years with low ice exports are used. The probability of the negative and positive persistence is shown in brackets.

ports accounts to about three-fourths after one and two years. The probability for anomalies exceeding one standard deviation amounts to slightly more than one-fourths. Similar values are reached for positive salinity anomalies after low ice exports. In 50 of 70 cases of the first and in 58 cases of the second year a positive salinity anomaly occurs, whereas in 25 and 26 cases salinity is largely enhanced, respectively.
For comparison the persistence of the salinity in the Labrador Sea in the first and second year after ice export events is calculated. It indicates for the one-year predictability of salinity similar values as the predictability using the ice export as predictor. For two years lead of the ice export, however, the predictability using the ice export clearly exceeds the persistence. The prediction for the salinity improves even more if only extreme ice export anomalies of more than one and a half or two standard deviations are used. Of course the number of years with the possibility for prediction is reduced then.

Table 8.9 presents the same quantities as table 8.8 for two meter air temperature. The predictability of temperature is slightly weaker than that of salinity. Probability values of about 70 % are reached for warmer (colder) temperatures than normal one and two years after low (large) ice export anomalies. However, the temperature persistence in the Labrador Sea is also slightly weaker than for salinity. Again, the prediction for two years in advance, using Fram Strait ice export as predictor, clearly exceeds the persistence. In contrast to the salinity, the predictability for air temperature only slightly improves with increasing ice export anomalies. An anomaly of one standard deviation seems to be sufficient to considerably reduce or even totally suppress Labrador Sea convection. A further increase of the fresh water input into the Labrador Sea cannot significantly

	ice $> 1std$ lag 1 year	ice $> 1std$ lag 2 years	ice $< -1std$ lag 1 year	ice $< -1std$ lag 2 years	distr. all years
$T > 1$	7.4 (6.3)	8.8 (12.6)	34.3 (29.8)	41.0 (22.6)	16.9
$T > 0$	29.5 (28.8)	30.9 (38.8)	70.0 (67.8)	70.0 (57.3)	48.2
$T < 0$	70.5 (71.2)	69.1 (61.2)	30.0 (32.2)	30.0 (42.7)	51.8
$T < -1$	26.4 (26.3)	25.0 (21.8)	7.1 (4.8)	8.6 (8.7)	16.5

Table 8.9: Same as table 8.8 but for 2 m air temperature after ice export events through Fram Strait.

enhance the heat flux to the atmosphere and hence the air temperature.
An investigation of the statistical probability of seasonal values one and two years after large and low ice exports shows similar results as for the entire year. The probability for temperature and salinity is in the range of 70 % and 80 % for all seasons, respectively. Thus, the impact of the ice export variability on climate is not limited to the winter season but is relevant for the entire year. Accordingly, the ice export through Fram Strait is a useful tool to improve the long-term predictability of the Labrador Sea climate.

9 Summary and Conclusions

The variability of the sea ice export through Fram Strait and related processes in the Arctic and North Atlantic have been studied by analysing a 500-year control integration of a global coupled atmosphere-ocean-sea ice model and by sensitivity studies.
A comparison of the simulated mean Arctic climate with observations and reanalyses indicated that the model provides a realistic mean climate state. Furthermore, the simulated variability captured a large part of the observed climate variations. The model turned out to be a useful tool to study Arctic climate variability.

The simulated ice transport is divergent in almost the entire Arctic Basin and convergent at the ice edges in the North Atlantic and North Pacific. This means that a net ice formation occurs in the Arctic Basin (up to 70 cm/year in the Kara Sea) while more ice is melted than formed in the Greenland, Barents, Labrador and Bering Seas. The ice volume both of the entire Arctic Basin and its sub regions shows high variability. The temporal ice volume change on shorter time scales is mainly determined by the dynamics of the ice transport while thermodynamic processes are dominant on a multi-decadal time scale.

The Fram Strait constitutes the main passage for sea ice out of the Arctic. The simulated annual mean ice export reaches about 100000 m^3/s with a standard deviation of 21000 m^3/s. Thus, the ice is responsible for 70 % of the total fresh water export through Fram Strait which accounts to 140000 m^3/s. Furthermore, the interannual variability of the total fresh water export through Fram Strait is governed by the ice export variability. However, it should be noted that the variability of the liquid fresh water flux becomes important on longer time scales.

After high ice export events, the associated ice/fresh water signal propagates southwards in the East Greenland Current, melts and enters as cold, fresh water the Labrador Sea. This input forms a large negative salinity anomaly one to two years after high ice exports. As a consequence, oceanic deep convection is reduced or even totally suppressed, which prevents a fast recovery of salinity in the Labrador Sea. In the coupled model used in this study, the sea ice export through Fram Strait is the main source for the formation of salinity anomalies in the Labrador Sea, which agrees well with results of Haak et al. (2003) and Häkkinen (1999). However, anomalous fresh water transports across the other three boundaries of the Labrador Sea as well as local processes contribute to the salinity anomalies. Although the knowledge of the amount of ice exported through the Canadian Archipelago is poor (H. Melling, pers. communication), it should be addressed that it seems to be underestimated in this model. Thus, it

cannot be ruled out that its impact on the variation of salinity in the Labrador Sea is also slightly underestimated.
The cold and fresh water anomaly in the Labrador Sea after large ice exports leads to an increase in sea ice concentration and thus to a reduction of the ocean heat release. This has a considerable impact on the atmospheric climate. Air temperatures in the Labrador Sea are significantly colder and even the large scale atmospheric circulation is influenced. Positive SLP anomalies occur over the North Atlantic and parts of Europe whereas SLP is reduced over the Nordic Seas. Although SLP anomalies are rather small at up to 0.6 hPa, a comparison with NCEP/NCAR-reanalysis shows that the pattern seems to be quite robust. After low ice exports, the entire process proceeds symmetrically.

Analyses of the variability of the ice export through Fram Strait confirm results of Kwok and Rothrock (1999) that almost 80 % of the ice export variability can be explained by the SLP gradient across Fram Strait. The NAO shows no significant influence on the SLP gradient in this study. This is in good agreement with the assumption that the recently observed high correlation between NAO-index and ice export through Fram Strait is due to an unusual state of the NAO (Jung and Hilmer, 2001). Nevertheless, a considerable influence of the large scale atmospheric circulation on the ice export could be assessed. In contrary to the NAO, the first zonal wave of SLP, averaged meridional over 70° to 80° N, is closely related to the ice export through Fram Strait. The phase of the first wave is determined by the position of the extensions of the Iceland Low and the Siberian High into the Arctic. According to Cavalieri and Häkkinen (2001), a shift of the phase to the east leads to an increased SLP gradient across Fram Strait in winter. A new index (WI1) has been defined in this study, combining the phase and amplitude of the first planetary wave between 70 and 80°N. The WI1 is significantly correlated with the ice export year-round with the highest correlation in winter. Moreover, the entire ice transport in the Arctic Basin is affected by variations of WI1. The first zonal wave turned out to be very important for climate variability in the entire Arctic. It is therefore essential to further analyse the processes determining its variability.
The stratospheric polar vortex has been identified as another source of Fram Strait ice export variability. During strong polar vortexes, both the SLP gradient across Fram Strait and the ice export are enhanced and vice versa during weak vortex regimes.
However, large scale atmospheric modes cannot explain the entire variability of the SLP gradient. A considerable part of the variation is due to regional processes in the Fram Strait area. This confirms results of Mikolajewicz et al. (submitted), who used a regional coupled model for the Arctic and split the variability into a regionally generated part and a part predefined by the lateral boundary forcing.

In spite of the close relationship between atmospheric forcing and sea ice export through Fram Strait, the atmospheric variability cannot fully explain the 9-year peak in the ice export. This study has presented a sea ice mode on a decadal time scale. It is characterised by the propagation of ice thickness anomalies within the Arctic Basin and leads to decadal ice export variability through Fram Strait. The mechanism of the mode is as follows: onshore winds form an ice thickness anomaly at the coasts of the Siberian and Chukchi Seas. This anomaly propagates with the mean ice drift along the Siberian coast to the west and crosses the Arctic in the TDS. It reaches Fram Strait four to five years after the formation and increases the ice export. The mode develops particularly well if atmospheric forcing strengthens the propagation of the ice anomaly. A combined EOF-analysis of sea ice thickness and SLP as well as a sensitivity study (EXP1) prescribing ice thickness anomalies at the Siberian coast indicate a weak feedback of the ice anomaly on SLP, which tends to maintain the mode. However, the feedback signal is small compared to the atmospheric variability. Thus, the propagation time from the formation area to the Fram Strait and the amount of anomalous ice volume reaching Fram Strait can vary considerably. In the sensitivity experiment (EXP1), about two-thirds of the prescribed ice volume anomaly at the Siberian coast are anomalously exported through Fram Strait in the following years. Simultaneous to the increased ice export, negative ice thickness anomalies occur at the Siberian coast due to offshore winds during high ice exports. They take the same way to Fram Strait in another four to five years. The ice export anomalies provoke the process of GSA-formation in the Labrador Sea and associated impact on atmospheric and oceanic climate as described above.
Extreme ice export events are produced by a combination of ice thickness anomaly and increased northerly winds in Fram Strait. The formation of ice thickness anomalies at the Siberian coast can be regarded as preconditioning for ice export events through Fram Strait. In agreement to this, model simulations of Haak et al. (2003) indicated that the large sea ice export 1967/68 that led to the GSA 1970/71 in the Labrador Sea was preceded by an ice thickness anomaly at the Siberian coast.

Once the ice signal passed Fram Strait, it reaches the Labrador Sea after about one and a half years and creates a salinity anomaly in most cases. This process is nearly independent from the atmospheric and oceanic conditions. To deflect the ice/fresh water signal before it attains the Labrador Sea, extreme wind anomalies must arise. Sensitivity experiments, which have prescribed large ice exports through Fram Strait and used different atmospheric and oceanic initial conditions, have confirmed these results. The oceanic and atmospheric conditions at the time of the ice export are of minor importance for the climate response. The increased ocean heat release and the cold temperatures in the Labrador Sea which lead to an increased meridional temperature gradient across the Gulf Stream after strong

ice export events have been identified as the main source for SLP anomalies in the North Atlantic and Arctic (EXP3). The predominant part of these anomalies can be reproduced by atmospheric only experiments forced with GSA's in the Labrador Sea. Coupled processes are thus of minor importance for their formation.

Knowledge of the decadal sea ice mode provides a good framework for predictability. A considerable increase of high ice exports through Fram Strait occurs after previous ice thickness anomalies at the coast of the Laptev Sea. However, the predictability of Labrador Sea climate using the ice export through Fram Strait as predictor seems to be even more promising because the associated processes are less affected by the highly variable atmosphere. The statistical predictability of 10 m salinity and 2 meter air temperature after large ice export anomalies has been calculated. The prediction of the sign of the anomaly reaches 75 % to 80 % for the salinity and 70 % to 75 % for temperature, both one and two years after high and low ice exports. For a two years lead of the ice export, the predictability clearly exceeds that derived from the assumption of persistence of salinity and temperature anomalies in the Labrador Sea.

In the future, hindcast experiments, initialised with reanalysis and satellite data, should be used to analyse the skill of predictability that can be obtained for real cases. Unfortunately, ice thickness data are very poor and satellites still have problems measuring the ice thickness. So, strong efforts providing reliable ice thickness data would be desirable.
The model experiments performed in this study clearly suggest that the processes taking place in the Labrador Sea are important for the SLP distribution over the North Atlantic and the Arctic. Further work is necessary to understand the mechanisms of the impact on SLP more precisely. This may provide the possibility to extend the predictability on SLP on other regions as e.g. Europe at least for extreme ice exports. Moreover, it is essential to understand the Arctic impact on mid-latitude SLP in the context of a possible future climate change. Related to this is the question whether the processes, presented in this thesis, will occur in a warmer future climate as well.

A Methods

The long control integration of the coupled climate model provides an excellent possibility for the usage of statistical methods. In this chapter, the used methods are introduced with a focus on the sketch and the advantages and disadvantages of each of the methods. The description is not in full detail but a comprehensive list of references is given, which allows further reading on methodological details and applications in different areas of climate research.

A.1 Spectral Analysis

The spectral analysis is a method to study the temporal variability of a time series. Both deterministic and stochastic processes can be characterised by a function of frequency f. This function $S(f)$ is called the power spectrum of the time series. A very irregular motion possesses a smooth and continuous spectrum, which indicates that all the frequencies in a given band are excited by such a process. On the other hand a purely periodic or quasiperiodic process is described by a single line or a number of lines in the frequency domain. Between these two extremes, processes can have spectral peaks superimposed on a continuous and wiggly background. Estimating the spectrum of $X(t) : t = 1, ...N$ by a discrete Fourier transform yields its periodogram, which is the Fourier transform squared:

$$\hat{S}_x(f) = \frac{\Delta t}{N} \mid \sum_{t=1}^{N} X(t) e^{-2\Pi i f t \Delta t} \mid^2 \tag{1.1}$$

There are several different approaches to reduce the estimate's bias and variance and attenuate the leakage effects of the periodogram. Often a lag window $(W_\mu(k) : k = -(N-1), ..., N-1)$ is used with a smoothing parameter μ. An example of such a window is the Bartlett window:

$$W_\mu(k) = 1 - \frac{|k|}{\mu} \tag{1.2}$$

The power spectrum estimate then becomes

$$\bar{S}_x(f) = \sum_{k=-(N-1)}^{N-1} W_\mu(k) \hat{\Phi}_x(k) e^{-2\Pi i f k} \tag{1.3}$$

with the Fourier transform of the autocorrelation function Φ_x. The windows traditionally have a compact support of length $m < N$, so that 1.3 becomes, with $\mu = m$,

$$\bar{S}_x(f) = \sum_{k=-(m-1)}^{m-1} W_m(k) \hat{\Phi}_x(k) e^{-2\Pi i f k} \tag{1.4}$$

m is called the truncation point or window width. It turned out that this method is quite efficient for estimating the continuous part of the spectrum, but it is less useful for the detection of components of the signal, which are purely sinusoidal or nearly so. Other methods for instance the multitaper method (MTM) or the maximum entropy method show an improvement by removing the noise. A description in detail of these methods is given in Ghil et al. (2002).

A.2 Regression and Correlation Analysis

The correlation analysis is used to analyse the quality of the linear relationship of several data sets. A vector series $\mathbf{y_t}$ (e.g., anomalous SLP or temperature fields) is related to an index x_t (e.g., NAO index):

$$\mathbf{y_t} = \mathbf{q}\overline{x}_t + noise \tag{1.5}$$

$\mathbf{y_t}$ represents anomalies, and $\overline{x}_t$ is a normalised index of x_t

$$\overline{x}_t = \frac{(x_t - \mu_x)}{\sigma_x} \tag{1.6}$$

with the average μ_x and the standard deviation σ_x of the index x_t. The normalisation of x_t ensures that the regression pattern $\mathbf{q}$ has the same units as $\mathbf{y_t}$. This means that $\mathbf{y_t}$ refers to one standard deviation of x_t.
To estimate the pattern $\mathbf{q}$ from the data, the mean square error has to be minimised. This leads to (von Storch and Zwiers, 1999)

$$q_i = \frac{1}{N-1}\sum_{t=1}^{N}\overline{x}_t y_{it}, \qquad i = 1, ..., L, \tag{1.7}$$

where L gives the number of components (grid points) of $\mathbf{y_t}$. Therefore regression patterns are estimated from the covariance between the normalised index x_t and anomalies of $\mathbf{y_t}$ at each grid point. If $\mathbf{y_t}$ is normalised at each grid point prior to the analysis, then the correlation pattern is obtained. For correlation/regression of two time series, the vector series $\mathbf{y_t}$ contains only one component and is therefore scalar.
The significance of the correlation/regression can be easily assessed by using standard tests for each grid point (von Storch and Zwiers, 1999). In this study, a correlation/regression is called significant if the level of significance reaches 95 % or more.
Care has to be taken by the interpretation of the correlation coefficient. It provides only a statistical relationship between two variables and not a physical one. Often it is influenced by other variables.
In this study, lag correlations and regressions are applied, as well, with the aim to detect the response of one variable on another after certain time periods. This is done by computing the linear relationship between the index x_t and the anomalies of $\mathbf{y_{t+dt}}$ where dt can be any time interval.

A.3 Composite Analysis

A composite analysis is a useful approach to determine the typical pattern $\mathbf{y_K}$ of the vector series $\mathbf{y_t}$ for a subset K of the index x_t:

$$\mathbf{y_K} = \frac{1}{N} \sum_{t \epsilon K} \mathbf{y_t} \tag{1.8}$$

N is the number of events meeting the criterion that is used to form K. $\mathbf{y_K}$ is called the composite pattern. Typically, all events with $x_t \geq \sigma_x$ or $x_t \leq -\sigma_x$ are used to define K. This criterion has been applied in most of the used composite patterns in this thesis. An advantage of the composite patterns approach over the regression pattern approach is that no assumption about the relationship between $\mathbf{y_t}$ and x_t is associated with the composite analysis. Therefore nonlinear relationships can be detected as well. Such a successful detection of a nonlinear relationship with a composite pattern analysis is presented by Hoerling et al. (1997) for El Niño, La Niña, and their teleconnections. A disadvantage of the composite analysis arises from the subjective choice of the subset K.
Because Eqn. 1.8 is an estimate for the mean, the significance of the pattern $\mathbf{y_K}$ can be calculated applying a Student's t-test (von Storch and Zwiers, 1999).
In this study, the composite analysis is mainly used to investigate the response of different variables to extreme events, for instance the response to large anomalies in the ice export through Fram Strait.

A.4 EOF Analysis

Empirical orthogonal function (EOF) analysis is a technique to study the spatial and temporal variability of a vector series $\mathbf{x_t}$. $\mathbf{x_t}$ can be written in a matrix form as $\mathbf{X}$ (with temporal anomalies in its columns). Since EOF analysis is well-known and widely used, only its essentials are discussed along with potential pitfalls. A detailed introduction is given, for instance, by von Storch (1995) and von Storch and Zwiers (1999).
The first EOF $\mathbf{e^1}$ of $\mathbf{X}$ is the pattern (with $||\mathbf{e^1}|| = 1$) whose associated principal component (PC) $\alpha_t^1 = \mathbf{X e^1}$ is the linear combination of elements of $\mathbf{X}$ explaining the largest amount of variance. The second EOF $\mathbf{e^2}$ (which is orthogonal to the first EOF) provides the second PC α_t^2 explaining the largest amount of variance under the constraint of zero correlation with the first PC, and so forth. The EOF's are obtained by diagonalizing the cross-covariance matrix $\mathbf{X^T X}$.
Since EOF analysis is an eigenvalues problem, the EOF's may be subject of degeneracy. North et al. (1982) illustrate this problem using synthetic data. Moreover, they provide a rule-of-thump, which allows to assess whether subsequent EOF's are mixed.
Care has to be taken with respect to the interpretation of EOF's. If the EOF's

are based on the cross-covariance matrix, then the patterns are constructed to maximise spatial covariance and not spatial coherence (correlation). Dominant patterns of spatial correlation can be obtained by normalizing $\mathbf{X}$ to unit variance prior to the decomposition, that is, by diagonalising the cross-correlation matrix (Wallace and Gutzler, 1981). Examples illustrating the difference between spatial patterns of covariance and correlation are given, for instance, by Richman (1986). To detect the maximised covariance for a given vector series at the times t and t+1 lagged EOF's are used. Thus, the vector series $\mathbf{x_t}$ is enlarged by $\mathbf{x_{t+1}}$ to a vector series $\mathbf{x_t^n}$. The resulting pattern has to be split into a pattern for t and t+1. A lag EOF analysis can be computed for any number of time steps giving the possibility to obtain a temporal continuous pattern.

B Abbreviations

AGCM	Atmosperic General Circulation Model
AMIP	Atmosphere Model Intercomparison Project
AO	Arctic Oscillation
DJF	December, January, February
EGC	East Greenland Current
EOF	Empirical Orthogonal Function
GSA	Great Salinity Anomaly
JJA	June, July, August
MAM	March, April, May
MOC	Meridional Overturning Circulation
NAO	North Atlantic Oscillation
NCAR	National Center for Atmospheric Research
NCEP	National Center for Environment Prediction
OAGCM	Ocean-Atmosphere General Circulation Model
PHC	Polar Science Center Hydrographic Climatology
PC	Principal Component
SLP	Sea Level Pressure
SON	September, October, November
SST	Sea Surface Temperature
TDS	Transpolar Drift Stream
WI1	Wave Index 1

List of Figures

List of Tables

References

Aagaard, K. and E. Carmack, 1989: The role of sea ice and other fresh water in the Arctic circulation. *J. Geophys. Res.*, **94**, 14485–14498.

Alekseev, G., V. Ivanov, and A. Korablev, 1994: Interannual variability of the thermohaline structure in the convective gyre of the Greenland Sea. *in: The Polar Oceans and their role in Shaping Global Environment, edited by O.M. Johannessen, R.D. Muench and J.E. Overland, Monograph 85, Amer. Geophys. U.*, pp. 199–209.

Alexander, M., U. Bhatt, J. Walsh, M. Timlin, J. Miller, and J. Scott, 2004: The atmospheric response to realistic Arctic sea ice anomalies in an AGCM during winter. *J. Climate*, **17**, 890–905.

Antonov, J., S. Levitus, T. Boyer, M. Conkright, T. O'Brien, and C. Stephens, 1998: World Ocean Atlas 1998 Vol.1: Temperature of the Atlantic Ocean. *NOAA Atlas NESDIS*, **27**, 166 pp.

Arfeuille, G., L. Mysak, and L.-B. Tremblay, 2000: Simulation of the interannual variability of the wind-driven Arctic sea-ice cover during 1958-1998. *Geophys. Res. Lett.*, **30**, doi:10.1029/2002GL016271.

Bacon, S., W. Gould, and Y. Jia, 2003: Open-ocean convection in the Irminger Sea. *GRL.*, **30**(5), Art. No. 1236.

Baldwin, M., D. Stephenson, D. Thompson, T. Dunkerton, A. Charlton, and A. O'Neill, 2003: Stratospheric Memory and Skill of Extended-range Weather Forecasts. *SCIENCE*, **301**, 636–640.

Belkin, I., S. Levitus, J. Antonov, and S.-A. Malmberg, 1998: "Great Salinity Anomalies" in the North Atlantic. *Progr. Oceanogr.*, **41**, 1–68.

Bitz, C., J. Fyfe, and G. Flato, 2002: Sea Ice Response to Wind Forcing from AMIP Models. *J. Climate*, **15**, 522–536.

Bojariu, R. and L. Gimeno, 2003: Predictability and numerical modelling of the North Atlantic Oscillation. *EARTH SCIENCES REVIEWS*, **63**(1-2), 145–168.

Boyer, T., S. Levitus, J. Antonov, M. Conkright, T. O'Brien, and C. Stephens, 1998: World Ocean Atlas 1998 Vol.4: Salinity of the Atlantic Ocean. *NOAA Atlas NESDIS*, **30**, 166 pp.

Brümmer, B., G. Müller, B. Affeld, R. Gerdes, M. Karcher, and F. Kauker, 2001: Cyclones over Fram Strait: impact on sea ice and variability. *Polar Research*, **20**(2), 147–152.

Brümmer, B., G. Müller, and H. Hober, 2003: A Fram Strait cyclone: Properties and impact on ice drift as measured by aircraft and buoys. *J. Geophys. Res.*, **108**(D7), 6/1–6/13.

Castanheira, J. and H.-F. Graf, 2003: North Pacific-North Atlantic relationships under stratospheric control. *J. Geophys. Res.*, **108**(D1), 11/1–11/10.

Cavalieri, D., 2002: A link between Fram Strait sea ice export and atmospheric planetary wave phase. *Geophys. Res. Lett.*, **29**(12), Art. No. 1614.

Cavalieri, D. and S. Häkkinen, 2001: Arctic climate and atmospheric planetary waves. *Geophys. Res. Lett.*, **28**(5), 791–794.

Charlton, A., W. Lahoz, A. Neill, and A. Massacand, 2004: Sensitivity of tropospheric forecasts to stratospheric initial conditions. *Quaterly J. Roy. Met. Soc.*, **130**(660), 1771–1792.

Charlton, A., A. Neill, D. Stephenson, W. Lahoz, and M. Baldwin, 2003: Can knowledge of the state of the stratosphere be used to improve statistical forecasts of the troposphere? *Quaterly J. Roy. Met. Soc.*, **129**(595), 3205–3224.

Christiansen, B., 2001: Downward propagation of zonal wind anomalies from the stratosphere to the troposphere: Model and reanalysis. *J. Geophys. Res.*, **105**, 27307–27322.

Christiansen, B., 2002: On the physical nature of the Arctic Oscillation. *Geophys. Res. Lett.*, **29**(16), Art. No. 1805.

Cohen, J., K. Saito, and D. Entekhabi, 2000: The role of the Siberian high in Northern Hemisphere climate variability. *Geophys. Res. Lett.*, **28**(2), 299–302.

Cullather, R., D. Bromwich, and M. Serreze, 2000: The Atmospheric Cycle over the Arctic Basin from Reanalysis. Part I: Comparison with Observations and Previous Studies. *Amer. Meteor. Soc.*, **13**, 923–937.

D'Andrea, S., S. Tibaldi, M. Blackburn, G. Boer, M. Deque, M. Dix, B. Dugas, L. Ferranti, T. Iwasaki, A. Kitoh, V. Pope, D. Randall, E. Roeckner, D. Straus, W. Stern, H. V. den Dool, and D. Williamson, 1998: Northern Hemisphere atmosperic blocking as simulated by 15 atmospheric general circulation models in the period 1979-1988. *Clim. Dyn.*, **14**, 385–407.

Deser, C., M. Holland, G. Reverdin, and M. Timlin, 2002: Decadal variations in Labrador Sea ice cover and North Atlantic sea surface temperature. *J. Geophys. Res.*, **107**(C5), 10.129/2000JC0000683.

Deser, C., G. Magnusdottir, R. Saravanan, and A. Phillips, 2004: The Effects of North Atlantic SST and Sea Ice Anomalies on the Winter Circulation in CCM3. Part 2: Direct and Indirect Components of the Response. *J. Climate*, **17**, 2160–2176.

Deser, C., J. Walsh, and M. Timlin, 2000: Arctic sea ice variability in the context of recent atmospheric circulation trends. *J. Climate*, **13**, 607–633.

Dickson, R., J. Meincke, S.-A. Malmberg, and A. Lee, 1988: The "Great Salinity Anomaly" in the northern North Atlantic, 1968-1982. *Progr. Oceanogr.*, **20**, 103–151.

Dickson, R., T. Osborn, J. Hurrell, J. Meincke, J. Blindheim, B. Adlandsvik, T. Vinje, G. Alekseev, and W. Maslowski, 2000: The Arctic Ocean Response to the North Atlantic Oscillation. *J. Climate*, **13**, 2671–2696.

Dorn, W., K. Dethloff, A. Rinke, and M. Botzet, 2000: Distinct circulation states of the Arctic atmosphere induced by natural climate variability. *J. Geophys. Res.*, **105**(D24), 29659–29668.

EWG, 1997: Joint U.S.-Russian Atlas of the Arctic Ocean for the Winter Period. *Natl. Snow and Ice Data Cent., CD-ROM*.

EWG, 1998: Joint U.S.-Russian Atlas of the Arctic Ocean for the Summer Period. *Natl. Snow and Ice Data Cent., CD-ROM*.

Ghil, M., M. Allen, M. Dettinger, K. Ide, D. Kondrashov, M. Mann, A. Robertson, A. Saunders, Y. Tian, F. Varadi, and P. Yiou, 2002: Advanced Spectral Methods for Climatic Time Series. *Reviews of Geophysics*, **40**(1), 1–41.

Gong, G., D. Entkhabi, and J. Cohen, 2003: Modeled Northern Hemisphere Winter Climate Response to Realistic Siberian Snow Anomalies. *J. Climate*, **16**, 3917–3931.

Goosse, H., T. Fichefet, and J.-M. Campin, 1997: The effects of the water flow through the Canadian Archipelago in a global ice-ocean model. *Geophys. Res. Lett.*, **24**(12), 1507–1510.

Goosse, H., F. Selten, R. Haarsma, and J. Opsteegh, 2002: A mechanism of decadal variability of the sea-ice volume in the Northern Hemisphere. *Clim. Dyn.*, **19**, 61–83.

Goosse, H., F. Selten, R. Haarsma, and J. Opsteegh, 2003: Large sea-ice volume anomalies simulated in a coupled climate model. *Clim. Dyn.*, **20**, 523–536.

Graversen, R. and B. Christiansen, 2003: Downward propagation from the stratosphere to the troposphere: A comparison of the two hemispheres. *J. Geophys. Res.*, **D24**, Art. No. 4780.

Gulev, S., O. Zulina, and S. Grigoriev, 2001: Extratropical cyclone variability in the Northern Hemsiphere winter from the NCEP/NCAR reanalysis data. *Clim. Dyn.*, **17**, 795–809.

Haak, H., J. Jungclaus, U. Mikolajewicz, and M. Latif, 2003: Formation and propagation of great salinity anomalies. *Geophys. Res. Lett.*, **30**(9), 26/1–26/4.

Haas, C., 2004: Late-summer sea ice thickness variability in the Arctic Transpolar Drift 1991-2001 derived from ground-based electromagnetic sounding. *Geophys. Res. Lett.*, **31**(L09402), doi:10.129/2003GL019394.

Haas, C. and H. Eicken, 2001: Interannual variability of summer sea ice thickness in the Siberian and central Arctic under different atmospheric circulation regimes. *J. Geophys. Res.*, **106**(C3), 4449–4462.

Hagemann, S. and L. Dümenil, 1998: A parameterisation of the lateral waterflow for the global scale. *Clim. Dyn.*, **14**(1), 17–31.

Hagemann, S. and L. Dümenil-Gates, 2003: Improving a subgrid runoff parameterisation scheme for climate models by the use of high resolution data derived from satellite observations. *Clim. Dyn.*, **21**(3-4), 349–359.

Häkkinen, S., 1993: An Arctic Source for the Great Salinity Anomaly: A Simulation of the Arctic Ice-Ocean System for 1955-1975. *J. Geophys. Res.*, **98**(C9), 16397–16410.

Häkkinen, S., 1999: A simulation of thermohaline effects of a Great Salinity Anomaly. *J. Climate*, **6**, 1781–1795.

Häkkinen, S., 2002: Surface salinity variability in the northern North Atlantic during recent decades. *J. Geophys. Res.*, **107**(C12), doi:10.129/2001JC000812.

Hall, M. and H. Byrden, 1982: Direct estimates and mechanisms of ocean heat transport. *Deep Sea Res.*, **29**, 339–359.

Harnik, N. and E. Chang, 2003: Storm Track Variations As Seen in Radiosonde Observations and Reanalysis Data. *J. Climate*, **16**, 480–495.

Hibler, W., 1979: A dynamic thermodynamic sea ice model. *J. Phys. Oceanogr.*, **9**, 815–846.

Hilmer, M., M. Harder, and P. Lemke, 1998: Sea ice transport: a highly variable link between Arctic and North Atlantic. *Geophys. Res. Lett.*, **25**(17), 3359–3362.

Hilmer, M. and T. Jung, 2000: Evidence for a recent change in the link between the North Atlantic Oscillation and Arctic sea ice export. *Geophys. Res. Lett.*, **27**(7), 989–992.

Hilmer, M. and P. Lemke, 2000: On the Decrease of Arctic Sea Ice Volume. *Geophys. Res. Lett.*, **27**(22), 3751–3754.

Hoerling, M., A. Kumar, and M. Zhong, 1997: El Nino, La Nina, and the nonlinearity of their teleconnections. *J. Climate*, **10**, 1769–1786.

Holland, M., 2003: The North Atlantic Oscillation - Arctic Oscillation in the CCSM2 and Its Influence on the Arctic Climate Variability. *J. Climate*, **16**, 2767–2781.

Holland, M. and C. Bitz, 2003: Polar amplification of climate change in coupled models. *Clim. Dyn.*, **21**, 221–232.

Houghton, R. and M. Visbeck, 2002: Quasi-decadal salinity fluctuations in the Labrador Sea. *J. Phys. Oceanogr.*, **32**, 687–701.

Hurrel, J., 1995: Decadal Trends in the North Atlantic Oscillation: Regional Temperatures and Precipitation. *Science*, **269**, 676–679.

Hurrel, J. and H. van Loon, 1997: Decadal variations in climate associated with the North Atlantic Oscillation. *Climate Change*, **36**, 301–326.

Hvidegaard, S. and R. Forsberg, 2002: Sea-ice thickness from airborne laser altimetry over the Arctic Ocean north of Greenland. *Geophys. Res. Lett.*, **29**(20), 13/1–13/4.

Itoh, H., 2002: True versus apparent arctic oscillation. *Geophys. Res. Lett.*, **29**(8), 109/1–109/4.

Johannessen, O. and C. Myrmehl, 2002: Ice cover data analysis - Arctic. *Technical Report 2, AICSEX*.

Jung, T. and M. Hilmer, 2001: The link between the North Atlantic Oscillation and Arctic sea ice export. *J. Climate*, **14**(19), 3932–3943.

Jungclaus, J., H. Haak, M. Latif, and U. Mikolajewicz, in press: Arctic-North Atlantic Interactions and Multidecadal Variability of the Meridional Overturning Circulation. *J. Climate*.

Kalnay, E., M. Kanamitsu, R. Kistler, W. Collins, D. Deaven, L. Gandin, M. Iredell, S. Saha, G. White, J. Woollen, Y. Zhu, M. Chelliah, W. Ebisuzaki, W. Higgins, J. Janowiak, K. Mo, C. Ropelewski, A. Wang, J.and Leetmaa, R. Reynolds, R. Jenne, and D. Joseph, 1996: The NCEP/NCAR 40-Year Reanalysis Project. *Bull. Amer. Meteor. Soc.*, **77**(3), 437–471.

Kistler, R., E. Kalnay, W. Collins, S. Saha, G. White, J. Woollen, M. Chelliah, W. Ebisusaki, M. Kanamitsu, V. Kousky, H. van den Dool, R. Jenne, and M. Fiorino, 2001: The NCEP/NCAR 50-Year Reanalysis: Monthly Means CD-ROM and Documentation. *Bull. Amer. Meteor. Soc.*, **82**(2), 247–267.

Koeberle, C. and R. Gerdes, 2003: Mechanisms Determining the Variability of Arctic Sea Ice Conditions and Export. *J. Climate*, **16**, 2843–2858.

Koeberle, C., R. Gerdes, and F. Kauker, 1999: Mechanisms determining Fram Strait ice export variability. *ICES-CM 1999/L:25*, p. 7 pp.

Koenigk, T., U. Mikolajewicz, J. Jungclaus, and H. Haak, accepted: Variability of Fram Strait Sea Ice Export: Causes, Impacts and Feedbacks in a Coupled Climate Model. *Clim. Dyn.*.

Kwok, R., 2000: Recent Changes in Arctic Ocean Sea Ice Motion Associated with the North Atlantic Oscillation. *Geophys. Res. Lett.*, **27**(6), 775–778.

Kwok, R. and D. A. Rothrock, 1999: Variability of Fram Strait ice flux and North Atlantic Oscillation. *J. Geophys. Res.*, **104**(C3), 5177–5189.

Latif, M., E. Roeckner, M. Botzet, M. Esch, H. Haak, S. Hagemann, J. Jungclaus, S. Legutke, S. Marsland, U. Mikolajewicz, and J. Mitchell, 2004: Reconstructing, monitoring and predicting multidecadal scale changes in the North Atlantic thermohaline circulation with sea surface temperatures. *J. Climate*, **17**(7), 1605–1614.

Lavender, K., R. Davis, and W. Owens, 2002: Observations of open-ocean deep convection in the Labrador Sea from subsurface floats. *J. Phys. Oceanogr.*, **32**(2), 511–526.

Lazier, J., 1995: The salinity decrease in the Labrador Sea over the past thirty years. *In: Natural Climate Variability on Decade-to-Century time scales (edited by D.G. Martinson, K. Bryan, M. Ghil, M.M. Hall, T.M. Karl, E.S. Sarachik, S. Sorooshian and L. Talley)*, pp. 295–304.

Legutke, S., E. Maier-Reimer, A. Stössel, and A. Hellbach, 1997: Ocean - sea-ice coupling in a global ocean general circulation model. *Ann. Glaciol.*, **25**, 116–120.

Levitus, S., T. Boyer, M. Conkright, T. O'Brian, J. Antonov, C. Stephens, L. Stathopolos, D. Johnson, and R. Gelfeld, 1998: World Ocean Database 1998: Volume 1: Introduction. *NOAA Atlas NESDIS 18, Ocean Climate Laboartory,National Oceanographic Data Center, U.S. Gov. Printing Office, Wash., D.C...*

Lin, H., J. Derome, and R. Greatbatch, 2002: Tropical links of the Arctic Oscillation. *Geophys. Res. Lett.*, **29**(20), Art. No. 1943.

Magnusdottir, G., C.Deser, and R. Saravanan, 2004: The Effects of North Atlantic SST and Sea Ice Anomalies on the Winter Circulation in CCM3. Part 1: Main Features and Storm Track Characteristics of the Response. *J. Climate*, **17**(5), 857–876.

Marsland, S., H. Haak, J. Jungclaus, M. Latif, and F. Röske, 2003: The Max-Planck-Institute global ocean/sea ice model with orthogonal curvilinear coordinates. *Ocean Modelling*, **5**, 91–127.

Martin, T. and T. Martin, submitted: Variability of Arctic Sea Ice Transports. *J. Geophys. Res.*.

Maslanik, J., M. Serreze, and R. Barry, 1996: Recent decreases in Arctic summer ice cover and linkages to atmospheric circulation anomalies. *Geophys. Res. Lett.*, **23**(13), 1677–1680.

Mauritzen, C. and S. Häkkinen, 1997: Influence of sea ice on the thermohaline circulation in the Arctic-North Atlantic Ocean. *Geophys. Res. Lett.*, **24**(24), 3257–3260.

Meincke, J., B. Rudels, and H. Friedrich, 1997: The Arctic ocean Nordic seas thermohaline system. *ICES Journal of Marine Science*, **54**(3), 283–299.

Mikolajewicz, U., D. Sein, D. Jacob, T. Kahl, R. Podzun, and T. Semmler, submitted: Simulating Arctic sea ice variability with a coupled regional atmosphere-ocean-sea ice model. *Meteor. Z.*.

Miletta Adams, J., N. Bond, and J. Overland, 2000: Regional Variability of the Arctic Heat Budget in Fall and Winter. *J. Climate*, **13**, 3500–3510.

Mo, K. and R. Higgins, 1996: Large-Scale Atmospheric Moisture Transport as Evaluated in the NCEP/NCAR and the NASA/DAO Reanalysis. *J. Climate*, **9**, 1531–1545.

Morawitz, W., P. Sutton, P. Worcester, B. Cornuelle, J. Lynch, and R. Pawlowitz, 1996: Three-dimensional observations of a deep convective chimney in the Greenland Sea during winter 1988/89. *J. Phys. Oceanogr.*, **26**, 2316–2343.

Moritz, R., C. Bitz, and E. Steig, 2002: Dynamics of Recent Climate Change in the Arctic. *Science*, **297**, 1497–1502.

Murray, R. and I. Simmonds, 1995: Responses of climate and cyclones to reductions in Arctic winter sea ice. *J. Geophys. Res.*, **100**(C3), 4791–4806.

Mysak, L. and S. Venegas, 1998: Decadal climate oscillations in the Arctic: A new feedback loop for atmosphere-ice-ocean interactions. *Geophys. Res. Lett.*, **25**(19), 3607–3610.

Noone, D., Y. Yung, and R. Shia, submitted: The Northern Annual Mode response to Arctic sea ice loss and the sensitivity of tropophere-stratosphere interactions. *J. Climate*.

North, G., T. Bell, and R. Cahalan, 1982: Sampling errors in the estimation of Empirical Orthogonal Functions. *Mon. Wea. Rev*, **110**, 699–706.

Norton, W., 2002: Sensitivity of Northern Hemisphere surface climate to simulations of the stratospheric polar vortex. *Atmospheric, Oceanic and Planetary Physics, University of Oxford, Oxford, UK*, pp. 1–5.

O'Hanlon, L., 2002: Making waves. *NATURE*, **415**, 360–362.

Orvik, K. and P. Niiler, 2002: Major pathways of Atlantic water in the northern North Atlantic and Nordic Seas toward Arctic. *Geophys. Res. Lett.*, **29**(29), 2/1–2/4.

Ostermeier, G. and J. Wallace, 2003: NOTES AND CORRESPONDENCE. Trends in the North Atlantic Oscillation-Northern Hemisphere Annular Mode during the Twentieth Century. *J. Climate*, **16**, 336–341.

Parkinson, C., D. Cavalieri, P. Gloersen, H. Zwally, and J. Comiso, 1999: Arctic sea ice extents, areas, and trends, 1978-1996. *J. Geophys. Res.*, **104**(C9), 20837–20856.

Pickart, R., M. Spall, M. Ribergaard, G. Moore, and R. Milliff, 2000: Deep convection in the Irminger Sea forced by the Greenland tip jet. *Nature*, **424**, 152–156.

Polyakov, I. and M. Johnson, 2000: Arctic decadal and interdecadal variability. *Geophys. Res. Lett.*, **27**(24), 4097–4100.

Polyakov, I., D. Walsh, I. Dmitrenko, and R. Colony, 2003: Arctic Ocean variability derived from historical observations. *Geophys. Res. Lett.*, **30**(6,1298), doi:10.1029/2002GL016441.

Power, S., A. Moore, D. Post, N. Smith, and R. Kleemann, 1994: Stability of North Atlantic Deep Water formation in a global ocean general circulation model. *J. Phys. Oceanogr.*, **24**, 904–916.

Proshutinsky, A. and M. Johnson, 1997: Two circulation regimes of the wind-driven Arctic Ocean. *J. Geophys. Res.*, **102**(C6), 12493–12514.

Rasmusson, E. and K. Mo, 1996: Large-Scale Atmospheric Moisture Cycling as Evaluated from NMC Global Analysis and Forecast Products. *Mon. Wea. Rev*, **95**, 403–426.

Richman, M., 1986: Rotation of principal components. *J. Climatol.*, **6**, 293–335.

Rigor, I., J. Wallace, and R. Colony, 2002: Response of Sea Ice to the Arctic Oscillation. *J. Climate*, **15**, 2648–2663.

Roeckner, E., G. Bäuml, L. Bonaventura, R. Brokopf, M. Esch, M. Giorgetta, S. Hagemann, I. Kirchner, L. Kornblueh, E. Manzini, A. Rhodin, U. Schlese, U. Schulzweida, and A. Tompkins, 2003: The atmosphere general circulation model ECHAM5, part 1: Model description. *Max-Planck-Institute für Meteorologie , Report No. 349*, p. 127 pp.

Rogers, J., 1990: Patterns of Low-Frequency Monthly Sea Level Pressure Variability (1899-1986) and Associated Wave Cyclone Frequencies. *J. Climate*, **3**, 1364–1379.

Rogers, J., 1997: North Atlantic Storm Track Variabilty and Its Association to the North Atlantic Oscillation and Climate Variability of Northern Europe. *J. Climate*, **10**, 1635–1647.

Rogers, J. and E. Mosley-Thompson, 1995: Atlantic Arctic Cyclones and the Mild Siberian Winters of the 1980s. *Geophys. Res. Lett.*, **22**(7), 799–802.

Rogers, J. M. M., 2002: On the separability of the North Atlantic oscillation and Arctic oscillation. *Clim. Dyn.*, **19**, 599–608.

Römmich, D. and C. Wunsch, 1985: Two transatlantic sections: meridional circulation and heat flux in the subtropical North Atlantic Ocean. *Deep Sea Res.*, **32**, 619–664.

Rothrock, D., Y. Yu, and G. Maycut, 1999: Thinning of Arctic sea ice cover. *Geophys. Res. Lett.*, **26**, 3469–3472.

Rudels, B., D. Quadfasel, H. Freidrich, and M. Houssais, 1989: Greenland Sea Convection in the winter of 1987-1988. *J. Geophys. Res.*, **94**(C3), 3223–3227.

Ruprecht, E. and T. Kahl, 2003: Investigation of the atmospheric water budget of the BALTEX area using NCEP/NCAR reanalysis data. *Tellus*, **55A**, 426–437.

Schmith, T. and C. Hansen, 2003: Fram Strait ice export during the 19^{th} and 20^{th} centuries: evidence for multidecadal variability. *J. Climate*, **16**(16), 2782–2791.

Serreze, 1994: Climatological Aspects of Cyclone Development and Decay in the Arctic. *Atmos. Ocean*, **33**(1), 1–23.

Serreze, M. and R. Barry, 1988: Synoptic Activity in the Arctic Basin, 1979-85. *J. Climate*, **1**, 1276–1295.

Steele, M., R. Morley, and W. Ermold, 2001: PHC: A global ocean hydrography with highquality Arctic Ocean. *J. Climate*, **14**, 2079–2087.

Stössel, A., 1992: The Hamburg sea-ice model. *Technical Report 3, DKRZ Hamburg, Germany*.

Terray, L., S. Valcke, and A. Piacentini, 1998: OASIS 2.2, ocean atmosphere sea ice soil user's guide and reference manual. *Tech. Rep. TR/CGMC/98-05,Centre Européen de Recherche et de Formation en Calcul Scientifique Avancé (CERFACS), Toulouse, France*.

Thompson, D., M. Baldwin, and J. Wallace, 2002: Stratospheric connection to the Northern Hemisphere wintertime weather: Implication for prediction. *J. Climate*, **15**(12), 1421–1428.

Thompson, D. and J. Wallace, 1998: The Arctic Oscillation signature in the wintertime geopotential height and temperature fields. *Geophys. Res. Lett.*, **25**(9), 1297–1300.

Thorndike, A. and R. Colony, 1982: Sea Ice Motion in Response to Geostrophic Winds. *J. Geophys. Res.*, **87**(C8), 5845–5852.

Tremblay, L. and L. Mysak, 1998: On the origin and evolution of sea-ice anomalies in the Beaufort-Chukchi Sea. *Clim. Dyn.*, **14**, 451–460.

Trenberth, K. and C. Guillemot, 1998: Evaluation of the atmospheric moisture and hydrological cycle in the NCEP/NCAR reanalyses. *Clim. Dyn.*, **14**, 213–231.

Vavrus, S. and S. Harrison, 2003: The impact of sea-ice dynamics on the Arctic climate system. *Clim. Dyn.*, **20**, 741–757, doi:10.1007/s00382–003–0309–5.

Venegas, S. and L. Mysak, 2000: Is There a Dominant Timescale of Natural Climate Variability in the Arctic? *J. Climate*, **13**, 3412–3434.

Vinje, T., 2001a: Anomalies and Trends of Sea-Ice Extent and Atmospheric Circulation in the Nordic Seas during the Period 1864-1998. *J. Climate*, **14**, 255–267.

Vinje, T., 2001b: Fram Strait Ice Fluxes and Atmospheric Circulation: 1950-2000. *J. Climate*, **14**, 3508–3517.

Vinje, T., N. Nordlund, and A. Kvambeck, 1998: Monitoring ice thickness in Fram Strait. *J. Geophys. Res.*, **103**, 10437–10449.

von Storch, H., 1995: Spatial patterns: EOFs and CCA. *In: H. von Storch and A. Navarra, eds., Analysis of Climate Variability: Application of Statistical Techniques, Springer Verlag.*, pp. 227–257.

von Storch, H. and F. Zwiers, 1999: Statistical Analysis in Climate Resaerch. *Cambridge University Press*, p. 484 pp.

Wadhams, P., G. Budeus, J. Wilkinson, T. Loyning, and V. Pavlov, 2004: The multi-year development of long-lived convective chimneys in the Greenland Sea. *Geophys. Res. Lett.*, **31**(L06306), doi:10.1029/2003GL019017.

Wadhams, P. and J. Comiso, 1991: Concurrent Remote-Sensing of Arctic Sea Ice from Submarine and Aircraft. *International Journal of Remote Sensing*, **12**(9), 1829–1840.

Wadhams, P., J. Holfort, E. Hansen, and J. Wilkinson, 2002: A deep chimney in the winter Greenland Sea. *Geophys. Res. Lett.*, **29**(10), doi:10.1029/2001GL014306.

Wallace, J. and D. Gutzler, 1981: Teleconnections in the geopotential height field during the Northern Hemisphere winter. *Mon. Wea. Rev*, **109**, 784–812.

Walsh, J. and W. Chapman, 1990: Arctic contribution to upper ocean variability in the North Atlantic. *J. Climate*, **3**(12), 1462–1473.

Wang, J. and M. Ikeda, 2000: Arctic Oscillation and Arctic Sea Ice Oscillation. *Geophys. Res. Lett.*, **27**(9), 1287–1290.

Weatherly, J., B. Briegleb, W. Large, and J. Maslanik, 1998: Sea ice and polar climate in the NCAR CSM. *JC*, **11**, 1472–1486.

Wettstein, J. and L. Mearns, 2002: The influence of the North Atlantic - Arctic Oscillation on mean, variance and extremes of temperatures in the northeastern United States and Canada. *J. Climate*, **15**(24), 3586–3600.

Winsor, P., 2001: Arctic Sea Ice Thickness Remained Constant During the 1990s. *Geophys. Res. Lett.*, **28**(6), 1039–1041.

Yu, Y., G. Maykut, and D. Rothrock, 2004: Changes in the thickness distribution of Arctic sea ice between 1958-1970 and 1993-1997. *J. Geophys. Res.*, **109**(C08004), doi:10.129/2003JC001982.

Zhang, J., W. Hibler, M. Steele, and D. Rothrock, 1998: Arctic Ice-Ocean Modeling with and without Climate Restoring. *J. Phys. Oceanogr.*, **28**, 191–217.

Acknowledgements

I am very grateful to Dr. Uwe Mikolajewicz and Prof. Dr. Jens Meincke for supervising this thesis and for supporting my scientific interest.
I thank my colleagues from the MPI Hamburg and the SFB 512 for numerous fruitful discussions. Furthermore they provided a stimulating atmosphere.
I am much obliged to Elijah Quetin, Dr. Matthias Gröger and Dr. Helmuth Haak. Special thanks go to my wife Cathérine for her patience and support.

The computations have been performed by the Deutsches Klima Rechenzentrum (DKRZ). The German Research Foundation provided financial support in the framework of the Sonderforschungsbereich 512 "Tiefdruckgebiete und Klimasystem des Nordatlantiks".

MPI-Examensarbeit-Referenz:

Examensarbeit Nr. 1-82 bei Bedarf bitte Anfragen:
MPI für Meteorologie, Abtlg.: PR, Bundesstr. 53, 20146 Hamburg

Examensarbeit Nr. 83 Juli 2001	**Aggregate models of climate change: development and applications** Kurt Georg Hooss
Examensarbeit Nr. 84 Februar 2002	**Ein Heterodyn-DIAL System für die simultane Messung von Wasserdampf und Vertikalwind: Aufbau und Erprobung** Stefan Lehmann
Examensarbeit Nr. 85 April 2002	**Der Wasser- und Energiehaushalt der arktischen Atmosphäre** Tido Semmler
Examensarbeit Nr. 86 April 2002	**Auswirkungen der Assimilation von Meereshöhen-Daten auf Analysen und Vorhersagen von El Niño** Sigrid Schöttle
Examensarbeit Nr. 87 Juni 2002	**Atmospheric Processes in a young Biomass Burning Plume - Radiation and Chemistry** Jörg Trentmann
Examensarbeit Nr. 88 August 2002	**Model Studies of the Tropical 30 to 60 Days Oscillation** Stefan Liess
Examensarbeit Nr. 89 Dezember 2002	**Influence of Sub-Grid Scale Variability of Clouds on the Solar Radiative Transfer Computations in the ECHAM5 Climate Model** Georg Bäuml
Examensarbeit Nr.90 Mai 2003	**Model studies on the response of the terrestrial carbon cycle to climate change and variability** Marko Scholze
Examensarbeit Nr.91 Juni 2003	**Integrated Assessment of Climate Change Using Structural Dynamic Models** Volker Barth
Examensarbeit Nr.92 Juli 2003	**Simulations of Indonesian Rainfall with a Hierarchy of Climate Models** Edvin Aldrian
Examensarbeit Nr.93 Juli 2003	**ENSO Teleconnections in High Resolution AGCM Experiments** Ute Merkel
Examensarbeit Nr.94 Juli 2003	**Application and Development of Water Vapor DIAL Systems** Klaus Ertel

MPI-Examensarbeit-Referenz:

Examensarbeit Nr. 1-82 bei Bedarf bitte Anfragen:
MPI für Meteorologie, Abtlg.: PR, Bundesstr. 53, 20146 Hamburg

Beginn einer neuen Veröffentlichungsreihe des MPIM, welche die vorherigen Reihen "Reports" und "Examensarbeiten" weiterführt:

„Berichte zur Erdsystemforschung" , „*Reports on Earth System Science*", ISSN 1614-1199
Sie enthält wissenschaftliche und technische Beiträge, inklusive Dissertationen.

Berichte zur Erdsystemforschung Nr.1 Juli 2004	**Simulation of Low-Frequency Climate Variability in the North Atlantic Ocean and the Arctic** Helmuth Haak
Berichte zur Erdsystemforschung Nr.2 Juli 2004	**Satellitenfernerkundung des Emissionsvermögens von Landoberflächen im Mikrowellenbereich** Claudia Wunram
Berichte zur Erdsystemforschung Nr.3 Juli 2004	**A Multi-Actor Dynamic Integrated Assessment Model (MADIAM)** Michael Weber
Berichte zur Erdsystemforschung Nr.4 November 2004	**The Impact of International Greenhouse Gas Emissions Reduction on Indonesia** Armi Susandi
Berichte zur Erdsystemforschung Nr.5 Januar 2005	**Proceedings of the first HyCARE meeting, Hamburg, 16-17 December 2004** Edited by Martin G. Schultz
Berichte zur Erdsystemforschung Nr.6 Januar 2005	**Mechanisms and Predictability of North Atlantic - European Climate** Holger Pohlmann
Berichte zur Erdsystemforschung Nr.7 November 2004	**Interannual and Decadal Variability in the Air-Sea Exchange of CO2 - a Model Study** Patrick Wetzel
Berichte zur Erdsystemforschung Nr.8 Dezember 2004	**Interannual Climate Variability in the Tropical Indian Ocean: A Study with a Hierarchy of Coupled General Circulation Models** Astrid Baquero Bernal
Berichte zur Erdsystemforschung Nr9 Februar 2005	**Towards the Assessment of the Aerosol Radiative Effects, A Global Modelling Approach** Philip Stier
Berichte zur Erdsystemforschung Nr.10 März 2005	**Validation of the hydrological cycle of ERA40** Stefan Hagemann, Klaus Arpe and Lennart Bengtsson
Berichte zur Erdsystemforschung Nr.11 Februar 2005	**Tropical Pacific/Atlantic Climate Variability and the Subtropical-Tropical Cells** Katja Lohmann


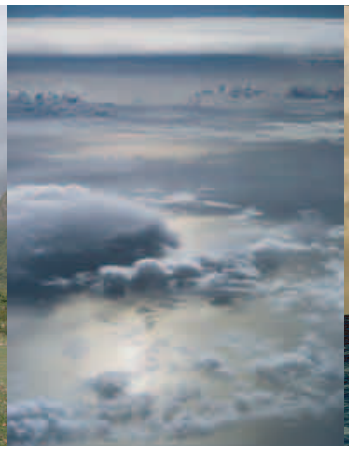


ISSN 1614-1199